Edwin A. Peraza Hernandez
Graduate Research Assistant
Department of Aerospace Engineering,
Texas A&M University,
College Station, TX 77843
e-mail: eperaza@tamu.edu

Darren J. Hartl
Research Assistant Professor
Department of Aerospace Engineering,
Texas A&M University,
College Station, TX 77843
e-mail: darren.hartl@tamu.edu

Dimitris C. Lagoudas[1]
Professor
Department of Aerospace Engineering,
Texas A&M University,
College Station, TX 77843;
Department of Materials
Science and Engineering,
Texas A&M University,
College Station, TX 77843
e-mail: lagoudas@tamu.edu

Kinematics of Origami Structures With Smooth Folds

Origami provides both inspiration and potential solutions to the fabrication, assembly, and functionality of various structures and devices. Kinematic modeling of origami-based objects is essential to their analysis and design. Models for rigid origami, in which all planar faces of the sheet are rigid and folds are limited to straight creases having only zeroth-order geometric continuity, are available in the literature. Many of these models include constraints on the fold angles to ensure that any initially closed strip of faces is not torn during folding. However, these previous models are not intended for structures with non-negligible fold thickness or with maximum curvature at the folds restricted by material or structural limitations. Thus, for general structures, creased folds of merely zeroth-order geometric continuity are not appropriate idealizations of structural response, and a new approach is needed. In this work, a novel model analogous to those for rigid origami with creased folds is presented for sheets having realistic folds of nonzero surface area and exhibiting higher-order geometric continuity, here termed smooth folds. The geometry of smooth folds and constraints on their associated shape variables are presented. A numerical implementation of the model allowing for kinematic simulation of sheets having arbitrary fold patterns is also described. Simulation results are provided showing the capability of the model to capture realistic kinematic response of origami sheets with diverse fold patterns. [DOI: 10.1115/1.4034299]

1 Introduction

Until recently, the term origami has been associated primarily with the ancient art of folding paper [1]. In origami, a goal shape is achieved from an initially planar sheet exclusively through folding. In this context, a *fold* is any deformation of the sheet in which the in-surface distance between any two points in the sheet is constant and the sheet does not self-intersect [2,3].

Engineering advantages of origami-inspired structures and devices include compact deployment/storage capability [4], a reduction in manufacturing complexity [5,6], and the potential for reconfigurability [7,8]. Existing and potential applications of origami solutions to device and structural design problems include deployable structures for space exploration [9–12], electronic components with improved properties [13–15], robotic components [16,17], foldable wings [18], cellular materials [19], metamaterials [20–23], and shelters [24,25], among others [26–28].

Rigid origami, the special case of origami for which the planar faces of the sheet are inflexible [29,30] has been studied in the past and remains an active subject [31]. Rigid origami has been utilized for the design of deployable structures and architectural constructions [30,32–34]. Theoretical modeling and simulation of rigid origami structures permit understanding of their kinematic behavior and the development of computational tools for their design. Rigid origami has been modeled using diverse approaches [29,35]. For example, Belcastro and Hull [36,37] presented a model for rigid origami derived by representing the deformation associated with folding using affine transformations. Their model provides constraints on the fold angles allowing for valid rigid origami configurations as well as mappings between unfolded and folded configurations. Tachi developed the *Rigid Origami Simulator* [29,38] for the simulation of rigid origami that also considered a set of constraints on the fold angles analogous to those presented in Refs. [36,37]. Using a similar approach, Tachi also developed *Freeform Origami* [39] for the simulation and design of freeform rigid origami structures represented as triangulated meshes [40].

Alternatively, truss representations [41] have been used wherein the polygonal faces of the sheet are triangulated, each fold or boundary edge end-point is represented by a truss joint, and each fold and boundary edge is represented by a truss member. The configurations for which the displacements of the truss joints do not cause elongations of the truss members represent valid rigid origami configurations. Additional constraints that allow the triangulated polygonal faces to remain planar are also considered for these models.

The majority of origami modeling approaches and design tools to date are based on the assumption of *creased folds* (see Fig. 1(*a*) for an example) that are straight line segments in the sheet that,

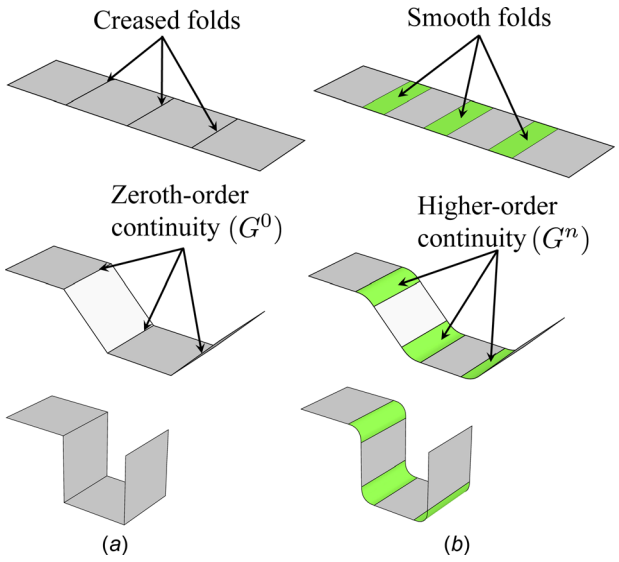

Fig. 1 (*a*) A conventional origami sheet having creased folds of zeroth-order geometric continuity (G^0). (*b*) A sheet having *smooth folds* of nonzero surface area and higher-order geometric continuity (G^n).

[1]Corresponding author.

Manuscript received April 24, 2016; final manuscript received July 13, 2016; published online October 11, 2016. Assoc. Editor: Robert J. Wood.

upon folding deformation, the sheet has zeroth-order geometric continuity (G^0) at such lines (i.e., the sheet tangent plane may be discontinuous at these folds). Curved creased folds are also allowed in origami (see Refs. [42–44]); nevertheless, the focus of this work is on rigid origami-based structures for which curved folds are not allowed because their folding deformation induces bending of the faces joined to such folds [43].

The idealization of physically folded structures as sheets having creased folds has been useful in the modeling and design of several origami-inspired structures in the past [20,23,32,45,46]. However, this simplification may not be appropriate for structures having non-negligible fold thickness or constructed from materials that do not provide sufficient strain magnitudes to generate the high curvatures required for a creased idealization. For these structures, the obtained folded regions may not be accurately represented as creases but rather as *bent* sheet regions having higher-order geometric continuity. These folded regions are referred to in this work as *smooth folds* (an example of a sheet with smooth folds is shown in Fig. 1(*b*)).

There have been past efforts to model and analyze surfaces that exhibit bent and creased folding. Origami-based bent and creased surfaces have been simulated using collections of developable surface subdomains [47–51]. Such advancements allow for the realistic animation and rendering of curved folds and combinations of creases and bent regions. However, none of the aforementioned works [47–51] have considered constraints on the geometry and deformation of the bent folded regions that are required to preserve rigid faces as in analogous rigid origami models, which are essential when fold intersections or holes are present in the sheet. In view of this, a novel model for the kinematic response of rigid origami-based structures having smooth folds is presented in this work. The proposed model for origami with smooth folds includes rigid origami with creased folds as a special case, hence being more general.

Modeling of origami-based morphing of plate structures having significant thickness at the fold regions requires the arbitrary order of continuity of smooth folds. The present model is also useful in the kinematic analysis of sheets folded via active material actuation, where the achievable curvature at the folds is limited by the maximum strain magnitude provided by such active materials [27]. Examples of these active material-based origami structures include liquid-crystal elastomer [52,53], shape memory alloy [54–57], dielectric elastomer [58,59], and optically responsive polymeric self-folding sheets [60–62], among others [27,63]. The different assumptions regarding strain distributions at the fold regions associated with the implementation of these various materials require the arbitrary order of continuity considered in this work.

The basic origami concepts and a review of the model for rigid origami with creased folds extended in this work are presented in Sec. 2. Section 3 presents the newly proposed model for origami with smooth folds. It includes the geometric description of smooth folds and the fold pattern, constraints required for valid configurations, and the numerical implementation of the model allowing for kinematic simulation of sheets having arbitrary patterns of smooth folds. Section 4 presents the simulation results of sheets with diverse fold patterns that demonstrate the model capabilities and the resulting realistic kinematic structural response captured by the model. Finally, Sec. 5 provides a summarizing discussion and concludes the paper.

2 Concepts and Review of Origami With Creased Folds

This section presents various concepts of origami and briefly reviews a model of rigid origami with creased folds for the purposes of developing the novel extensions proposed in this work. The notation used in this work is also introduced.

The origami modeling approach adopted and extended herein is largely based on Refs. [36,37]. The considered continuum body denoted as the *sheet*, and the shape variables associated with the creased folds in the sheet (e.g., *fold angles*) are first described. The layout of the folds in the sheet (i.e., the *fold pattern*) is then determined by *vertices* (start-points and end-points of the line segments coincident with the creased folds in a planar reference configuration) and their connectivity. After the geometric parameters of the fold pattern are determined, *constraints* on the fold shape variables required for valid rigid origami configurations are described. The set of configurations that satisfy the stated constraints comprises the constrained configuration space. *Continuous motion* of the sheet is achieved by continuously altering the fold shape variables such that any attained configuration is contained in the constrained configuration space (i.e., the motion of the sheet is a continuous path in the constrained configuration space).

In the present approach, the required fold pattern data (e.g., vertex coordinates and fold connectivity) are provided as inputs. Information on methods to design fold patterns for specific applications is provided in Refs. [3,46,64–71] and the references therein. The simulation of the continuous motion of the sheet is executed by incrementally updating the values of the fold shape variables using input guess increments and subsequently applies corrections such that the resulting set of fold shape variables satisfies the proposed constraints. Here, input guess increments for the fold shape variables are arbitrary and not obtained via any specific method. Motion planning in origami for various applications is being addressed by various researchers, and the reader is referred to Refs. [72–76] for such works.

To begin, the various concepts of origami previously introduced must be formalized. The considered continuum body is denoted as the *sheet*, which in this work is a three-dimensional, orientable, path-connected surface with boundary. A detailed description of a sheet for origami with creased folds is provided in Ref. [3]. For origami with creased folds, the sheet is divided into various *faces* that are connected by straight edges corresponding to the *creased folds*. Every face comprising the sheet has the same aforementioned characteristics of the sheet (i.e., they are three-dimensional, orientable, path-connected surfaces with boundary).

The orthonormal vectors $\mathbf{e}_i \in \mathbb{R}^3$, $i = 1, 2, 3$, with $\mathbf{e}_3 := \mathbf{e}_1 \times \mathbf{e}_2$ form the basis $\{\mathbf{e}_1, \mathbf{e}_2, \mathbf{e}_3\}$ that defines the fixed global coordinate system. The *reference configuration* of the sheet, denoted $\mathcal{S}_0$, is defined such that it is contained in the plane spanned by $\mathbf{e}_1$ and $\mathbf{e}_2$ with its faces not overlapping each other, except at their shared boundary edges. Although several applications that utilize origami concepts do not start from a planar, nonoverlapping configuration (e.g., Refs. [17,23,77]), the reference configuration $\mathcal{S}_0$ has such characteristics in this work to agree with conventional origami modeling approaches [36,37] and for the sake of simplicity. The configuration of the faces comprising $\mathcal{S}_0$ is denoted $\mathcal{P}_0^i \subset \mathcal{S}_0,\ i = 1, ..., N_\mathcal{P}$, where $N_\mathcal{P}$ is the number of faces in the sheet (i.e., $\mathcal{S}_0 = \cup_{i=1}^{N_\mathcal{P}} \mathcal{P}_0^i$). The side of $\mathcal{S}_0$ with normal $\mathbf{e}_3$ is selected as the *positive side* of the sheet. An example of a sheet in its reference configuration $\mathcal{S}_0$ is provided in Fig. 2(*a*).

A *current configuration* of the sheet is denoted $\mathcal{S}_t$ where the parameter t indicates the history of deformation from the reference configuration ($t = 0$) to a current configuration ($t > 0$). Examples of a sheet in the reference configuration and a current configuration are presented in Figs. 2(*a*) and 2(*b*), respectively. The configuration of the faces comprising $\mathcal{S}_t$ is denoted $\mathcal{P}_t^i \subset \mathcal{S}_t,\ i = 1, ..., N_\mathcal{P}$, i.e., $\mathcal{S}_t = \cup_{i=1}^{N_\mathcal{P}} \mathcal{P}_t^i$. As previously stated, the focus of this work is on rigid origami, which imposes the following constraints for the configurations $\mathcal{S}_t$ [36,37]:

DEFINITION 2.1. Valid configuration: *A valid current configuration $\mathcal{S}_t$ has the following characteristics: (i) the faces undergo only rigid deformations (i.e., they are neither stretched nor bent), (ii) the sheet is not torn (initially joined faces remain joined), and (iii) the sheet does not self-intersect.*

The only nonrigid body deformations of the sheet are thus achieved by rotating adjacent faces relative to one another along their connecting creased fold in such a manner that the sheet only

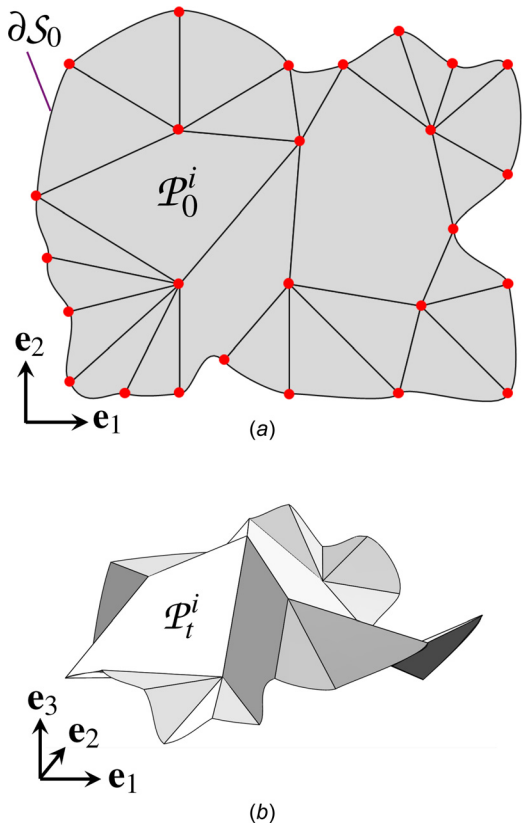

Fig. 2 Sheet with creased folds in its reference configuration $\mathcal{S}_0$ (*a*) and a current configuration $\mathcal{S}_t$ (*b*). The planar faces comprising the sheet undergo only rigid deformations.

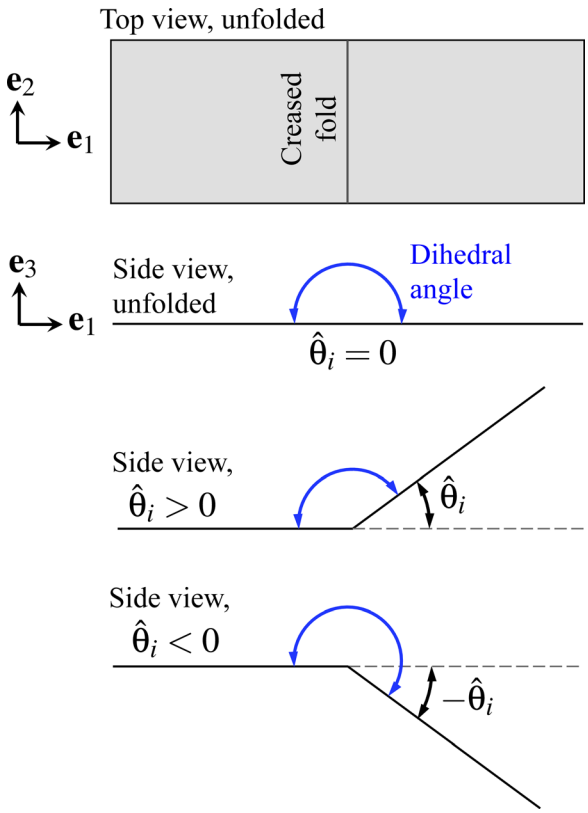

Fig. 3 Schematics showing unfolded and folded configurations of a creased fold

attains valid configurations during such deformations. Therefore, the sheet is G^0 continuous at the creased folds.

Any configuration of the sheet is fully described by the set of the *shape variables* associated with the creased folds. The only shape variable associated with a creased fold describes the relative rotation between the two faces joined by such a fold and is denoted as *fold angle*.

DEFINITION 2.2. *Fold angle*: *The fold angle $\hat{\theta}_i(t)$ is defined as π minus the dihedral angle between the positive sides of the two faces joined by the ith creased fold.*

Schematics showing the concept of fold angle are provided in Fig. 3. It is noted in the previous definition that each fold angle is a function of the parameter t. Specifically, each fold angle $\hat{\theta}_i(t)$, $i = 1, ..., N_{\mathcal{F}}$ (where $N_{\mathcal{F}}$ is the number of creased folds in the sheet) is a *continuous* function with respect to t since the motion of the sheet must be continuous (see Chap. 11 of Ref. [3]). For the remainder of this section, the dependence of $\hat{\theta}_i$ on t is left implicit to simplify the notation.

To avoid self-intersection of any pair of faces joined by a creased fold, the value of the associated fold angle must be contained in the interval $[-\pi, \pi]$. The vector $\hat{\boldsymbol{\theta}} \in \mathbb{R}^{N_{\mathcal{F}}}$ is constructed by collecting the fold angles as follows:

$$\hat{\boldsymbol{\theta}} = [\,\hat{\theta}_1 \quad \cdots \quad \hat{\theta}_{N_{\mathcal{F}}}\,]^\top \tag{1}$$

2.1 Fold Pattern. The layout of the creased folds in $\mathcal{S}_0$ is presented in a *fold pattern*, often referred to as *crease pattern* in this context of origami with creased folds [3,36,37]. To describe the fold pattern, the *vertices* are introduced:

DEFINITION 2.3. *Vertices*: *The vertices are the start-points and end-points of the line segments coincident with the creased folds in $\mathcal{S}_0$. Each vertex has an associated position vector denoted $\mathbf{v}^j \in \text{span}(\mathbf{e}_1, \mathbf{e}_2)$.*

The number of vertices located at the interior of $\mathcal{S}_0$ is denoted $N_{\mathcal{I}}$, and the number of vertices located at $\partial\mathcal{S}_0$ (the boundary of $\mathcal{S}_0$, see Fig. 2(*a*)) is denoted $N_{\mathcal{B}}$. The vertices are enumerated starting from those located at the interior of $\mathcal{S}_0$ (with corresponding position vectors $\mathbf{v}^1, ..., \mathbf{v}^{N_{\mathcal{I}}}$) followed by those located at $\partial\mathcal{S}_0$ (with corresponding position vectors $\mathbf{v}^{N_{\mathcal{I}}+1}, ..., \mathbf{v}^{N_{\mathcal{I}}+N_{\mathcal{B}}}$). The vector $\mathbf{V} \in \mathbb{R}^{3(N_{\mathcal{I}}+N_{\mathcal{B}})}$ is formed by concatenating the vertex position vectors $\mathbf{v}^j$, $j = 1, ..., N_{\mathcal{I}} + N_{\mathcal{B}}$, as follows:

$$\mathbf{V} = \begin{bmatrix} \mathbf{v}^1 \\ \vdots \\ \mathbf{v}^{N_{\mathcal{I}}+N_{\mathcal{B}}} \end{bmatrix} \tag{2}$$

The line segment coincident with a creased fold in $\mathcal{S}_0$, simply denoted as *fold line*, is defined by its start-point and end-point (both points corresponding to vertices by Definition 2.3). As such, to define the fold lines in $\mathcal{S}_0$, the matrix $\hat{\mathbf{C}} \in \{-1, 0, 1\}^{N_{\mathcal{F}} \times (N_{\mathcal{I}}+N_{\mathcal{B}})}$ with elements $\hat{C}_{ij}$ is introduced

$$\hat{C}_{ij} = \begin{cases} -1; & \mathbf{v}^j \text{ is the position of the } i\text{th fold line start} - \text{point} \\ 1; & \mathbf{v}^j \text{ is the position of the } i\text{th fold line end} - \text{point} \\ 0; & \text{otherwise, i.e., } \mathbf{v}^j \text{ is not connected to the } i\text{th} \\ & \text{fold line} \end{cases} \tag{3}$$

Let n_j, $j = 1, ..., N_{\mathcal{I}}$, be the number of fold lines incident to each interior vertex (i.e., those vertices located at the interior of $\mathcal{S}_0$). Also, let $\mathbf{m}^{jk} \in \text{span}(\mathbf{e}_1, \mathbf{e}_2)$, $j = 1, ..., N_{\mathcal{I}}$, $k = 1, ..., n_j$, be the vector along the length of the kth fold line incident to the jth interior vertex that emanates from such a vertex (see Fig. 4).

DEFINITION 2.4. *The angle between the vector $\mathbf{y} \in \text{span}(\mathbf{e}_1, \mathbf{e}_2)$ and $\mathbf{e}_1$, which starts at $\mathbf{e}_1$ and is measured in the counterclockwise direction, is denoted $\varphi(\mathbf{y}) : \text{span}(\mathbf{e}_1, \mathbf{e}_2) \to [0, 2\pi)$ and is determined as follows:*[2]

[2] $\|\cdot\|$ denotes the two-norm, i.e., $\|\mathbf{y}\| = (\mathbf{y} \cdot \mathbf{y})^{1/2}$.

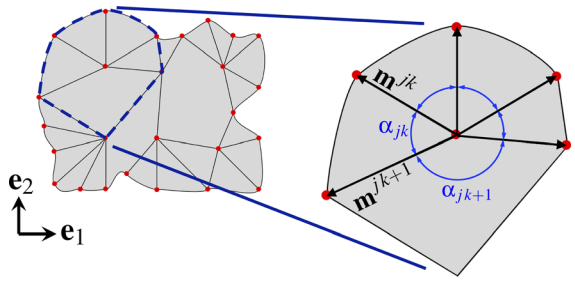

Fig. 4 Schematic showing faces and folds connected to an interior vertex and their associated geometric parameters

$$\varphi(\mathbf{y}) := \begin{cases} \cos^{-1}\left(\dfrac{\mathbf{y}}{\|\mathbf{y}\|}\cdot\mathbf{e}_1\right); & \mathbf{e}_2\cdot\mathbf{y}\geq 0 \\ 2\pi-\cos^{-1}\left(\dfrac{\mathbf{y}}{\|\mathbf{y}\|}\cdot\mathbf{e}_1\right); & \mathbf{e}_2\cdot\mathbf{y}<0 \end{cases} \tag{4}$$

For each interior vertex, its associated vectors $\mathbf{m}^{jk}$, $k=1,...,n_j$, are arranged in a counterclockwise ordering such that $\varphi(\mathbf{m}^{j1})<\varphi(\mathbf{m}^{j1})<\cdots<\varphi(\mathbf{m}^{jn_j})\quad \forall j\in\{1,...,N_{\mathcal{I}}\}$. Let $\mathbf{M}^j\in\mathbb{R}^{3n_j}$ be the vector constructed by concatenating the vectors $\mathbf{m}^{jk}$, $k=1,...,n_j$, as follows:

$$\mathbf{M}^j=\begin{bmatrix}\mathbf{m}^{j1}\\ \vdots\\ \mathbf{m}^{jn_j}\end{bmatrix} \tag{5}$$

The matrices $\mathbf{C}^j\in\{-1,0,1\}^{n_j\times N_{\mathcal{F}}}$, $j=1,...,N_{\mathcal{I}}$, with elements C^j_{ki} are used for the identification and ordering of the folds incident to the jth interior vertex and are defined as follows:

$$C^j_{ki}=\begin{cases} 1; & \mathbf{m}^{jk}\text{ is a vector along the }i\text{th fold line and}\\ & \text{emanates from the }i\text{th fold line start}-\text{point}\\ -1; & \mathbf{m}^{jk}\text{ is a vector along the }i\text{th fold line and}\\ & \text{emanates from the }i\text{th fold line end}-\text{point}\\ 0; & \text{otherwise}\end{cases} \tag{6}$$

The mapping from the vertex position vectors $\mathbf{v}^j$, $j=1,...,N_{\mathcal{I}}+N_{\mathcal{B}}$, to the vectors $\mathbf{m}^{jk}$, $k=1,...,n_j$, is then compactly given as follows:[3]

$$\mathbf{M}^j=((\mathbf{C}^j\hat{\mathbf{C}})\otimes\mathbf{I}_3)\mathbf{V} \tag{7}$$

where $\mathbf{I}_n$ denotes the $\mathbb{R}^{n\times n}$ identity matrix.

The face corner angles surrounding each interior vertex are denoted as $\alpha_{jk}\in(0,2\pi]$, $j=1,...,N_{\mathcal{I}}$, $k=1,...,n_j$, and are calculated as follows (see Fig. 4):

$$\alpha_{jk}=\begin{cases}\varphi(\mathbf{m}^{jk+1})-\varphi(\mathbf{m}^{jk}); & k=1,...,n_j-1\\ 2\pi+\varphi(\mathbf{m}^{j1})-\varphi(\mathbf{m}^{jk}); & k=n_j\end{cases} \tag{8}$$

2.2 Constraints. Once the geometry of the fold pattern is defined, constraints on the fold shape variables (corresponding to the fold angles for creased folds) are formulated such that every current configuration is valid according to Definition 2.1.[4] In addition to constraints for valid configurations, *developability* [40] is also conventionally imposed in origami. Developability allows a surface to be flattened onto a plane without stretching or overlapping. A developable surface has zero Gaussian curvature everywhere [79]. Since valid configurations of the sheet consist of planar faces joined at straight creased folds, the only location where the Gaussian curvature is nontrivially zero is at the interior fold intersections. The definition of Gaussian curvature as the product of the two principal curvatures is not valid at a singular interior fold intersection [80]; hence, the *discrete Gaussian curvature*, denoted K_j, is considered [54,80,81]. It is given as 2π less the sum of face corner angles surrounding each interior fold intersection [82], and it must be zero for the fold intersection to be developable

$$K_j=2\pi-\sum_{k=1}^{n_j}\alpha_{jk}=0\qquad\forall j\in\{1,...,N_{\mathcal{I}}\} \tag{9}$$

In this work, the angles α_{jk} are defined in $\mathcal{S}_0$, which is planar and having its faces only overlapping at their shared boundary edges, and thus, these angles clearly sum to 2π for each interior vertex. Therefore, the developability constraint in Eq. (9) is satisfied in $\mathcal{S}_0$. No further consideration of this constraint is required since the face corner angles are constant during the deformation history of the sheet (since the faces undergo only rigid deformations for valid configurations), and thus, they hold their associated values α_{jk} as defined in $\mathcal{S}_0$. As a consequence, developability is assured for any valid current configuration $\mathcal{S}_t$.

Nontrivial and important are the constraints on the fold angles that define the constrained configuration space. The set of constraints for $\hat{\theta}_i$, $i=1,...,N_{\mathcal{F}}$, required for a valid configuration can be formulated as a set of constraints for the fold angles associated with the folds incident to each interior vertex (assuming that the sheet has no holes) [32].

The fold angle associated with the kth fold incident to the jth interior vertex is denoted θ_{jk}. The vectors $\boldsymbol{\theta}^j\in\mathbb{R}^{n_j}$, $j=1,...,N_{\mathcal{I}}$, are formed by collecting the fold angles θ_{jk}, $k=1,...,n_j$, as follows:

$$\boldsymbol{\theta}^j=\begin{bmatrix}\theta_{j1} & \cdots & \theta_{jn_j}\end{bmatrix}^{\top} \tag{10}$$

and the mapping from the vector $\hat{\boldsymbol{\theta}}$ with elements corresponding to the fold angles of the sheet (defined in Eq. (1)) to each vector $\boldsymbol{\theta}^j$ is given as follows:

$$\boldsymbol{\theta}^j=|\mathbf{C}^j|_*\,\hat{\boldsymbol{\theta}} \tag{11}$$

where the elements of the matrix $\mathbf{C}^j$ are defined in Eq. (6), and $|\cdot|_*:\mathbb{R}^{m\times n}\to\mathbb{R}^{m\times n}_{\geq 0}$ denotes the elementwise absolute value of a matrix where $[|\mathbf{Y}|_*]_{ij}=|Y_{ij}|$.

Let $\mathbf{R}_1(\phi)\in\mathbb{R}^{3\times 3}$ be the transformation matrix associated with a rotation by ϕ about an axis of rotation aligned to $\mathbf{e}_1$

$$\mathbf{R}_1(\phi):=\begin{bmatrix}1 & 0 & 0\\ 0 & \cos(\phi) & -\sin(\phi)\\ 0 & \sin(\phi) & \cos(\phi)\end{bmatrix} \tag{12}$$

and $\mathbf{R}_3(\phi)\in\mathbb{R}^{3\times 3}$ be the transformation matrix associated with a rotation by ϕ about an axis of rotation aligned to $\mathbf{e}_3$

$$\mathbf{R}_3(\phi):=\begin{bmatrix}\cos(\phi) & -\sin(\phi) & 0\\ \sin(\phi) & \cos(\phi) & 0\\ 0 & 0 & 1\end{bmatrix} \tag{13}$$

The fold angles associated with the folds incident to each interior vertex θ_{jk}, $k=1,...,n_j$, must be constrained to prevent tearing of closed strip of faces joined to each interior vertex [36,37]. For this purpose, the following constraint is proposed:

PROPOSITION 2.1. *For the initially closed strip of faces joined to the jth interior vertex to remain closed with each face undergoing a rigid deformation, the following constraint must hold [3,32]:*

[3]The matrix Kronecker product $\otimes$ is defined as [78]: $\mathbf{Y}\otimes\mathbf{Z}:\{\mathbb{R}^{m\times n},\mathbb{R}^{p\times q}\}\to\mathbb{R}^{mp\times nq}$, where $[\mathbf{Y}\otimes\mathbf{Z}]_{ij\,\text{block}}\in\mathbb{R}^{p\times q}=Y_{ij}\mathbf{Z}$.

[4]Self-intersection avoidance is an essential restriction in origami as stated in Definition 2.1. It remains an open problem to provide constraints on fold angles that would allow for three-dimensional folded configurations free of self-intersection [3,36]. This restriction is not considered in this work.

$$\mathbf{R}^j := \prod_{k=1}^{n_j} \mathbf{R}_1(\theta_{jk})\mathbf{R}_3(\alpha_{jk}) = \mathbf{I}_3 \tag{14}$$

It is shown in Appendix A that this constraint for origami with creased folds is a special case of the constraints for origami with smooth folds to be presented in Sec. 3.3.

COROLLARY 2.1.

(i) *If the jth interior vertex has a single incident creased fold, it allows for a valid configuration if* $\theta_{j1} = 0$.
(ii) *If the jth interior vertex has two incident creased folds, it allows for a valid configuration if (ii,1)* $\alpha_{j1} \neq \pi, \theta_{j1} = \theta_{j2} = 0$ *or (ii,2)* $\alpha_{j1} = \pi, \theta_{j1} = \theta_{j2}$.
(iii) *If the jth interior vertex has three incident creased folds, it allows for a valid configuration if (iii,1)* $\alpha_{j1} \neq \pi, \alpha_{j2} \neq \pi, \alpha_{j3} \neq \pi, \theta_{j1} = \theta_{j2} = \theta_{j3} = 0$, *or (iii,2)* $\alpha_{j1} = \pi, \theta_{j1} = \theta_{j2}, \theta_{j3} = 0$, *or (iii,3)* $\alpha_{j2} = \pi, \theta_{j2} = \theta_{j3}, \theta_{j1} = 0$, *or (iii,4)* $\alpha_{j3} = \pi, \theta_{j3} = \theta_{j1}, \theta_{j2} = 0$.

Proof. Case (*i*): The matrix $\mathbf{R}^j$ associated with an interior vertex having one incident creased fold is $\mathbf{R}^j = \mathbf{R}_1(\theta_{j1})\mathbf{R}_3(\alpha_{j1})$. The angle α_{j1} is equal to 2π for a single fold incident to an interior vertex, thus $\mathbf{R}_3(\alpha_{j1}) = \mathbf{I}_3$. This requires $\mathbf{R}_1(\theta_{j1}) = \mathbf{I}_3$ which in the domain $\theta_{j1} \in [-\pi, \pi]$ holds true only when $\theta_{j1} = 0$. Cases (*ii*) and (*iii*) can be verified in a similar manner. □

Thus, for nontrivial folding deformation, any interior vertex must have at least four incident creased folds. It can be shown that each face in the sheet undergoes a rigid deformation and no tearing occurs provided the constraint in Eq. (14) is satisfied for each interior vertex of the sheet (see Refs. [36,37,83] for details). Therefore, the constraints on the fold angles defining the constrained configuration space for a sheet with creased folds (excluding self-intersection avoidance) are then the following:

$$\mathbf{R}^j = \mathbf{I}_3 \qquad \forall j \in \{1, ..., N_{\mathcal{I}}\} \tag{15}$$

For the sake of brevity, the formulation of the map from the reference configuration to a valid current configuration, constructed using the set of the shape variables of all the folds in the sheet, is not included here for origami creased folds and can be found in Refs. [36,37]. It is reminded that the model for origami with creased folds reviewed in this section is a special case of the more general model for origami with smooth folds presented in Sec. 3. Thus, the map from reference to current configurations for origami with smooth folds provided in Sec. 3.4 covers such a map for origami with creased folds.

3 Origami With Smooth Folds

The model for origami presented in the preceding section is based on the assumption of creased folds. Such a simplification may not be appropriate for structures having folds of non-negligible thickness or constructed from materials that do not provide sufficient strain magnitudes to generate the high curvatures needed for a creased idealization. For such structures, the folded regions may not be accurately represented as creases but instead as *bent* sheet regions exhibiting higher-order geometric continuity (termed *smooth folds* in this work). A novel model for the kinematic response of origami structures having smooth folds is presented in this section.

The approach used to develop a model for origami with smooth folds follows that outlined at the beginning of Sec. 2. First, the *sheet* and the *shape variables* associated with the *smooth folds* in the sheet are described. The layout of the smooth folds in the sheet (i.e., the *fold pattern*) is determined by *vertices* (start-points and end-points of the smooth fold *centerlines* in a planar reference configuration), their connectivity, and the initial *width* of each smooth fold. Subsequently, *constraints* on the fold shape variables that define the constrained configuration space are derived. The *continuous motion* of the sheet represents a continuous path in such a constrained configuration space.

The studied continuum body is denoted as the *sheet* which is a three-dimensional, orientable, path-connected surface with boundary (same properties of a sheet in origami with creased folds, see Sec. 2). For origami with smooth folds, the sheet is divided into various surface subdomains denoted as *faces*, *smooth folds*, and *fold intersections*. Every surface subdomain comprising the sheet has the same aforementioned characteristics of the sheet (i.e., they are three-dimensional, orientable, path-connected surfaces with boundary). Following the notation of Sec. 2, the orthonormal vectors $\mathbf{e}_i \in \mathbb{R}^3$, $i = 1, 2, 3$, with $\mathbf{e}_3 := \mathbf{e}_1 \times \mathbf{e}_2$ form the basis $\{\mathbf{e}_1, \mathbf{e}_2, \mathbf{e}_3\}$ that defines the fixed global coordinate system.

The *reference configuration* of the sheet is denoted $\mathcal{S}_0$ and is defined such that it is contained in the plane spanned by $\mathbf{e}_1$ and $\mathbf{e}_2$ with its surface subdomains not overlapping each other, except at their shared boundary edges. The configuration of the $N_{\mathcal{P}}$ faces, $N_{\mathcal{F}}$ smooth folds, and $N_{\mathcal{I}}$ fold intersections subdomains in $\mathcal{S}_0$ is denoted $\mathcal{P}_0^i$, $i = 1, ..., N_{\mathcal{P}}$, $\mathcal{F}_0^i$, $i = 1, ..., N_{\mathcal{F}}$, and $\mathcal{I}_0^i$, $i = 1, ..., N_{\mathcal{I}}$, respectively. Therefore, $\mathcal{S}_0 = (\cup_{i=1}^{N_{\mathcal{P}}} \mathcal{P}_0^i) \cup (\cup_{i=1}^{N_{\mathcal{F}}} \mathcal{F}_0^i) \cup (\cup_{i=1}^{N_{\mathcal{I}}} \mathcal{I}_0^i)$. The side of $\mathcal{S}_0$ with normal $\mathbf{e}_3$ is selected as the positive side of the sheet. An example of a sheet with smooth folds in its reference configuration $\mathcal{S}_0$ is shown in Fig. 5(*a*).

A *current configuration* of the sheet is denoted $\mathcal{S}_t$ where t is a parameter that indicates the history of deformation from the reference configuration ($t = 0$) to a current configuration ($t > 0$). Refer to Fig. 5(*b*) for an example. The configuration of the $N_{\mathcal{P}}$ faces, $N_{\mathcal{F}}$ smooth folds, and $N_{\mathcal{I}}$ fold intersections comprising $\mathcal{S}_t$ is denoted $\mathcal{P}_t^i$, $i = 1, ..., N_{\mathcal{P}}$, $\mathcal{F}_t^i$, $i = 1, ..., N_{\mathcal{F}}$, and $\mathcal{I}_t^i$, $i = 1, ..., N_{\mathcal{I}}$, respectively. Thus, $\mathcal{S}_t = (\cup_{i=1}^{N_{\mathcal{P}}} \mathcal{P}_t^i) \cup (\cup_{i=1}^{N_{\mathcal{F}}} \mathcal{F}_t^i) \cup (\cup_{i=1}^{N_{\mathcal{I}}} \mathcal{I}_t^i)$. As stated in Sec. 1, the focus of this work is on rigid origami-based structures. As such, the following definition provides the characteristics of a *valid* current configuration for origami with smooth folds:

DEFINITION 3.1. *Valid configuration*: *A valid current configuration* $\mathcal{S}_t$ *has the following characteristics: (i) the faces undergo only rigid deformations, (ii) the sheet is not torn (initially joined*

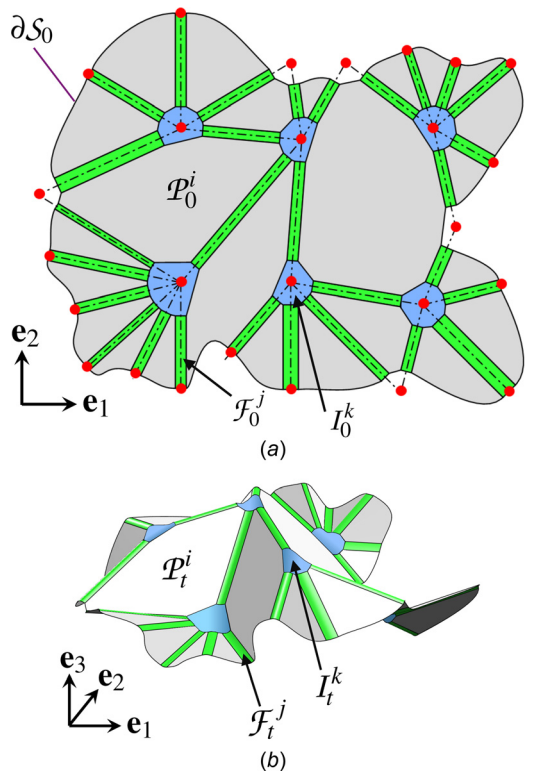

Fig. 5 Sheet with smooth folds in its reference configuration $\mathcal{S}_0$ (*a*) and a current configuration $\mathcal{S}_t$ (*b*)

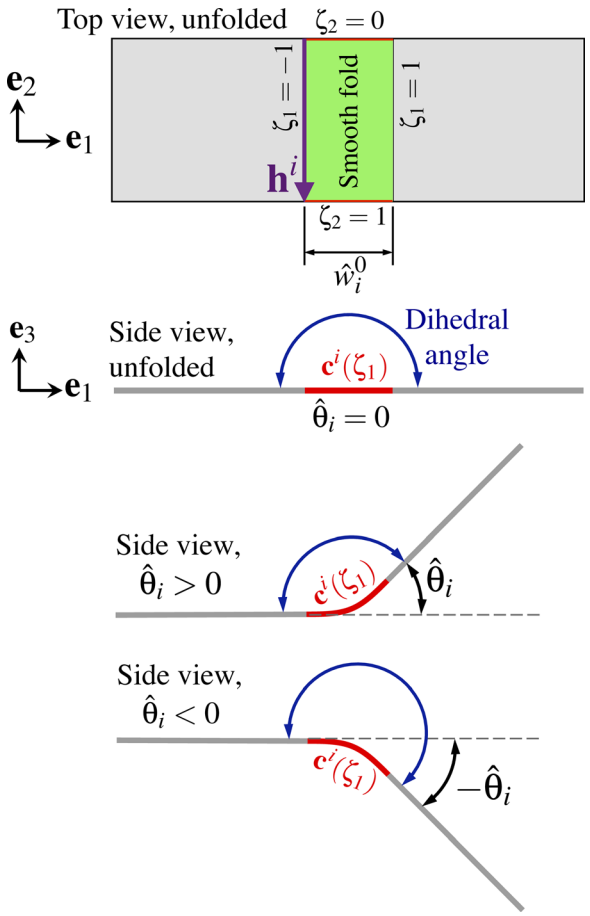

Fig. 6 Schematics showing unfolded and folded configurations of a smooth fold, cf. Fig. 3

surface subdomains of the sheet remain joined), and (iii) the sheet does not self-intersect.

The characteristics of a valid configuration provided in Definition 3.1 are the same as those of a valid configuration for a sheet with creased folds presented in Definition 2.1. However, it is noted that unlike a sheet with creased folds, a sheet with smooth folds is also comprised of other surface subdomains besides the faces (smooth folds and fold intersections) for which bending and stretching are permitted.

DEFINITION 3.2. *Smooth folds*: *The smooth folds are ruled surfaces*[5] *of the following form:*

$$\boldsymbol{\mathcal{F}}_t^i(\zeta_1, \zeta_2) = \mathbf{c}_t^i(\zeta_1) + \zeta_2 \mathbf{h}_t^i, \quad \frac{\mathrm{d}\mathbf{c}_t^i(\zeta_1)}{\mathrm{d}\zeta_1} \cdot \mathbf{h}_t^i = 0 \tag{16}$$

where $\boldsymbol{\mathcal{F}}_t^i(\zeta_1, \zeta_2) \in \mathbb{R}^3$ *is a parameterization of* $\mathcal{F}_t^i$. *Without loss of generality, the parameters* ζ_1 *and* ζ_2 *are contained in the intervals* $[-1, 1]$ *and* $[0, 1]$, *respectively.*

An example of a smooth fold is shown in Fig. 6. In Definition 3.2, $\mathbf{h}_t^i \in \mathbb{R}^3$ provides the direction of the rulings comprising $\mathcal{F}_t^i$ while $\mathbf{c}_t^i(\zeta_1) \in \mathbb{R}^3$ is the parametric ruled surface directrix curve that defines the cross section of $\mathcal{F}_t^i$. The curve parameterized by $\mathbf{c}_t^i(\zeta_1)$ is contained in a plane orthogonal to $\mathbf{h}_t^i$ as stated in Eq. (16). It is assumed that $\| \mathbf{h}_t^i \|$ is constant for all configurations. As a consequence, the only nonrigid deformations allowed for the smooth folds are achieved through continuous bending or stretching of its cross section defined by $\mathbf{c}_t^i(\zeta_1)$. To simplify the notation, the dependence of $\boldsymbol{\mathcal{F}}_t^i(\zeta_1, \zeta_2)$, $\mathbf{c}_t^i(\zeta_1)$, and $\mathbf{h}_t^i$ on t is left implicit for the remainder of the paper and these vectors are denoted as $\boldsymbol{\mathcal{F}}^i(\zeta_1, \zeta_2)$, $\mathbf{c}^i(\zeta_1)$, and $\mathbf{h}^i$, respectively.

The reference configuration of the smooth folds is simplified here to a rectangular shape and their deformation only includes stretching and bending of the fold cross section. However, the modeling framework proposed in this work can be extended for the consideration of folds having a trapezoidal reference configuration (that deform into conical sections) or folds that exhibit torsional deformation. Such extensions are recommended for future studies.

Remark 3.1. Deformation of a sheet with creased folds is the special limiting case of the more general deformation of a sheet with smooth folds. Specifically, creased folds are obtained when the curve parameterized by $\mathbf{c}^i(\zeta_1)$ is degenerated to a single point, thereby degenerating the smooth fold surface $\mathcal{F}_t^i$ to a single straight line segment.

Each smooth fold is joined to a face at each of its two boundary rulings (i.e., $\boldsymbol{\mathcal{F}}^i(-1, \zeta_2)$ and $\boldsymbol{\mathcal{F}}^i(1, \zeta_2)$, refer to Fig. 6). The remaining boundaries of $\mathcal{F}_t^i$ (i.e., $\boldsymbol{\mathcal{F}}^i(\zeta_1, 0)$ and $\boldsymbol{\mathcal{F}}^i(\zeta_1, 1)$) are either at the boundary of $\mathcal{S}_t$ or joined to a fold intersection. A parameterization for the fold intersections ($\mathcal{I}_t^i$, $i = 1, ..., N_{\mathcal{I}}$) is not provided here. It is noted, however, that the model proposed herein is independent of the parameterization of $\mathcal{I}_t^i$.

A nonrigid body deformation of the sheet is achieved by rotating pairs of faces joined to smooth folds relative to one another in such a manner that the sheet only attains valid configurations during such a deformation. One of the *shape variables* associated with a smooth fold describes the relative rotation between the two faces joined by such a fold and is denoted as *fold angle*.

DEFINITION 3.3. *Fold angle*: *The fold angle* $\hat{\theta}_i(t)$ *is defined as* π *minus the dihedral angle between the positive sides of the two faces joined to the ith smooth fold.*

The dependence of the fold angles on t is left implicit for the remainder of the paper. The vector $\hat{\boldsymbol{\theta}} \in \mathbb{R}^{N_{\mathcal{F}}}$ was constructed by collecting the fold angles $\hat{\theta}_i$, $i = 1, ..., N_{\mathcal{F}}$, and is defined in Eq. (1). Schematics showing the concept of fold angle for smooth folds are provided in Fig. 6.

3.1 Geometry of Smooth Folds. This section presents the detailed geometrical description of smooth folds. The conditions required for various orders of geometric continuity and particular formulations for $\mathbf{c}^i(\zeta_1)$ are also provided.

The distance between the two end-points of $\mathbf{c}^i(\zeta_1)$ with position vectors $\mathbf{c}^i(-1)$ and $\mathbf{c}^i(1)$ in any configuration is denoted $\hat{w}_i$

$$\hat{w}_i := \| \mathbf{c}^i(1) - \mathbf{c}^i(-1) \| \tag{17}$$

A schematic of a smooth fold cross section showing $\hat{w}_i$ is provided in Fig. 7. The vector $\hat{\boldsymbol{w}} \in \mathbb{R}^{N_{\mathcal{F}}}$ is constructed by collecting the variables $\hat{w}_i$ as follows:

$$\hat{\boldsymbol{w}} = [\, \hat{w}_1 \quad \cdots \quad \hat{w}_{N_{\mathcal{F}}} \,]^\top \tag{18}$$

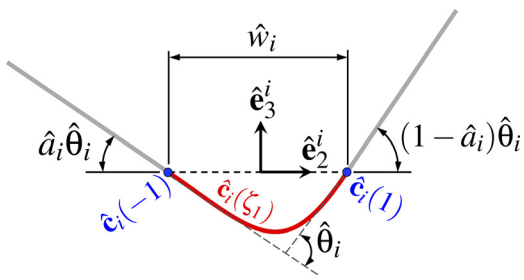

Fig. 7 Cross section of a smooth fold. The fold shape variables and the fold-attached coordinate system are shown.

[5]A ruled surface is formed by the union of straight lines, called the rulings or generators of the surface [79].

The *fold width* $\hat{w}_i^0$ is the value of $\hat{w}_i$ at $t=0$. The vector $\hat{\boldsymbol{w}}^0 \in \mathbb{R}^{N_\mathcal{F}}$ is constructed as follows:

$$\hat{\boldsymbol{w}}^0 = \begin{bmatrix} \hat{w}_1^0 & \cdots & \hat{w}_{N_\mathcal{F}}^0 \end{bmatrix}^\top \tag{19}$$

The fold-attached orthonormal vectors $\hat{\mathbf{e}}_j^i \in \mathbb{R}^3$, $i = 1, ..., N_\mathcal{F}$, $j = 1, 2, 3$, with $\hat{\mathbf{e}}_3^i := \hat{\mathbf{e}}_1^i \times \hat{\mathbf{e}}_2^i$ form the bases $\{\hat{\mathbf{e}}_1^i, \hat{\mathbf{e}}_2^i, \hat{\mathbf{e}}_3^i\}$ that define the local *fold coordinate system* of each smooth fold $\mathcal{F}_t^i$. The origin of this coordinate system is located at $(1/2)(\mathbf{c}^i(-1) + \mathbf{c}^i(1))$. The director vector $\mathbf{h}^i$ is aligned to $\hat{\mathbf{e}}_1^i$ (i.e., $\mathbf{h}^i \cdot \hat{\mathbf{e}}_1^i = \| \mathbf{h}^i \|$) and $(\mathbf{c}^i(1) - \mathbf{c}^i(-1)) \in \text{span}(\hat{\mathbf{e}}_2^i)$.

The face adjacent to a smooth fold at the boundary $\boldsymbol{\mathcal{F}}^i(-1, \zeta_2)$ makes an angle of $\hat{a}_i\hat{\theta}_i$ with $-\hat{\mathbf{e}}_2^i$ in the plane spanned by $\hat{\mathbf{e}}_2^i$ and $\hat{\mathbf{e}}_3^i$, and the face adjacent to a smooth fold at the boundary $\boldsymbol{\mathcal{F}}^i(1, \zeta_2)$ makes an angle of $(1 - \hat{a}_i)\hat{\theta}_i$ with $\hat{\mathbf{e}}_2^i$ in such a plane. This is shown schematically in Fig. 7. The vector $\hat{\boldsymbol{a}} \in \mathbb{R}^{N_\mathcal{F}}$ is constructed by collecting the variables $\hat{a}_i$ as follows:

$$\hat{\boldsymbol{a}} = \begin{bmatrix} \hat{a}_1 & \cdots & \hat{a}_{N_\mathcal{F}} \end{bmatrix}^\top \tag{20}$$

Let $\hat{\mathbf{c}}^i(\zeta_1)$ be the parametric curve $\mathbf{c}^i(\zeta_1)$ expressed in the fold coordinate system of $\mathcal{F}_t^i$

$$\hat{\mathbf{c}}^i(\zeta_1) = \begin{bmatrix} \hat{\mathbf{e}}_1^i & \hat{\mathbf{e}}_2^i & \hat{\mathbf{e}}_3^i \end{bmatrix}^\top \left[\mathbf{c}^i(\zeta_1) - \frac{1}{2}\left(\mathbf{c}^i(-1) + \mathbf{c}^i(1)\right) \right] \tag{21}$$

If $\hat{\mathbf{c}}^i(\zeta_1)$ is at least first-order differentiable for $\zeta_1 \in [-1, 1]$, the total arc length of the fold cross section, denoted s_i^{tot}, is determined as follows:

$$s_i^{\text{tot}} = \int_{-1}^{1} \left\| \frac{\mathrm{d}\hat{\mathbf{c}}^i(\zeta_1)}{\mathrm{d}\zeta_1} \right\| \mathrm{d}\zeta_1 \tag{22}$$

and the arc length $s_i(\zeta_1)$ measured from $\zeta_1 = -1$ to any value of $\zeta_1 \in [-1, 1]$ is determined as follows:

$$s_i(\zeta_1) = \int_{-1}^{\zeta_1} \left\| \frac{\mathrm{d}\hat{\mathbf{c}}^i(\zeta)}{\mathrm{d}\zeta} \right\| \mathrm{d}\zeta \tag{23}$$

The tangent direction of the parametric curve $\hat{\mathbf{c}}^i(\zeta_1)$ is determined by the unit tangent vector $\mathbf{t}^i(\zeta_1) \in \text{span}(\hat{\mathbf{e}}_2^i, \hat{\mathbf{e}}_3^i)$ and is defined at the points where $\hat{\mathbf{c}}^i(\zeta_1)$ is at least first-order differentiable

$$\mathbf{t}^i(\zeta_1) = \frac{\mathrm{d}\hat{\mathbf{c}}^i(\zeta_1)}{\mathrm{d}\zeta_1} \Bigg/ \left\| \frac{\mathrm{d}\hat{\mathbf{c}}^i(\zeta_1)}{\mathrm{d}\zeta_1} \right\| \tag{24}$$

The curvature $\kappa_i(\zeta_1)$ is defined at the points where $\hat{\mathbf{c}}_i(\zeta_1)$ is at least second-order differentiable

$$\kappa_i(\zeta_1) = \left\| \frac{\mathrm{d}\hat{\mathbf{c}}_i(\zeta_1)}{\mathrm{d}\zeta_1} \times \frac{\mathrm{d}^2\hat{\mathbf{c}}_i(\zeta_1)}{\mathrm{d}\zeta_1^2} \right\| \Bigg/ \left\| \frac{\mathrm{d}\hat{\mathbf{c}}_i(\zeta_1)}{\mathrm{d}\zeta_1} \right\|^3 \tag{25}$$

and the signed curvature is given as follows:[6]

$$\kappa_i^s(\zeta_1) = \kappa_i(\zeta_1)\, \text{sgn}\left(\left(\frac{\mathrm{d}\hat{\mathbf{c}}^i(\zeta_1)}{\mathrm{d}\zeta_1} \times \frac{\mathrm{d}^2\hat{\mathbf{c}}^i(\zeta_1)}{\mathrm{d}\zeta_1^2} \right) \cdot \hat{\mathbf{e}}_1^i \right) \tag{26}$$

The order of geometric continuity of $\mathcal{S}_t$ at the interior rulings of $\mathcal{F}_t^i$ is determined by the order of geometric continuity of $\hat{\mathbf{c}}^i(\zeta_1)$, $\zeta_1 \in (-1, 1)$, while that at the joints with the planar faces adjacent to $\mathcal{F}_t^i$ depends on the particular values of $\hat{\mathbf{c}}_i(\zeta_1)$ and its derivatives at $\zeta_1 = \pm 1$. For instance, G^0 continuous joints with the faces adjacent to $\mathcal{F}_t^i$ require the following conditions on $\hat{\mathbf{c}}^i(\zeta_1)$ at $\zeta_1 = \pm 1$ (refer to Fig. 7):

$$\hat{\mathbf{c}}^i(-1) = \begin{bmatrix} 0 \\ -\frac{\hat{w}_i}{2} \\ 0 \end{bmatrix} =: \hat{\mathbf{c}}_{L_0}^i, \qquad \hat{\mathbf{c}}^i(1) = \begin{bmatrix} 0 \\ \frac{\hat{w}_i}{2} \\ 0 \end{bmatrix} =: \hat{\mathbf{c}}_{R_0}^i \tag{27}$$

Continuity of the unit tangent vector $\mathbf{t}^i(\zeta_1)$ at $\zeta_1 = \pm 1$ is required for G^1 continuous joints with the planar faces adjacent to $\mathcal{F}_t^i$ in addition to G^0 continuity [84,85]. The following values of $\mathbf{t}^i(\zeta_1)$ at $\zeta_1 = \pm 1$ are then required for G^1 continuity in addition to those conditions of Eq. (27):

$$\mathbf{t}^i(-1) = \begin{bmatrix} 0 \\ \cos(\hat{a}_i\hat{\theta}_i) \\ -\sin(\hat{a}_i\hat{\theta}_i) \end{bmatrix}, \qquad \mathbf{t}^i(1) = \begin{bmatrix} 0 \\ \cos((1-\hat{a}_i)\hat{\theta}_i) \\ \sin((1-\hat{a}_i)\hat{\theta}_i) \end{bmatrix} \tag{28}$$

Therefore, the following conditions on the first derivatives of $\hat{\mathbf{c}}^i(\zeta_1)$ at $\zeta_1 = \pm 1$ are required for G^1 continuity at the joints with the planar faces adjacent to $\mathcal{F}_t^i$:

$$\begin{aligned} \left.\frac{\mathrm{d}\hat{\mathbf{c}}^i(\zeta_1)}{\mathrm{d}\zeta_1}\right|_{\zeta_1=-1} &= \beta_{L_1}^i \begin{bmatrix} 0 \\ \cos(\hat{a}_i\hat{\theta}_i) \\ -\sin(\hat{a}_i\hat{\theta}_i) \end{bmatrix} =: \hat{\mathbf{c}}_{L_1}^i \\ \left.\frac{\mathrm{d}\hat{\mathbf{c}}^i(\zeta_1)}{\mathrm{d}\zeta_1}\right|_{\zeta_1=1} &= \beta_{R_1}^i \begin{bmatrix} 0 \\ \cos\left((1-\hat{a}_i)\hat{\theta}_i\right) \\ \sin\left((1-\hat{a}_i)\hat{\theta}_i\right) \end{bmatrix} =: \hat{\mathbf{c}}_{R_1}^i \end{aligned} \tag{29}$$

where $\beta_{L_1}^i, \beta_{R_1}^i \in \mathbb{R}_{>0}$.

Continuity of the curvature vector (or the signed curvature) is required for G^2 continuity [85] in addition to G^1 continuity. This requires the curvature of $\hat{\mathbf{c}}^i(\zeta_1)$ at $\zeta_1 = \pm 1$ to be zero since $\mathcal{F}_t^i$ is connected to planar faces at its boundary rulings. Zero curvature at the boundary rulings of $\mathcal{F}_t^i$ requires the following according to Eq. (25):

$$\begin{aligned} \left(\frac{\mathrm{d}\hat{\mathbf{c}}^i(\zeta_1)}{\mathrm{d}\zeta_1} \times \frac{\mathrm{d}^2\hat{\mathbf{c}}^i(\zeta_1)}{\mathrm{d}\zeta_1^2} \right)\Bigg|_{\zeta_1=-1} &= \mathbf{0}_3 \\ \left(\frac{\mathrm{d}\hat{\mathbf{c}}^i(\zeta_1)}{\mathrm{d}\zeta_1} \times \frac{\mathrm{d}^2\hat{\mathbf{c}}^i(\zeta_1)}{\mathrm{d}\zeta_1^2} \right)\Bigg|_{\zeta_1=1} &= \mathbf{0}_3 \end{aligned} \tag{30}$$

where $\mathbf{0}_n$ is the zero vector in $\mathbb{R}^n$. Considering Eqs. (29) and (30), the following conditions on the second derivatives of $\hat{\mathbf{c}}^i(\zeta_1)$ are needed in addition to the conditions provided in Eqs. (27) and (29) for G^2 continuity at the joints with the planar faces adjacent to $\mathcal{F}_t^i$:

$$\begin{aligned} \frac{\mathrm{d}^2\hat{\mathbf{c}}^i(\zeta_1)}{\mathrm{d}\zeta_1^2}|_{\zeta_1=-1} &= \beta_{L_2}^i \begin{bmatrix} 0 \\ \cos(\hat{a}_i\hat{\theta}_i) \\ -\sin(\hat{a}_i\hat{\theta}_i) \end{bmatrix} =: \hat{\mathbf{c}}_{L_2}^i \\ \frac{\mathrm{d}^2\hat{\mathbf{c}}^i(\zeta_1)}{\mathrm{d}\zeta_1^2}|_{\zeta_1=1} &= \beta_{R_2}^i \begin{bmatrix} 0 \\ -\cos\left((1-\hat{a}_i)\hat{\theta}_i\right) \\ -\sin\left((1-\hat{a}_i)\hat{\theta}_i\right) \end{bmatrix} =: \hat{\mathbf{c}}_{R_2}^i \end{aligned} \tag{31}$$

where $\beta_{L_2}^i, \beta_{R_2}^i \in \mathbb{R}$. Conditions on higher-order derivatives of $\hat{\mathbf{c}}^i(\zeta_1)$ required for higher-order geometric continuity can be provided in a similar manner [84,85].

[6]The sign function is defined as follows: $\text{sgn}(y) := \begin{cases} -1; & y < 0 \\ 1; & y > 0 \\ 0; & y = 0 \end{cases}$.

3.1.1 Fold Shape Examples. Polynomials of the minimum order required to satisfy the previous conditions for continuity of $\hat{\mathbf{c}}^i(\zeta_1)$ and its derivatives at $\zeta_1 = \pm 1$ are used to define this parametric curve. Hermite interpolation polynomials [86] are used to represent $\hat{\mathbf{c}}^i(\zeta_1)$ in this work. Alternative representations (e.g., Bezier curves) are also applicable as long as they satisfy the conditions required for the considered order of geometric continuity. For G^1 continuity at the boundary rulings of $\mathcal{F}_t^i$, $\hat{\mathbf{c}}^i(\zeta_1)$ is expressed as follows:

$$\hat{\mathbf{c}}^i(\zeta_1) = h_{30}(\zeta_1)\hat{\mathbf{c}}^i_{L_0} + h_{31}(\zeta_1)\hat{\mathbf{c}}^i_{R_0} + h_{32}(\zeta_1)\hat{\mathbf{c}}^i_{L_1} + h_{33}(\zeta_1)\hat{\mathbf{c}}^i_{R_1} \quad (32)$$

where the utilized cubic Hermite interpolation polynomials $h_{3i}(\zeta)$, $i = 0, ..., 3$, are given as follows:

$$\begin{aligned} h_{30}(\zeta) &= \frac{1}{4}\zeta^3 - \frac{3}{4}\zeta + \frac{1}{2} \\ h_{31}(\zeta) &= -\frac{1}{4}\zeta^3 + \frac{3}{4}\zeta + \frac{1}{2} \\ h_{32}(\zeta) &= \frac{1}{4}\zeta^3 - \frac{1}{4}\zeta^2 - \frac{1}{4}\zeta + \frac{1}{4} \\ h_{33}(\zeta) &= \frac{1}{4}\zeta^3 + \frac{1}{4}\zeta^2 - \frac{1}{4}\zeta - \frac{1}{4} \end{aligned} \quad (33)$$

For G^2 continuity at the boundary rulings of $\mathcal{F}_t^i$, $\hat{\mathbf{c}}^i(\zeta_1)$ is expressed as follows:

$$\begin{aligned} \hat{\mathbf{c}}^i(\zeta_1) = {} & h_{50}(\zeta_1)\hat{\mathbf{c}}^i_{L_0} + h_{51}(\zeta_1)\hat{\mathbf{c}}^i_{R_0} + h_{52}(\zeta_1)\hat{\mathbf{c}}^i_{L_1} \\ & + h_{53}(\zeta_1)\hat{\mathbf{c}}^i_{R_1} + h_{54}(\zeta_1)\hat{\mathbf{c}}^i_{L_2} + h_{55}(\zeta_1)\hat{\mathbf{c}}^i_{R_2} \end{aligned} \quad (34)$$

where the utilized quintic Hermite interpolation polynomials $h_{5i}(\zeta)$, $i = 0, ..., 5$, are given as follows:

$$\begin{aligned} h_{50}(\zeta) &= -\frac{3}{16}\zeta^5 + \frac{5}{8}\zeta^3 - \frac{15}{16}\zeta + \frac{1}{2} \\ h_{51}(\zeta) &= \frac{3}{16}\zeta^5 - \frac{5}{8}\zeta^3 + \frac{15}{16}\zeta + \frac{1}{2} \\ h_{52}(\zeta) &= -\frac{3}{16}\zeta^5 + \frac{1}{16}\zeta^4 + \frac{5}{8}\zeta^3 - \frac{3}{8}\zeta^2 - \frac{7}{16}\zeta + \frac{5}{16} \\ h_{53}(\zeta) &= -\frac{3}{16}\zeta^5 - \frac{1}{16}\zeta^4 + \frac{5}{8}\zeta^3 + \frac{3}{8}\zeta^2 - \frac{7}{16}\zeta - \frac{5}{16} \\ h_{54}(\zeta) &= -\frac{1}{16}\zeta^5 + \frac{1}{16}\zeta^4 + \frac{1}{8}\zeta^3 - \frac{1}{8}\zeta^2 - \frac{1}{16}\zeta + \frac{1}{16} \\ h_{55}(\zeta) &= \frac{1}{16}\zeta^5 + \frac{1}{16}\zeta^4 - \frac{1}{8}\zeta^3 - \frac{1}{8}\zeta^2 + \frac{1}{16}\zeta + \frac{1}{16} \end{aligned} \quad (35)$$

3.2 Fold Pattern. The layout of the smooth folds in $\mathcal{S}_0$ is presented in a fold pattern. To describe the fold pattern, the *vertices* are first introduced.

DEFINITION 3.4. *Vertices*: *The vertices are the start-points and end-points of the line segments coincident with the centerlines of the smooth folds in* $\mathcal{S}_0$. *Each vertex has an associated position vector denoted* $\mathbf{v}^j \in \text{span}(\mathbf{e}_1, \mathbf{e}_2)$.

As in Sec. 2.1, the number of vertices located at the interior of $\mathcal{S}_0$ is denoted $N_\mathcal{I}$, and the number of vertices located at $\partial\mathcal{S}_0$ or outside $\mathcal{S}_0$ is denoted $N_\mathcal{B}$. The vertices are enumerated starting from those located at the interior of $\mathcal{S}_0$ (with corresponding position vectors $\mathbf{v}^1, ..., \mathbf{v}^{N_\mathcal{I}}$) followed by those at the located at $\partial\mathcal{S}_0$ or outside $\mathcal{S}_0$ (with corresponding position vectors $\mathbf{v}^{N_\mathcal{I}+1}, ..., \mathbf{v}^{N_\mathcal{I}+N_\mathcal{B}}$). The vertices in origami with smooth folds are used only to indicate end-points of the fold centerlines in $\mathcal{S}_0$. The points of the sheet coincident with the vertices in $\mathcal{S}_0$ do not occupy any especial location in $\mathcal{S}_t$, $t > 0$. This is in contrast to origami with creased folds where the points of the sheet coincident with the vertices in $\mathcal{S}_0$, which correspond to fold line end-points, and also correspond to fold line end-points in $\mathcal{S}_t$, $t > 0$ (see Sec. 2).

Following Sec. 2.1, the vector $\mathbf{V} \in \mathbb{R}^{3(N_\mathcal{I}+N_\mathcal{B})}$ formed by concatenating the vertex position vectors is provided in Eq. (2). The definition of the matrix $\hat{\mathbf{C}} \in \{-1, 0, 1\}^{N_\mathcal{F} \times (N_\mathcal{I}+N_\mathcal{B})}$ that identifies which vertices are the start-points and end-points of the fold centerlines follows that provided in Eq. (3). Let $\hat{\mathbf{v}}^{i1}, \hat{\mathbf{v}}^{i2} \in \text{span}(\mathbf{e}_1, \mathbf{e}_2)$, $i = 1, ..., N_\mathcal{F}$, be the position vectors of the vertices from which each fold centerline emanates and ends, respectively. The vectors $\hat{\mathbf{V}}^1, \hat{\mathbf{V}}^2 \in \mathbb{R}^{3N_\mathcal{F}}$ are constructed by concatenating the vectors $\hat{\mathbf{v}}^{i1}$, $\hat{\mathbf{v}}^{i2}$, $i = 1, ..., N_\mathcal{F}$, as follows:

$$\hat{\mathbf{V}}^1 = \begin{bmatrix} \hat{\mathbf{v}}^{11} \\ \vdots \\ \hat{\mathbf{v}}^{N_\mathcal{F}1} \end{bmatrix}, \qquad \hat{\mathbf{V}}^2 = \begin{bmatrix} \hat{\mathbf{v}}^{12} \\ \vdots \\ \hat{\mathbf{v}}^{N_\mathcal{F}2} \end{bmatrix} \quad (36)$$

The mappings from the collection of all the vertex position vectors $\mathbf{V}$ to those corresponding to the position vectors of the start-points and end-points of the fold centerlines ($\hat{\mathbf{V}}^1$ and $\hat{\mathbf{V}}^2$, respectively) are given as follows:

$$\begin{aligned} \hat{\mathbf{V}}^1 &= \left(\frac{1}{2}\left(|\hat{\mathbf{C}}|_* - \hat{\mathbf{C}}\right) \otimes \mathbf{I}_3\right)\mathbf{V} \\ \hat{\mathbf{V}}^2 &= \left(\frac{1}{2}\left(|\hat{\mathbf{C}}|_* + \hat{\mathbf{C}}\right) \otimes \mathbf{I}_3\right)\mathbf{V} \end{aligned} \quad (37)$$

The four corner points of $\mathcal{F}_0^i$ having associated position vectors $\hat{\mathbf{p}}_1^i, \hat{\mathbf{p}}_2^i, \hat{\mathbf{p}}_3^i, \hat{\mathbf{p}}_4^i \in \text{span}(\mathbf{e}_1, \mathbf{e}_2)$, $i = 1, ..., N_\mathcal{F}$, are then determined as follows:

$$\begin{aligned} \hat{\mathbf{p}}_1^i &= \hat{\mathbf{v}}^{i1} - \frac{\hat{w}_i^0}{2}\left(\mathbf{e}_3 \times \frac{\hat{\mathbf{v}}^{i2} - \hat{\mathbf{v}}^{i1}}{\| \hat{\mathbf{v}}^{i2} - \hat{\mathbf{v}}^{i1} \|}\right) + \hat{r}_1^i \frac{\hat{\mathbf{v}}^{i2} - \hat{\mathbf{v}}^{i1}}{\| \hat{\mathbf{v}}^{i2} - \hat{\mathbf{v}}^{i1} \|} \\ \hat{\mathbf{p}}_2^i &= \hat{\mathbf{v}}^{i2} - \frac{\hat{w}_i^0}{2}\left(\mathbf{e}_3 \times \frac{\hat{\mathbf{v}}^{i2} - \hat{\mathbf{v}}^{i1}}{\| \hat{\mathbf{v}}^{i2} - \hat{\mathbf{v}}^{i1} \|}\right) - \hat{r}_2^i \frac{\hat{\mathbf{v}}^{i2} - \hat{\mathbf{v}}^{i1}}{\| \hat{\mathbf{v}}^{i2} - \hat{\mathbf{v}}^{i1} \|} \\ \hat{\mathbf{p}}_3^i &= \hat{\mathbf{v}}^{i2} + \frac{\hat{w}_i^0}{2}\left(\mathbf{e}_3 \times \frac{\hat{\mathbf{v}}^{i2} - \hat{\mathbf{v}}^{i1}}{\| \hat{\mathbf{v}}^{i2} - \hat{\mathbf{v}}^{i1} \|}\right) - \hat{r}_2^i \frac{\hat{\mathbf{v}}^{i2} - \hat{\mathbf{v}}^{i1}}{\| \hat{\mathbf{v}}^{i2} - \hat{\mathbf{v}}^{i1} \|} \\ \hat{\mathbf{p}}_4^i &= \hat{\mathbf{v}}^{i1} + \frac{\hat{w}_i^0}{2}\left(\mathbf{e}_3 \times \frac{\hat{\mathbf{v}}^{i2} - \hat{\mathbf{v}}^{i1}}{\| \hat{\mathbf{v}}^{i2} - \hat{\mathbf{v}}^{i1} \|}\right) + \hat{r}_1^i \frac{\hat{\mathbf{v}}^{i2} - \hat{\mathbf{v}}^{i1}}{\| \hat{\mathbf{v}}^{i2} - \hat{\mathbf{v}}^{i1} \|} \end{aligned} \quad (38)$$

where $\hat{r}_1^i, \hat{r}_2^i \in \mathbb{R}$ and the resulting fold length orthogonal to the width direction must be positive

$$\| \hat{\mathbf{v}}^{i2} - \hat{\mathbf{v}}^{i1} \| - \hat{r}_1^i - \hat{r}_2^i > 0 \qquad \forall i \in \{1, ..., N_\mathcal{F}\} \quad (39)$$

The geometric parameters that define the corner points of $\mathcal{F}_0^i$ are shown in Fig. 8.

The vectors $\hat{\mathbf{P}}^j \in \mathbb{R}^{3N_\mathcal{F}}$, $j = 1, ..., 4$, are constructed by concatenating the vectors $\hat{\mathbf{p}}_j^i$, $i = 1, ..., N_\mathcal{F}$, as follows:

$$\hat{\mathbf{P}}^j = \begin{bmatrix} \hat{\mathbf{p}}_j^1 \\ \vdots \\ \hat{\mathbf{p}}_j^{N_\mathcal{F}} \end{bmatrix} \quad (40)$$

As in Sec. 2.1, let n_j, $j = 1, ..., N_\mathcal{I}$, be the number of fold centerlines incident to each interior vertex (i.e., those vertices located at the interior of $\mathcal{S}_0$). Also, let $\mathbf{m}^{jk} \in \text{span}(\mathbf{e}_1, \mathbf{e}_2)$, $j = 1, ..., N_\mathcal{I}$, $k = 1, ..., n_j$, be the vector along the length of the kth fold centerline incident to the jth interior vertex that emanates from this vertex. The vectors $\mathbf{m}^{jk}$, $k = 1, ..., n_j$, have a counterclockwise ordering, i.e., $\varphi(\mathbf{m}^{j1}) < \varphi(\mathbf{m}^{j1}) < \cdots < \varphi(\mathbf{m}^{jn_j})$ $\forall j \in \{1, ..., N_\mathcal{I}\}$, where $\varphi(\cdot)$ is defined in Eq. (4).

The mapping from the vertex position vectors $\mathbf{v}^j$, $j = 1, ..., N_\mathcal{I} + N_\mathcal{B}$, to the vectors $\mathbf{m}^{jk}$, $k = 1, ..., n_j$, is provided in Eq. (7). The angles between adjacent fold centerlines intersecting at a common interior vertex α_{jk}, $j = 1, ..., N_\mathcal{I}$, $k = 1, ..., n_j$, are

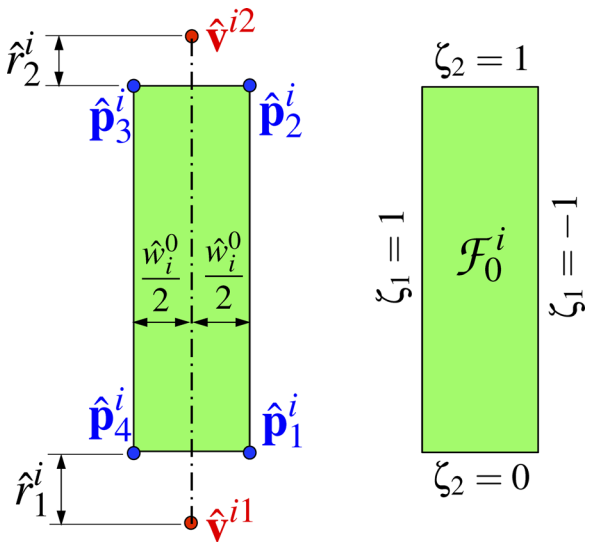

Fig. 8 Geometric parameters defining $\mathcal{F}_0^i$

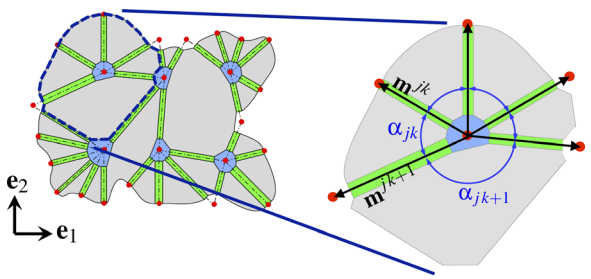

Fig. 9 Schematic showing faces and smooth folds adjacent to an interior fold intersection and associated geometric parameters

calculated using Eq. (8). A schematic showing the vectors $\mathbf{m}^{jk}$ and the angles α_{jk} is provided in Fig. 9.

3.3 Constraints. As in conventional origami with creased folds [36,37], constraints are required for origami with smooth folds to ensure that every current configuration $\mathcal{S}_t$ is valid[7] (according to Definition 3.1).

The angles α_{jk}, $k = 1, ..., n_j$, satisfy the following constraint since they are defined in $\mathcal{S}_0$:

$$K_j := 2\pi - \sum_{k=1}^{n_j} \alpha_{jk} = 0 \qquad \forall j \in \{1, ..., N_{\mathcal{I}}\} \tag{41}$$

Since the faces undergo only rigid deformations, the angles α_{jk} are constant during the deformation history of the sheet, i.e., independent of t, and therefore, Eq. (41) holds at every configuration $\mathcal{S}_t$. Equation (41) represents the developability constraint for origami with creased folds (see Eq. (9)). However, pointwise isometric deformation is relaxed here for origami with smooth folds since stretching is permitted within the subdomains $\mathcal{F}_t^i$ and $\mathcal{I}_t^i$, and thus, only $\mathcal{S}_0$ is in general pointwise developable. It is remarked that isometry is assumed for the smooth folds $\mathcal{F}_t^i$ in the direction of $\mathbf{h}^i$ (see Fig. 6). However, the arc length of the curve parameterized by $\hat{\mathbf{c}}^i(\zeta_1)$ may change in general during deformation, and thus, stretching of the smooth folds in such a direction may be allowed. Refer to Definition 3.2 and its subsequent discussion.

The variables describing the deformation associated with the folding of the smooth folds are constrained such that every configuration $\mathcal{S}_t$ is valid. These variables correspond to the fold angle $\hat{\theta}_i$, the distance $\hat{w}_i$ between the end-points of the cross section parametric curve $\hat{\mathbf{c}}^i(\zeta_1)$, and $\hat{a}_i$, $i = 1, ..., N_{\mathcal{F}}$ (refer to Sec. 3.1). Following Sec. 2.2, a new set of constraints for the variables associated with the smooth folds adjacent to each interior fold intersection are now proposed.

The variables θ_{jk}, w_{jk}, and a_{jk} are those associated with the kth smooth fold adjacent to $\mathcal{I}_0^j$. The vectors $\boldsymbol{\theta}^j \in \mathbb{R}^{n_j}$, $j = 1, ..., N_{\mathcal{I}}$, constructed by collecting the fold angles θ_{jk}, $k = 1, ..., n_j$, are defined in Eq. (10). The vectors $\boldsymbol{w}^j$, $\boldsymbol{a}^j \in \mathbb{R}^{n_j}$, $j = 1, ..., N_{\mathcal{I}}$, are constructed by collecting the variables w_{jk} and a_{jk}, $k = 1, ..., n_j$, and are defined as follows:

$$\boldsymbol{w}^j = [\, w_{j1} \quad \cdots \quad w_{jn_j} \,]^\top, \qquad \boldsymbol{a}^j = [\, a_{j1} \quad \cdots \quad a_{jn_j} \,]^\top \tag{42}$$

The mapping from the vector $\hat{\boldsymbol{\theta}}$ with elements corresponding to the fold angles of the sheet to each vector $\boldsymbol{\theta}^j$ with elements corresponding to the fold angles of the smooth folds adjacent to $\mathcal{I}_0^j$ is provided in Eq. (11). The mapping from the vector $\hat{\boldsymbol{w}}$, defined in Eq. (18), to each vector $\boldsymbol{w}^j$ is the following:

$$\boldsymbol{w}^j = |\mathbf{C}^j|_* \, \hat{\boldsymbol{w}} \tag{43}$$

where the definition of the matrix $\mathbf{C}^j$ in Eq. (6) holds in the context of connectivity of fold centerlines. Taking into account the orientation of the adjacent smooth folds with respect to the considered fold intersection $\mathcal{I}_0^j$ (i.e., whether the interior vertex associated with $\mathcal{I}_0^j$ is the start-point or the end-point of the adjacent smooth fold centerline), the mapping from the vector $\hat{\boldsymbol{a}}$, defined in Eq. (20), to each vector $\boldsymbol{a}^j$ is as follows:

$$\boldsymbol{a}^j = [\, \mathbf{C}^j \quad {}^A\mathbf{C}^j \,] \begin{bmatrix} \hat{\boldsymbol{a}} \\ 1 \end{bmatrix} \tag{44}$$

where ${}^A\mathbf{C}^j \in \mathbb{R}^{n_j}$ is a vector with elements ${}^AC_k^j$ that are determined as follows:

$${}^AC_k^j = \frac{1}{2}\left(1 - \sum_{i=1}^{N_{\mathcal{F}}} C_{ki}^j\right) \tag{45}$$

Note that if the vector $\mathbf{m}^{jk}$ is coincident with and has the *same* orientation as the ith fold centerline, then $a_{jk} = \hat{a}_i$. Conversely, if the vector $\mathbf{m}^{jk}$ is coincident with and has the *opposite* orientation as the ith fold centerline, then $a_{jk} = 1 - \hat{a}_i$. This is obtained from the mapping provided in Eq. (44).

The fold widths associated with the smooth folds adjacent to $\mathcal{I}_0^j$ are denoted w_{jk}^0, $k = 1, ..., n_j$, and are required in the subsequent derivations. Let $\boldsymbol{w}^{0,j} \in \mathbb{R}^{n_j}$ be the vector constructed by collecting the fold widths w_{jk}^0, $k = 1, ..., n_j$. Such a vector and its mapping from $\hat{\boldsymbol{w}}^0$ (defined in Eq. (19)) are as follows:

$$\boldsymbol{w}^{0,j} = [\, w_{j1}^0 \quad \cdots \quad w_{jn_j}^0 \,]^\top = |\mathbf{C}^j|_* \, \hat{\boldsymbol{w}}^0 \tag{46}$$

Let $\boldsymbol{\gamma}_j(\eta) : [0, 1] \to \mathcal{S}_0$ be any simple closed path (i.e., $\boldsymbol{\gamma}_j(0) = \boldsymbol{\gamma}_j(1)$) enclosing $\mathcal{I}_0^j$ and crossing each smooth fold adjacent to $\mathcal{I}_0^j$ once. An example of a path $\boldsymbol{\gamma}_j(\eta)$ is shown in Fig. 10. The point having position $\boldsymbol{\gamma}_j(0) = \boldsymbol{\gamma}_j(1)$ is defined such that it is located at the face adjacent to the smooth folds with corresponding vectors $\mathbf{m}^{j1}$ and $\mathbf{m}^{jn_j}$. Also, the path $\boldsymbol{\gamma}_j(\eta)$ is defined such that it crosses the smooth folds with associated vectors $\mathbf{m}^{jk}$ in counterclockwise order (i.e., $\mathbf{m}^{j1}, \mathbf{m}^{j2}, ..., \mathbf{m}^{jn_j}$).

The position vectors of the points where $\boldsymbol{\gamma}_j(\eta)$ crosses each boundary ruling of the smooth folds with associated vector $\mathbf{m}^{jk}$ are denoted $\mathbf{b}_L^{jk} \in \text{span}(\mathbf{e}_1, \mathbf{e}_2)$ (point where $\boldsymbol{\gamma}_j(\eta)$ enters the smooth fold) and $\mathbf{b}_R^{jk} \in \text{span}(\mathbf{e}_1, \mathbf{e}_2)$ (point where $\boldsymbol{\gamma}_j(\eta)$ exits the smooth fold). This is shown schematically in Fig. 10(*a*).

Let $\mathbf{Q}_1(\phi) \in \mathbb{R}^{4\times4}$ be the transformation matrix in homogeneous coordinates associated with a rotation by ϕ about an axis of rotation aligned to $\mathbf{e}_1$

[7] As stated in Sec. 2.2, self-intersection avoidance is not considered in this work.

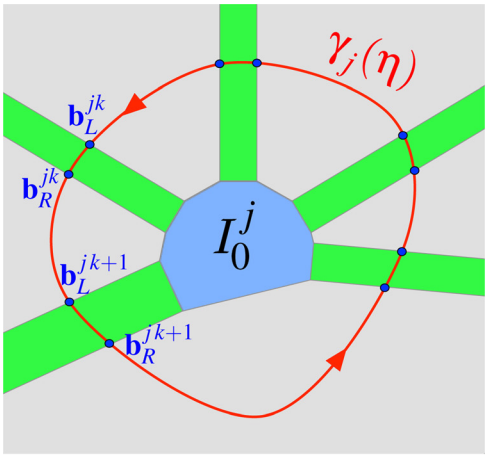

(*a*)

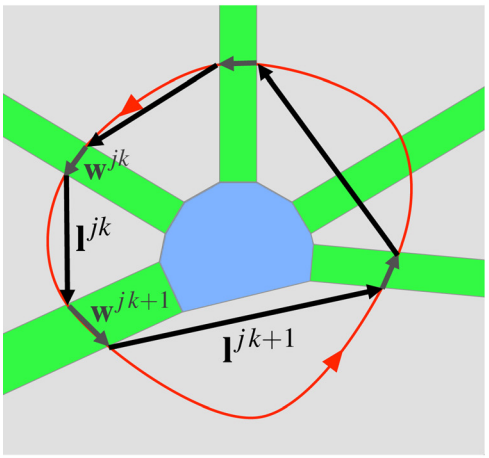

(*b*)

Fig. 10 (*a*) Path $\gamma_j(\eta)$ crossing the faces and smooth folds joined to $\mathcal{I}_0^j$. (*b*) Vectors $\mathbf{w}^{jk}$ and $\mathbf{l}^{jk}$ with start-points and end-points corresponding to the points where the path $\gamma_j(\eta)$ crosses the boundary rulings of the smooth folds.

$$\mathbf{Q}_1(\phi) := \begin{bmatrix} 1 & 0 & 0 & 0 \\ 0 & \cos(\phi) & -\sin(\phi) & 0 \\ 0 & \sin(\phi) & \cos(\phi) & 0 \\ 0 & 0 & 0 & 1 \end{bmatrix} = \begin{bmatrix} \mathbf{R}_1(\phi) & \mathbf{0}_3 \\ \mathbf{0}_3^\top & 1 \end{bmatrix} \tag{47}$$

and $\mathbf{Q}_3(\phi) \in \mathbb{R}^{4\times4}$ be the transformation matrix associated with a rotation by ϕ about an axis of rotation aligned to $\mathbf{e}_3$

$$\mathbf{Q}_3(\phi) := \begin{bmatrix} \cos(\phi) & -\sin(\phi) & 0 & 0 \\ \sin(\phi) & \cos(\phi) & 0 & 0 \\ 0 & 0 & 1 & 0 \\ 0 & 0 & 0 & 1 \end{bmatrix} = \begin{bmatrix} \mathbf{R}_3(\phi) & \mathbf{0}_3 \\ \mathbf{0}_3^\top & 1 \end{bmatrix} \tag{48}$$

Let $\mathbf{T}(\mathbf{b}) \in \mathbb{R}^{4\times4}$ be the matrix representing the transformation associated with a translation by vector $\mathbf{b} \in \mathbb{R}^3$ with elements b_i

$$\mathbf{T}(\mathbf{b}) := \begin{bmatrix} 1 & 0 & 0 & b_1 \\ 0 & 1 & 0 & b_2 \\ 0 & 0 & 1 & b_3 \\ 0 & 0 & 0 & 1 \end{bmatrix} = \begin{bmatrix} \mathbf{I}_3 & \mathbf{b} \\ \mathbf{0}_3^\top & 1 \end{bmatrix} \tag{49}$$

Considering an axis with direction aligned to a vector $\mathbf{y} \in \text{span}(\mathbf{e}_1, \mathbf{e}_2)$ that crosses a point with position vector $\mathbf{b} \in \text{span}(\mathbf{e}_1, \mathbf{e}_2)$, the transformation associated with a rotation by ϕ about such an axis can be represented as follows [36,37]:

$$\mathbf{T}(\mathbf{b})\,\mathbf{Q}_3(\varphi(\mathbf{y}))\,\mathbf{Q}_1(\phi)\,\mathbf{Q}_3^{-1}(\varphi(\mathbf{y}))\,\mathbf{T}^{-1}(\mathbf{b}) \tag{50}$$

THEOREM 3.1. *The transformation matrix $\mathbf{L}^{jk}$ describing the deformation associated with the folding of the kth smooth fold crossed by the path $\boldsymbol{\gamma}_j(\eta)$ is determined as follows:*[8]

$$\begin{aligned} \mathbf{L}^{jk} = {} & (\mathbf{T}(\mathbf{b}_L^{jk} - \mathbf{g}^{j\,k-1})\,\mathbf{Q}_3(\varphi(\mathbf{m}^{jk}))\,\mathbf{Q}_1(a_{jk}\theta_{jk}) \\ & \mathbf{Q}_3^{-1}(\varphi(\mathbf{m}^{jk}))\,\mathbf{T}^{-1}(\mathbf{b}_L^{jk} - \mathbf{g}^{j\,k-1}) \\ & \mathbf{T}(\mathbf{b}_R^{jk} - \mathbf{g}^{jk})\,\mathbf{Q}_3(\varphi(\mathbf{m}^{jk}))\,\mathbf{Q}_1((1-a_{jk})\theta_{jk}) \\ & \mathbf{Q}_3^{-1}(\varphi(\mathbf{m}^{jk}))\,\mathbf{T}^{-1}(\mathbf{b}_R^{jk} - \mathbf{g}^{jk})) \end{aligned} \tag{51}$$

where the vectors $\mathbf{g}^{jk} \in \text{span}(\mathbf{e}_1, \mathbf{e}_2)$, $k = 0, ..., n_j$, account for the change in the distance between the boundary rulings of the smooth folds in a current configuration and are determined recursively as follows:

$$\begin{aligned} & \mathbf{g}^{j0} = \mathbf{0}_3, \\ & \mathbf{g}^{jk} = \mathbf{g}^{j\,k-1} + \left(w_{jk}^0 - w_{jk}\right)\left(\mathbf{e}_3 \times \frac{\mathbf{m}^{jk}}{\| \mathbf{m}^{jk} \|}\right) \qquad \forall k \in \{1, ..., n_j\} \end{aligned} \tag{52}$$

Proof. Referring to Figs. 11(*c*) and 11(*d*), the transformation associated with the folding of the *k*th smooth fold crossed by $\boldsymbol{\gamma}_j(\eta)$ can be discretized by two consecutive rotation transformations. The first transformation corresponds to a rotation by $(1 - a_{jk})\theta_{jk}$ about an axis aligned to $\mathbf{m}^{jk}$ and crossing a point with position vector $\mathbf{b}_R^{jk} - \mathbf{g}^{jk}$. Using Eq. (50), the transformation matrix associated with this rotation is the following:

$$\begin{aligned} & (\mathbf{T}(\mathbf{b}_R^{jk} - \mathbf{g}^{jk})\mathbf{Q}_3(\varphi(\mathbf{m}^{jk}))\mathbf{Q}_1((1-a_{jk})\theta_{jk}) \\ & \mathbf{Q}_3^{-1}(\varphi(\mathbf{m}^{jk}))\mathbf{T}^{-1}(\mathbf{b}_R^{jk} - \mathbf{g}^{jk})) \end{aligned} \tag{53}$$

The second transformation corresponds to a rotation by $a_{jk}\theta_{jk}$ about an axis aligned to $\mathbf{m}^{jk}$ and a crossing point with position vector $\mathbf{b}_L^{jk} - \mathbf{g}^{j\,k-1}$. The transformation matrix associated with this rotation has the form

$$\begin{aligned} & (\mathbf{T}(\mathbf{b}_L^{jk} - \mathbf{g}^{j\,k-1})\mathbf{Q}_3(\varphi(\mathbf{m}^{jk}))\mathbf{Q}_1(a_{jk}\theta_{jk}) \\ & \mathbf{Q}_3^{-1}(\varphi(\mathbf{m}^{jk}))\mathbf{T}^{-1}(\mathbf{b}_L^{jk} - \mathbf{g}^{j\,k-1})) \end{aligned} \tag{54}$$

The composition of the transformations shown in Eqs. (53) and (54) results in the transformation matrix $\mathbf{L}^{jk}$ provided in Eq. (51).

Referring to Figs. 11(*a*) and 11(*b*), the change in the distance between the boundary rulings of a smooth fold in a current configuration is given by $-(w_{jk}^0 - w_{jk})$. To define the position of the axes of rotation for the transformations composing $\mathbf{L}^{jk}$, the vector $\sum_{l=1}^{k-1}(w_{jl}^0 - w_{jl})[\mathbf{e}_3 \times (\mathbf{m}^{jl}/\,\|\,\mathbf{m}^{jl}\,\|)]$ must be subtracted from $\mathbf{b}_L^{jk}$ while $\sum_{l=1}^{k}(w_{jl}^0 - w_{jl})[\mathbf{e}_3 \times (\mathbf{m}^{jl}/\,\|\,\mathbf{m}^{jl}\,\|)]$ must be subtracted from $\mathbf{b}_R^{jk}$. The recursive definition of the vectors $\mathbf{g}^{jk}$, $k = 0, ..., n_j$, in Eq. (52) allows for a simplified form of these vector subtractions. □

Utilizing the block matrix expressions for the rotation and translation matrices given in Eqs. (47)–(49), the transformation matrices $\mathbf{L}^{jk}$ provided in Eq. (51) can be partitioned into four blocks: ($[\mathbf{L}^{jk}]_{11\,\text{block}} \in \mathbb{R}^{3\times3}$, $[\mathbf{L}^{jk}]_{12\,\text{block}} \in \mathbb{R}^{3\times1}$, $[\mathbf{L}^{jk}]_{21\,\text{block}} \in \mathbb{R}^{1\times3}$, and $[\mathbf{L}^{jk}]_{22\,\text{block}} \in \mathbb{R}^{1\times1}$) as follows:

[8]Alternative approaches for modeling the large rotations resulting from folding include quaternions-based [35] and geometric algebra-based approaches [1]. However, such approaches are not explored in this work.

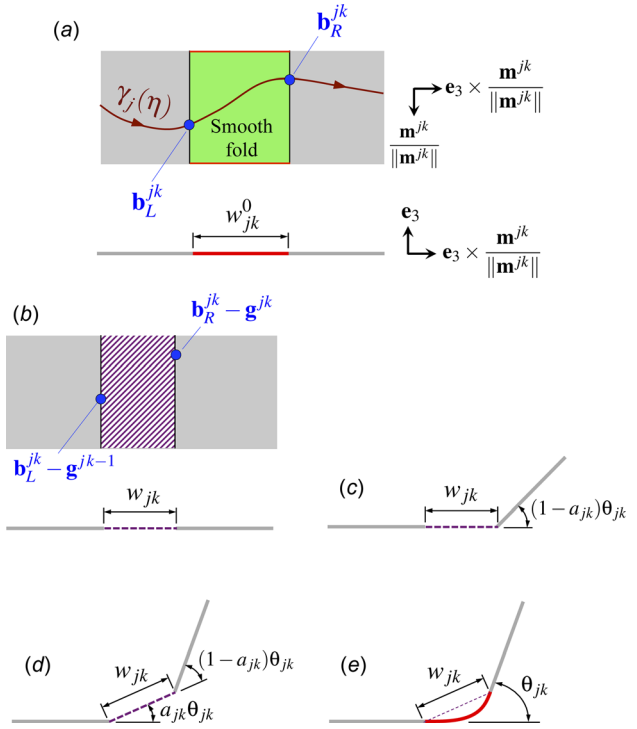

Fig. 11 Schematics illustrating the transformation associated with folding of the *k*th smooth fold crossed by $\gamma_j(\eta)$. (*a*) Reference configuration of the fold. (*b*) Intermediate step to determine the location of the axes of rotation taking into account the change in the distance between the boundary rulings of the smooth fold in a current configuration. Note that the vector $\mathbf{g}^{jk-1}$ is subtracted from $\mathbf{b}_L^{jk}$ to account for the previous smooth folds crossed by $\gamma_j(\eta)$. (*c*) Rotation by $(1-a_{jk})\theta_{jk}$ about an axis aligned to $\mathbf{m}^{jk}$ and crossing a point with position vector $\mathbf{b}_R^{jk}-\mathbf{g}^{jk}$. (*d*) Rotation by $a_{jk}\theta_{jk}$ about an axis aligned to $\mathbf{m}^{jk}$ and a crossing point with position vector $\mathbf{b}_L^{jk}-\mathbf{g}^{jk-1}$. (*e*) Resulting configuration of the smooth fold and its adjacent faces.

$$[\mathbf{L}^{jk}]_{11\,\text{block}} = \mathbf{R}_3(\varphi(\mathbf{m}^{jk}))\mathbf{R}_1(\theta_{jk})\mathbf{R}_3^{-1}(\varphi(\mathbf{m}^{jk})) \tag{55}$$

$$\begin{aligned}[\mathbf{L}^{jk}]_{12\,\text{block}} = {} & \mathbf{b}_L^{jk} - \mathbf{g}^{jk-1} \\ & + (\mathbf{R}_3(\varphi(\mathbf{m}^{jk}))\mathbf{R}_1(a_{jk}\theta_{jk})\mathbf{R}_3^{-1}(\varphi(\mathbf{m}^{jk})) \\ & \times (\mathbf{b}_R^{jk} - \mathbf{g}^{jk} - \mathbf{b}_L^{jk} + \mathbf{g}^{jk-1})) \\ & - (\mathbf{R}_3(\varphi(\mathbf{m}^{jk}))\mathbf{R}_1(\theta_{jk})\mathbf{R}_3^{-1}(\varphi(\mathbf{m}^{jk})) \\ & \times (\mathbf{b}_R^{jk} - \mathbf{g}^{jk}))\end{aligned} \tag{56}$$

$$[\mathbf{L}^{jk}]_{21\,\text{block}} = \mathbf{0}_3^\top \tag{57}$$

$$[\mathbf{L}^{jk}]_{22\,\text{block}} = 1 \tag{58}$$

The vectors $\mathbf{w}^{jk}$, $\mathbf{l}^{jk} \in \text{span}(\mathbf{e}_1, \mathbf{e}_2)$ are defined as follows:

$$\mathbf{w}^{jk} := \mathbf{b}_R^{jk} - \mathbf{g}^{jk} - \mathbf{b}_L^{jk} + \mathbf{g}^{jk-1} \tag{59}$$

$$\mathbf{l}^{jk} := \begin{cases} \mathbf{b}_L^{jk+1} - \mathbf{b}_R^{jk}; & k = 1, \ldots, n_j - 1 \\ \mathbf{b}_L^{j1} - \mathbf{b}_R^{jk}; & k = n_j \end{cases} \tag{60}$$

The vectors $\mathbf{w}^{jk}$ and $\mathbf{l}^{jk}$ for the example in Fig. 10(*a*) are shown in Fig. 10(*b*). Let the vectors $\tilde{\mathbf{w}}^{jk}$ and $\tilde{\mathbf{l}}^{jk}$ be $\mathbf{w}^{jk}$ and $\mathbf{l}^{jk}$, respectively, expressed in a coordinate system with the one-axis aligned to $\mathbf{m}^{jk}$ and the three-axis aligned to $\mathbf{e}_3$

$$\tilde{\mathbf{w}}^{jk} = \mathbf{R}_3^{-1}(\varphi(\mathbf{m}^{jk}))\mathbf{w}^{jk} \tag{61}$$

$$\tilde{\mathbf{l}}^{jk} = \mathbf{R}_3^{-1}(\varphi(\mathbf{m}^{jk}))\mathbf{l}^{jk} \tag{62}$$

Following the process presented in Refs. [36,37], to formulate constraints for the shape variables associated with the folds, the map from the reference to current configurations considering only the faces and smooth folds adjacent to an interior fold intersection is first constructed. The face containing the point with position $\gamma_j(0)$ is assumed *fixed* in space (not translating or rotating) for the derivation of constraints. Let $\mathbf{X} \in \text{span}(\mathbf{e}_1, \mathbf{e}_2)$ be the position vector of a point in a face adjacent to $\mathcal{I}_0^j$ in the reference configuration and let $\mathbf{x} \in \mathbb{R}^3$ be the position vector of such a point in a current configuration. The map $\mathbf{X} \mapsto \mathbf{x}$ is constructed as the composition of transformations $\mathbf{L}^{jk}$ associated with the folds crossed by the segment of path $\gamma_j(\eta)$ that connects $\gamma_j(0)$ to the face containing the point with initial position $\mathbf{X}$

$$\begin{aligned}\begin{bmatrix}\mathbf{x}\\1\end{bmatrix} &= \left(\prod_{k=1}^{n_y}\mathbf{L}^{jk}\right)\mathbf{T}^{-1}(\mathbf{g}^{jn_y})\begin{bmatrix}\mathbf{X}\\1\end{bmatrix} \\ &= \left(\prod_{k=1}^{n_y}\mathbf{H}^{jk}\right)\begin{bmatrix}\mathbf{X}\\1\end{bmatrix}\end{aligned} \tag{63}$$

where the matrices $\mathbf{H}^{jk}$, $j = 1, \ldots, N_{\mathcal{I}}$, $k = 1, \ldots, n_j$, are expressed as follows:

$$\begin{aligned}\mathbf{H}^{jk} = {} & \left(\mathbf{T}\left(\mathbf{b}_L^{jk}\right)\mathbf{Q}_3\left(\varphi(\mathbf{m}^{jk})\right)\mathbf{Q}_1\left(a_{jk}\theta_{jk}\right)\right. \\ & \mathbf{Q}_3^{-1}\left(\varphi(\mathbf{m}^{jk})\right)\mathbf{T}^{-1}\left(\mathbf{b}_L^{jk}\right) \\ & \mathbf{T}^{-1}\left(\left(w_{jk}^0 - w_{jk}\right)\left(\mathbf{e}_3 \times \frac{\mathbf{m}^{jk}}{\|\mathbf{m}^{jk}\|}\right)\right) \\ & \mathbf{T}\left(\mathbf{b}_R^{jk}\right)\mathbf{Q}_3\left(\varphi(\mathbf{m}^{jk})\right)\mathbf{Q}_1\left((1-a_{jk})\theta_{jk}\right) \\ & \left.\mathbf{Q}_3^{-1}\left(\varphi(\mathbf{m}^{jk})\right)\mathbf{T}^{-1}\left(\mathbf{b}_R^{jk}\right)\right)\end{aligned} \tag{64}$$

and n_y is the number of smooth folds crossed by the segment of the path $\gamma_j(\eta)$ that connects $\gamma_j(0)$ and the face containing the point with position vector $\mathbf{X}$. Note that $\mathbf{x}$ is the position vector of such a point in a current configuration determined by θ_{jk}, a_{jk}, and w_{jk}, $k = 1, \ldots, n_j$. Since such a mapping is a composition of translation and rotation matrices, each face undergoes a rigid deformation (required for a valid configuration). In order to prevent tearing among the surface subdomains joined to $\mathcal{I}_t^j$, the following constraints are proposed:

THEOREM 3.2. *For the initially closed strip of faces and smooth folds joined to $\mathcal{I}_0^j$ to remain closed with each face undergoing a rigid deformation, two constraints must hold. These are the rotation constraint*

$$\mathbf{R}^j := \prod_{k=1}^{n_j}\mathbf{R}_1(\theta_{jk})\mathbf{R}_3(\alpha_{jk}) = \mathbf{I}_3 \tag{65}$$

and the translation constraint

$$\begin{aligned}\mathbf{d}^j := \sum_{k=1}^{n_j}\left(\left(\prod_{l=1}^{k-1}\mathbf{R}_1(\theta_{jl})\mathbf{R}_3(\alpha_{jl})\right)\mathbf{R}_1(a_{jk}\theta_{jk})\tilde{\mathbf{w}}^{jk}\right. \\ \left. + \left(\prod_{l=1}^{k-1}\mathbf{R}_1(\theta_{jl})\mathbf{R}_3(\alpha_{jl})\right)\mathbf{R}_1(\theta_{jk})\tilde{\mathbf{l}}^{jk}\right) = \mathbf{0}_3\end{aligned} \tag{66}$$

Proof. The deformation map of a point in the face containing the point with position $\gamma_j(0)$ must be the identity transformation since

such a face is assumed fixed (i.e., if $n_y = n_j$ in Eq. (63) is considered, then $\mathbf{x} = \mathbf{X}$). This requires the following:

$$\mathbf{I}_4 = \left(\prod_{k=1}^{n_j} \mathbf{H}^{jk}\right) = \left(\prod_{k=1}^{n_j} \mathbf{L}^{jk}\right)\mathbf{T}^{-1}(\mathbf{g}^{jn_j}) \tag{67}$$

Utilizing Eqs. (55)–(58), Eq. (67) can be partitioned into four blocks. The 11 block is the following:

$$\begin{aligned}\mathbf{I}_3 &= \prod_{j=1}^{n_j} \mathbf{R}_3(\varphi(\mathbf{m}^{jk}))\mathbf{R}_1(\theta_{ij})\mathbf{R}_3^{-1}(\varphi(\mathbf{m}^{ik})) \\ &= \left(\mathbf{R}_3(\varphi(\mathbf{m}^{j1}))\left(\prod_{k=1}^{n_j-1}\mathbf{R}_1(\theta_{jk})\mathbf{R}_3(\alpha_{jk})\right)\right. \\ &\quad \left.\times\, \mathbf{R}_1(\theta_{jn_j})\mathbf{R}_3^{-1}(\varphi(\mathbf{m}^{jn_j}))\right)\end{aligned} \tag{68}$$

where the following equality was used:

$$\mathbf{R}_3(\alpha_{jk}) = \begin{cases} \mathbf{R}_3^{-1}(\varphi(\mathbf{m}^{jk}))\mathbf{R}_3(\varphi(\mathbf{m}^{jk+1})); & k = 1, \ldots, n_j - 1 \\ \mathbf{R}_3^{-1}(\varphi(\mathbf{m}^{jk}))\mathbf{R}_3(\varphi(\mathbf{m}^{j1})); & k = n_j \end{cases} \tag{69}$$

Multiplying the last expression in Eq. (68) by $\mathbf{R}_3^{-1}(\varphi(\mathbf{m}^{j1}))$ from the left and by $\mathbf{R}_3(\varphi(\mathbf{m}^{j1}))$ from the right, the following is obtained:

$$\begin{aligned}\mathbf{I}_3 &= \left(\left(\prod_{k=1}^{n_j-1}\mathbf{R}_1(\theta_{jk})\mathbf{R}_3(\alpha_{jk})\right)\right. \\ &\quad \left.\mathbf{R}_1(\theta_{jn_j})\mathbf{R}_3^{-1}(\varphi(\mathbf{m}^{jn_j}))\mathbf{R}_3(\varphi(\mathbf{m}^{j1}))\right) \\ &= \left(\prod_{k=1}^{n_j-1}\mathbf{R}_1(\theta_{jk})\mathbf{R}_3(\alpha_{jk})\right)\mathbf{R}_1(\theta_{jn_j})\mathbf{R}_3(\alpha_{jn_j}) \\ &= \prod_{k=1}^{n_j}\mathbf{R}_1(\theta_{jk})\mathbf{R}_3(\alpha_{jk}) = \mathbf{R}^j\end{aligned} \tag{70}$$

cf. Eq. (65). The 12 block of Eq. (67) is the following:

$$\begin{aligned}\mathbf{0}_3 = \sum_{k=1}^{n_j}\Bigg(&\left(\prod_{l=1}^{k-1}\mathbf{R}_3(\varphi(\mathbf{m}^{jl}))\mathbf{R}_1(\theta_{jl})\mathbf{R}_3^{-1}(\varphi(\mathbf{m}^{jl}))\right) \\ &\times (\mathbf{b}_L^{jk} - \mathbf{g}^{jk-1} + (\mathbf{R}_3(\varphi(\mathbf{m}^{jk}))\mathbf{R}_1(a_{jk}\theta_{jk}) \\ &\mathbf{R}_3^{-1}(\varphi(\mathbf{m}^{ik}))(\mathbf{b}_R^{jk} - \mathbf{g}^{jk} - \mathbf{b}_L^{jk} + \mathbf{g}^{jk-1})) \\ &-(\mathbf{R}_3(\varphi(\mathbf{m}^{ik}))\mathbf{R}_1(\theta_{jk})\mathbf{R}_3^{-1}(\varphi(\mathbf{m}^{ik}))(\mathbf{b}_R^{jk} - \mathbf{g}^{jk}))) \\ &-\left(\prod_{k=1}^{n_j}\mathbf{R}_3(\varphi(\mathbf{m}^{ik})\right)\mathbf{R}_1(\theta_{jk})\mathbf{R}_3^{-1}(\varphi(\mathbf{m}^{jk}))\Bigg)\mathbf{g}^{jn_j}\end{aligned} \tag{71}$$

Substituting the second expression of Eq. (68) and Eqs. (61) and (62) into Eq. (71), the following is obtained:

$$\begin{aligned}\mathbf{0}_3 = \sum_{k=1}^{n_j}\Bigg(&\left(\prod_{l=1}^{k-1}\mathbf{R}(\varphi(\mathbf{m}^{jl})\right)\mathbf{R}_1(\theta_{jl})\mathbf{R}_3^{-1}(\varphi(\mathbf{m}^{jl}))\Bigg) \\ &(\mathbf{R}_3(\varphi(\mathbf{m}^{jk}))\mathbf{R}_1(a_{jk}\theta_{jk})\tilde{\mathbf{w}}^{jk} \\ &+\mathbf{R}_3(\varphi(\mathbf{m}^{jk}))\mathbf{R}_1(\theta_{jk})\tilde{\mathbf{l}}^{jk}))\end{aligned} \tag{72}$$

Finally multiplying both sides of the previous expression by $\mathbf{R}_3^{-1}(\varphi(\mathbf{m}^{j1}))$ and simplifying using Eq. (69), the following is obtained:

$$\begin{aligned}\mathbf{0}_3 &= \sum_{k=1}^{n_j}\left(\left(\prod_{l=1}^{k-1}\mathbf{R}_1(\theta_{jl})\mathbf{R}_3(\alpha_{jl})\right)\mathbf{R}_1(a_{jk}\theta_{jk})\tilde{\mathbf{w}}^{jk}\right. \\ &\quad \left.+\left(\prod_{l=1}^{k-1}\mathbf{R}_1(\theta_{jl})\mathbf{R}_3(\alpha_{jl})\right)\mathbf{R}_1(\theta_{jk})\tilde{\mathbf{l}}^{jk}\right) \\ &= \mathbf{d}^j\end{aligned} \tag{73}$$

cf. Eq. (66). The 21 and the 22 blocks of the right side of Eq. (67) are equal to $\mathbf{0}_3^\top$ and 1, respectively. □

COROLLARY 3.1.

(i) *If $\mathcal{I}_0^j$ has a single adjacent smooth fold, it allows for a valid configuration if $\theta_{j1} = 0$.*
(ii) *If $\mathcal{I}_0^j$ has two adjacent smooth folds, it allows for a valid configuration if (ii,1) $\alpha_{j1} \neq \pi, \theta_{j1} = \theta_{j2} = 0$ or (ii,2) $\alpha_{j1} = \pi, \theta_{j1} = \theta_{j2}$.*
(iii) *If $\mathcal{I}_0^j$ has three adjacent smooth folds, it allows for a valid configuration if (iii,1) $\alpha_{j1} \neq \pi, \alpha_{j2} \neq \pi, \alpha_{j3} \neq \pi$, $\theta_{j1} = \theta_{j2} = \theta_{j3} = 0$, or (iii,2) $\alpha_{j1} = \pi, \theta_{j1} = \theta_{j2}, \theta_{j3} = 0$, or (iii,3) $\alpha_{j2} = \pi, \theta_{j2} = \theta_{j3}, \theta_{j1} = 0$, or (iii,4) $\alpha_{j3} = \pi$, $\theta_{j3} = \theta_{j1}, \theta_{j2} = 0$.*

Since the rotation constraint for smooth folds ($\mathbf{R}^j = \mathbf{I}_3$, cf. Eq. (65)) also holds for creased folds (cf. Eq. (14)), the proof of this corollary is the same as that provided for Corollary 2.1.

The selection of the vectors $\mathbf{b}_L^{jk}, \mathbf{b}_R^{jk}$, $k = 1, \ldots, n_j$ is not unique and depends on the particular choice of the closed path $\boldsymbol{\gamma}_j(\eta)$ (see Fig. 10(*a*)). The corner points of the smooth folds defined in Eq. (38) provide a simple choice for the points where $\boldsymbol{\gamma}_j(\eta)$ crosses the boundary rulings of each smooth fold adjacent to $\mathcal{I}_0^j$. Thus, they can be used to define $\mathbf{b}_L^{jk}, \mathbf{b}_R^{jk}$, $k = 1, \ldots, n_j$. First, let $\mathbf{B}_L^j, \mathbf{B}_R^j \in \mathbb{R}^{3n_j}$ be the vectors constructed by concatenating the vectors $\mathbf{b}_L^{jk}, \mathbf{b}_R^{jk}$, $k = 1, \ldots, n_j$, as follows:

$$\mathbf{B}_L^j = \begin{bmatrix} \mathbf{b}_L^{j1} \\ \vdots \\ \mathbf{b}_L^{jn_j} \end{bmatrix}, \quad \mathbf{B}_R^j = \begin{bmatrix} \mathbf{b}_R^{j1} \\ \vdots \\ \mathbf{b}_R^{jn_j} \end{bmatrix} \tag{74}$$

Taking into account the orientation of the adjacent smooth folds with respect to the considered fold intersection $\mathcal{I}_0^j$ (i.e., whether the interior vertex associated with $\mathcal{I}_0^j$ is the start-point or the end-point of the adjacent smooth fold centerline), the mapping from the corner points of the smooth folds to $\mathbf{B}_L^j$ and $\mathbf{B}_R^j$ is compactly given as follows:

$$\begin{bmatrix} \mathbf{B}_L^j \\ \mathbf{B}_R^j \end{bmatrix} = \begin{bmatrix} \frac{1}{2}\left(|\mathbf{C}^j|_* + \mathbf{C}^j\right) \otimes \mathbf{I}_3 & \frac{1}{2}\left(|\mathbf{C}^j|_* - \mathbf{C}^j\right) \otimes \mathbf{I}_3 \\ \frac{1}{2}\left(|\mathbf{C}^j|_* - \mathbf{C}^j\right) \otimes \mathbf{I}_3 & \frac{1}{2}\left(|\mathbf{C}^j|_* + \mathbf{C}^j\right) \otimes \mathbf{I}_3 \end{bmatrix} \begin{bmatrix} \hat{\mathbf{P}}^1 \\ \hat{\mathbf{P}}^4 \end{bmatrix} \tag{75}$$

where the vectors $\hat{\mathbf{P}}^i$ are defined in Eq. (40). Note that the mapping provided in Eq. (75) results in $\mathbf{b}_L^{jk} = \hat{\mathbf{p}}_1^i$, $\mathbf{b}_R^{jk} = \hat{\mathbf{p}}_4^i$ if $\mathbf{m}^{jk}$ is coincident with and has the same orientation as the ith smooth fold centerline and $\mathbf{b}_L^{jk} = \hat{\mathbf{p}}_4^i$, $\mathbf{b}_R^{jk} = \hat{\mathbf{p}}_1^i$ if $\mathbf{m}^{jk}$ is coincident with and has the opposite orientation as the ith smooth fold centerline.

Finally, the constraints on the fold shape variables that allow for a valid configuration (excluding self-intersection avoidance) for a sheet with smooth folds are then the following:

$$\mathbf{R}^j = \mathbf{I}_3, \quad \mathbf{d}^j = \mathbf{0}_3 \quad \forall j \in \{1, \ldots, N_{\mathcal{I}}\} \tag{76}$$

cf. Eq. (15).

In general, the variables $\hat{\theta}_i$, $\hat{w}_i$, and $\hat{a}_i$ for each individual smooth fold represent its shape variables (i.e., degrees-of-freedom) that describe its configuration. If certain assumptions hold regarding the deformation of each individual smooth fold, the associated variables $\hat{\theta}_i$, $\hat{w}_i$, and $\hat{a}_i$ may not vary independently but

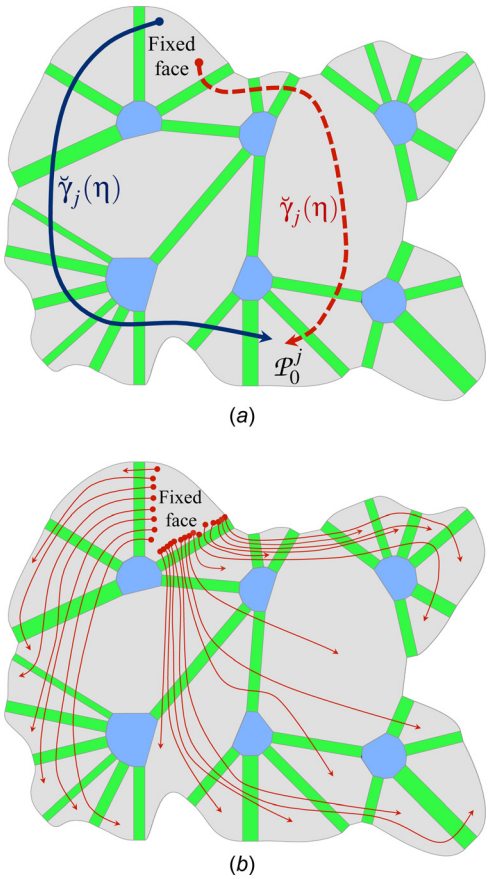

Fig. 12 (*a*) Two equivalent paths $\breve{\gamma}_j(\eta)$ connecting the fixed face to $\mathcal{P}_0^j$. (*b*) Paths $\breve{\gamma}^j(\eta)$, $j = 1, ..., N_{\mathcal{P}}$, connecting the fixed face to every other face in $\mathcal{S}_0$.

rather relations among them can be derived. For simplicity in the implementation of the proposed model, assumptions on the extensibility and curvature field of the curve $\hat{\mathbf{c}}^i(\zeta_1)$ are taken such that the overall deformation of a smooth fold becomes a function of the fold angle $\hat{\theta}_i$ and the fold width $\hat{w}_i^0$ (i.e., $\hat{w}_i = \hat{w}_i(\hat{\theta}_i, \hat{w}_i^0)$, $\hat{a}_i = \hat{a}_i(\hat{\theta}_i, \hat{w}_i^0)$ for each fold). Such a process involves nondimensionalization of the parametric curve $\hat{\mathbf{c}}^i(\zeta_1)$ and is presented in detail in Appendix B for the case of smooth folds exhibiting G^2 continuity (Eq. (34)).

3.4 Folding Map. The formulation of the deformation map that relates the reference and current configurations (termed *folding map* here) is provided in this section. A folding map considering only the smooth folds and faces adjacent to an interior fold intersection was provided in Eq. (63). Here such a formulation is extended for the folding map of all the smooth folds and faces in the sheet.

First, an arbitrary face in the sheet is assumed fixed in its reference configuration.[9] Let $\breve{\gamma}_j(\eta) : [0, 1] \to \mathcal{S}_0$, $j = 1, ..., N_{\mathcal{P}}$, be paths connecting the fixed face to $\mathcal{P}_0^j$, $j = 1, ..., N_{\mathcal{P}}$, respectively (see Fig. 12 for an example). The paths $\breve{\gamma}_j(\eta)$, $j = 1, ..., N_{\mathcal{P}}$, may not cross any fold intersection (i.e., they pass only through faces and smooth folds of $\mathcal{S}_0$). Following the formulation of Eq. (63), the map for points located in the faces is constructed as the composition of transformations associated with the smooth folds crossed by the path $\breve{\gamma}^j(\eta)$ between $\breve{\gamma}^j(0)$ (located at the fixed face) and $\breve{\gamma}^j(1)$ (located at $\mathcal{P}_0^j$). Each path $\breve{\gamma}^j(\eta)$ crosses a number of p_j smooth folds.

[9]A breve (˘) is used to distinguish the symbols related to the folding map from the symbols used in Sec. 3.3.

The path $\breve{\gamma}^j(\eta)$ crosses a smooth fold *positively* if it enters such a fold from the ruling $\mathcal{F}^i(-1, \zeta_2)$ and exits at the ruling $\mathcal{F}^i(1, \zeta_2)$. Conversely, the path $\breve{\gamma}^j(\eta)$ crosses a smooth fold *negatively* if it crosses such a fold in the opposite direction. The matrices $\breve{\mathbf{C}}^j \in \{-1, 0, 1\}^{p_j \times N_{\mathcal{F}}}$, $j = 1, ..., N_{\mathcal{P}}$, with elements $\breve{C}^j_{ki}$ are used for the identification and ordering of the folds crossed by $\breve{\gamma}^j(\eta)$

$$\breve{C}^j_{ki} = \begin{cases} 1; & \mathcal{F}_0^i \text{ is the } k\text{th fold crossed by } \breve{\gamma}^j(\eta) \text{ and is positively crossed} \\ -1; & \mathcal{F}_0^i \text{ is the } k\text{th fold crossed by } \breve{\gamma}^j(\eta) \text{ and is negatively crossed} \\ 0; & \text{otherwise} \end{cases} \tag{77}$$

Let $\breve{\mathbf{m}}^{jk}$ be the vector along the length of the centerline of the kth smooth fold crossed by $\breve{\gamma}_j(\eta)$. Such a vector has the same orientation as the fold centerline if $\breve{\gamma}_j(\eta)$ crosses the fold positively and opposite orientation if $\breve{\gamma}_j(\eta)$ crosses the fold negatively. The vector $\breve{\mathbf{M}}^j \in \mathbb{R}^{3p_j}$ is constructed by concatenating the vectors $\breve{\mathbf{m}}^{jk}$, $k = 1, ..., p_j$, as follows:

$$\breve{\mathbf{M}}^j = \begin{bmatrix} \breve{\mathbf{m}}^{j1} \\ \vdots \\ \breve{\mathbf{m}}^{jp_j} \end{bmatrix} \tag{78}$$

The mapping from the vertex position vectors collected in the vector V to each vector $\breve{\mathbf{M}}^j$ is compactly given as follows:

$$\breve{\mathbf{M}}^j = ((\breve{\mathbf{C}}^j \hat{\mathbf{C}}) \otimes \mathbf{I}_3)\mathbf{V} \tag{79}$$

Let $\breve{\theta}_{jk}$, $\breve{w}_{jk}$, and $\breve{a}_{jk}$, $k = 1, ..., p_j$, be the shape variables associated with the ordered smooth folds crossed by $\breve{\gamma}_j(\eta)$. The vectors $\breve{\boldsymbol{\theta}}^j, \breve{\mathbf{w}}^j, \breve{\mathbf{a}}^j \in \mathbb{R}^{p_j}$ are constructed by collecting the variables $\breve{\theta}_{jk}$, $\breve{w}_{jk}$, and $\breve{a}_{jk}$, $k = 1, ..., p_j$, as follows:

$$\begin{aligned} \breve{\boldsymbol{\theta}}^j &= [\breve{\theta}_{j1} \quad \cdots \quad \breve{\theta}_{jp_j}]^\top, \quad \breve{\mathbf{w}}^j = [\breve{w}_{j1} \quad \cdots \quad \breve{w}_{jp_j}]^\top \\ \breve{\mathbf{a}}^j &= [\breve{a}_{j1} \quad \cdots \quad \breve{a}_{jp_j}]^\top \end{aligned} \tag{80}$$

Following the formulation presented in Sec. 3.3, the vectors $\breve{\boldsymbol{\theta}}^j$, $\breve{\mathbf{w}}^j$, and $\breve{\mathbf{a}}^j$ are determined from the shape variables of the smooth folds in the sheet as follows (cf. Eqs. (11), (43), and (44)):

$$\breve{\boldsymbol{\theta}}^j = |\breve{\mathbf{C}}^j|_* \hat{\boldsymbol{\theta}}, \quad \breve{\boldsymbol{w}}^j = |\breve{\mathbf{C}}^j|_* \hat{\boldsymbol{w}}, \quad \breve{\boldsymbol{a}}^j = [\breve{\mathbf{C}}^j \quad {}^A\breve{\mathbf{C}}^j] \begin{bmatrix} \hat{\boldsymbol{a}} \\ 1 \end{bmatrix} \tag{81}$$

where ${}^A\breve{\mathbf{C}}^j \in \mathbb{R}^{p_j}$ is a vector with elements ${}^A\breve{C}^j_k$ determined as follows (cf. Eq. (45)):

$${}^A\breve{C}^j_k = \frac{1}{2} - \frac{1}{2}\sum_{i=1}^{N_{\mathcal{F}}} \breve{C}^j_{ki} \tag{82}$$

The fold widths associated with the smooth folds crossed by $\breve{\gamma}_j(\eta)$ are denoted $\breve{w}^0_{jk}$, $k = 1, ..., n_j$, and are required in the formulation of the folding map. As such, let $\breve{\mathbf{w}}^{0,j} \in \mathbb{R}^{p_j}$ be the vector constructed by collecting the fold widths $\breve{w}^0_{jk}$, $k = 1, ..., p_j$. Such a vector and its mapping from $\hat{\boldsymbol{w}}^0$ (defined in Eq. (19)) are as follows:

$$\breve{\mathbf{w}}^{0,j} = \begin{bmatrix} \breve{w}^0_{j1} & \cdots & \breve{w}^0_{jn_j} \end{bmatrix}^\top = |\breve{\mathbf{C}}^j|_* \hat{\boldsymbol{w}}^0 \tag{83}$$

The position vectors of the points where $\breve{\gamma}_j(\eta)$ crosses the boundary rulings of the smooth folds are denoted $\breve{\mathbf{b}}^{jk}_L \in \mathbb{R}^3$ (point

where $\breve{\gamma}_j(\eta)$ enters the smooth fold) and $\breve{\mathbf{b}}_R^{jk} \in \mathbb{R}^3$ (point where $\breve{\gamma}_j(\eta)$ exits the smooth fold). Let $\breve{\mathbf{B}}_L^{\,j}, \breve{\mathbf{B}}_R^{\,j} \in \mathbb{R}^{3p_j}$ be the vectors constructed by concatenating the vectors $\breve{\mathbf{b}}_L^{jk}, \breve{\mathbf{b}}_R^{jk}$, $k = 1, ..., p_j$, respectively, as follows:

$$\breve{\mathbf{B}}_L^{\,j} = \begin{bmatrix} \breve{\mathbf{b}}_L^{j1} \\ \vdots \\ \breve{\mathbf{b}}_L^{jp_j} \end{bmatrix}, \quad \breve{\mathbf{B}}_R^{\,j} = \begin{bmatrix} \breve{\mathbf{b}}_R^{j1} \\ \vdots \\ \breve{\mathbf{b}}_R^{jp_j} \end{bmatrix} \tag{84}$$

The corner points of the smooth folds in $\mathcal{S}_0$ defined in Eq. (38) provide a simple choice for the locations where the path $\breve{\gamma}_j(\eta)$ crosses the boundary rulings of the smooth folds. Thus, as in Sec. 3.3, the position vectors of such corner points are utilized to define the vectors $\breve{\mathbf{b}}_L^{jk}, \breve{\mathbf{b}}_R^{jk}$, $k = 1, ..., p_j$ (cf. Eq. (75))

$$\begin{bmatrix} \breve{\mathbf{B}}_L^{\,j} \\ \breve{\mathbf{B}}_R^{\,j} \end{bmatrix} = \begin{bmatrix} \frac{1}{2}\left(|\breve{\mathbf{C}}^j|_* + \breve{\mathbf{C}}^j\right) \otimes \mathbf{I}_3 & \frac{1}{2}\left(|\breve{\mathbf{C}}^j|_* - \breve{\mathbf{C}}^j\right) \otimes \mathbf{I}_3 \\ \frac{1}{2}\left(|\breve{\mathbf{C}}^j|_* - \breve{\mathbf{C}}^j\right) \otimes \mathbf{I}_3 & \frac{1}{2}\left(|\breve{\mathbf{C}}^j|_* + \breve{\mathbf{C}}^j\right) \otimes \mathbf{I}_3 \end{bmatrix} \begin{bmatrix} \hat{\mathbf{P}}^1 \\ \hat{\mathbf{P}}^4 \end{bmatrix} \tag{85}$$

After defining all the shape variables and geometric parameters associated with the smooth folds crossed by each path $\breve{\gamma}^j(\eta)$, $j = 1, ..., N_{\mathcal{P}}$, the folding map for points in the faces is obtained as the composition of transformations $\breve{\mathbf{H}}^{jk}$ associated with the smooth folds crossed by these paths (cf. Eq. (63))

$$\mathbf{x} = \chi(\mathbf{X}, t) \quad \text{where} \quad \begin{bmatrix} \mathbf{x} \\ 1 \end{bmatrix} = \left(\prod_{k=1}^{p_j} \breve{\mathbf{H}}^{jk}\right) \begin{bmatrix} \mathbf{X} \\ 1 \end{bmatrix} \tag{86}$$

where $\mathbf{X} \in \text{span}(\mathbf{e}_1, \mathbf{e}_2)$ is the position vector of a point in $\mathcal{P}_0^j \subset \mathcal{S}_0$ and $\mathbf{x} \in \mathbb{R}^3$ is the position vector of such a point in $\mathcal{P}_t^j \subset \mathcal{S}_t$. Since the results of Theorem 3.1 and Eqs. (63) and (64) are also applicable for the smooth folds crossed by the paths $\breve{\gamma}^j(\eta)$, the matrices $\breve{\mathbf{H}}^{jk}$ follow the same formulation presented in Eq. (64)

$$\begin{aligned} \breve{\mathbf{H}}^{jk} = & \left(\mathbf{T}\left(\breve{\mathbf{b}}_L^{jk}\right) \mathbf{Q}_3\left(\varphi\left(\breve{\mathbf{m}}^{jk}\right)\right) \mathbf{Q}_1\left(\breve{a}_{jk}\breve{\theta}_{jk}\right)\right. \\ & \times \mathbf{Q}_3^{-1}\left(\varphi\left(\breve{\mathbf{m}}^{jk}\right)\right) \mathbf{T}^{-1}\left(\breve{\mathbf{b}}_L^{jk}\right) \\ & \times \mathbf{T}^{-1}\left(\left(\breve{w}_{jk}^{\,0} - \breve{w}_{jk}\right)\left(\mathbf{e}_3 \times \frac{\breve{\mathbf{m}}^{jk}}{\|\breve{\mathbf{m}}^{jk}\|}\right)\right) \\ & \times \mathbf{T}\left(\breve{\mathbf{b}}_R^{jk}\right) \mathbf{Q}_3\left(\varphi\left(\breve{\mathbf{m}}^{jk}\right)\right) \mathbf{Q}_1\left(\left(1 - \breve{a}_{jk}\right)\breve{\theta}_{jk}\right) \\ & \left. \times \mathbf{Q}_3^{-1}\left(\varphi\left(\breve{\mathbf{m}}^{jk}\right)\right) \mathbf{T}^{-1}\left(\breve{\mathbf{b}}_R^{jk}\right)\right) \end{aligned} \tag{87}$$

Determining the folding map for the smooth folds requires further steps since these surface subdomains undergo nonrigid deformations in addition to rotations and translations. The position vector of a point in $\mathcal{F}_t^i$ expressed in its associated fold coordinate system (with basis $\{\hat{\mathbf{e}}_1^i, \hat{\mathbf{e}}_2^i, \hat{\mathbf{e}}_3^i\}$ and origin at $(1/2)(\mathbf{c}^i(-1) + \mathbf{c}^i(1))$, see Sec. 3.1) is denoted $\hat{\mathbf{x}} \in \mathbb{R}^3$. Since the current configuration of a smooth fold $\mathcal{F}_t^i$ is known in its associated fold coordinate system for a given set of fold shape variables, the focus here is on the formulation of the map $\mathbf{x} = \hat{\chi}(\hat{\mathbf{x}}(t), t)$. To construct this map, a transformation represented by the matrix $\hat{\mathbf{L}}^{\,i} \in \mathbb{R}^{4\times4}$ is first applied to the vector $\hat{\mathbf{x}}$. This transformation returns the position of the deformed smooth fold as joined to the reference configuration of the face adjacent to its boundary ruling $\mathcal{F}^i(-1, \zeta_2)$ (denoted $\mathcal{P}_0^{i_{\mathcal{F}}}$). The transformation $\hat{\mathbf{L}}^{\,i}$ is obtained by first aligning position of the smooth fold expressed in its associated fold coordinate system with the plane spanned by $\mathbf{e}_1$ and $\mathbf{e}_2$ (performed via the transformation $\mathbf{Q}_1(\hat{a}_i\hat{\theta}_i)\mathbf{T}([0, \hat{w}_i/2, 0]^\top)$), and then aligning such a resulting position to $\mathcal{P}_0^{i_{\mathcal{F}}}$ (performed through the transformation $\mathbf{T}(\hat{\mathbf{p}}_1^i)\mathbf{Q}_3(\varphi(\hat{\mathbf{v}}^{i2} - \hat{\mathbf{v}}^{i1}))$. Therefore, $\hat{\mathbf{L}}^{\,i}$ is given as follows:

$$\hat{\mathbf{L}}^{\,i} = \mathbf{T}(\hat{\mathbf{p}}_1^i)\mathbf{Q}_3(\varphi(\hat{\mathbf{v}}^{i2} - \hat{\mathbf{v}}^{i1}))\mathbf{Q}_1(\hat{a}_i\hat{\theta}_i)\mathbf{T}([0, \hat{w}_i/2, 0]^\top) \tag{88}$$

Subsequently, the folding map associated with the face $\mathcal{P}_0^{i_{\mathcal{F}}}$ is applied to determine the position of the smooth fold in the current configuration expressed in the global coordinate system. Thus, the folding map for points in the smooth folds is defined as follows:

$$\mathbf{x} = \hat{\chi}(\hat{\mathbf{x}}(t), t) \quad \text{where} \quad \begin{bmatrix} \mathbf{x} \\ 1 \end{bmatrix} = \left(\prod_{k=1}^{p_{i_{\mathcal{F}}}} \mathbf{H}^{i_{\mathcal{F}}k}\right) \hat{\mathbf{L}}^{\,i} \begin{bmatrix} \hat{\mathbf{x}}(t) \\ 1 \end{bmatrix} \tag{89}$$

where $\hat{\mathbf{x}}$ is the position vector of a point in $\mathcal{F}_t^i \subset \mathcal{S}_t$ expressed in the ith fold coordinate system with basis $\{\hat{\mathbf{e}}_1^i, \hat{\mathbf{e}}_2^i, \hat{\mathbf{e}}_3^i\}$ and $\mathbf{x} \in \mathbb{R}^3$ is the position vector of such a point expressed in the global coordinate system with basis $\{\mathbf{e}_1, \mathbf{e}_2, \mathbf{e}_3\}$. Note that the position vector of a point in $\mathcal{F}_0^i \subset \mathcal{S}_0$ is obtained as $\mathbf{X} = \hat{\chi}(\hat{\mathbf{x}}(0), 0) \in \text{span}(\mathbf{e}_1, \mathbf{e}_2)$

$$\begin{aligned} & \mathbf{X} = \hat{\chi}(\hat{\mathbf{x}}(0), 0) \quad \text{where} \\ & \begin{bmatrix} \mathbf{X} \\ 1 \end{bmatrix} = \mathbf{I}_4 \hat{\mathbf{L}}^{\,i}|_{t=0} \begin{bmatrix} \hat{\mathbf{x}}(0) \\ 1 \end{bmatrix} \\ & \quad = \mathbf{T}(\hat{\mathbf{p}}_1^i)\mathbf{Q}_3(\varphi(\hat{\mathbf{v}}^{i2} - \hat{\mathbf{v}}^{i1}))\mathbf{T}([0, \hat{w}_i^0/2, 0]^\top) \begin{bmatrix} \hat{\mathbf{x}}(0) \\ 1 \end{bmatrix} \end{aligned} \tag{90}$$

3.5 Numerical Implementation. As stated at the beginning of Sec. 3, the *continuous motion* of the sheet is achieved by continuously altering the values of the fold shape variables ($\hat{\theta}_i$, $\hat{w}_i$, and $\hat{a}_i$, $i = 1, ..., N_{\mathcal{F}}$) such that any attained configuration satisfies the constraints presented in Eq. (76) (i.e., the motion of the sheet is a continuous path in the constrained configuration space).

The simulation of the continuous motion of the sheet is executed by *incrementally* updating the values of the fold shape variables using input guess increments and then iteratively applying any required corrections such that the resulting set of fold shape variables satisfies the constraints of Eq. (76). The iterative procedure used to perform such corrections is outlined in this section. As stated in Sec. 3.3, the full set of fold shape variables $\hat{\theta}_i$, $\hat{w}_i$, and $\hat{a}_i$, $i = 1, ..., N_{\mathcal{F}}$, is reduced to only the set of fold angles $\hat{\theta}_i$, $i = 1, ..., N_{\mathcal{F}}$, by establishing relations $\hat{w}_i(\hat{\theta}_i, \hat{w}_i^0)$ and $\hat{a}_i(\hat{\theta}_i, \hat{w}_i^0)$ following certain assumptions on the extensibility and curvature field of the smooth folds (see Appendix B for details).

3.5.1 Constraints. Given a guess set of fold angles ordered in the vector ${}_l^k\hat{\boldsymbol{\theta}} \in \mathbb{R}^{N_{\mathcal{F}}}$ where the subscript l denotes to incremental step number and the superscript k denotes to the correction iteration number, the matrices $\mathbf{R}^j({}_l^k\hat{\boldsymbol{\theta}})$ and the vectors $\mathbf{d}^j({}_l^k\hat{\boldsymbol{\theta}})$, $j = 1, ..., N_{\mathcal{I}}$, are calculated. If the vector of fold angles ${}_l^k\hat{\boldsymbol{\theta}}$ does not yield a configuration that satisfies Eq. (76), $\mathbf{R}^j({}_l^k\hat{\boldsymbol{\theta}}) - \mathbf{I}_3$ is not equal to the zero matrix in $\mathbb{R}^{3\times3}$ and/or $\mathbf{d}^j({}_l^k\hat{\boldsymbol{\theta}})$ is not equal to $\mathbf{0}_3$.

Let $\boldsymbol{\mathcal{R}}({}_l^k\hat{\boldsymbol{\theta}}) \in \mathbb{R}^{6N_{\mathcal{I}}+2N_{\mathcal{F}}}$ with components $\Re_j({}_l^k\hat{\boldsymbol{\theta}})$ be the vector of residuals from constraints of Eq. (76) ($6N_{\mathcal{I}}$ in total) and from constraints imposing the upper and lower fold angle bounds ($2N_{\mathcal{F}}$ in total). Since $\mathbf{R}^j({}_l^k\hat{\boldsymbol{\theta}})$ is an orthogonal matrix, only three of its scalar components are independent. Thus, the matrix-type constraint in Eq. (65) provides the following three scalar constraints that contribute to the residual vector [40]:

$$\Re_{6j-5}\left({}^{k}_{l}\hat{\boldsymbol{\theta}}\right)=\frac{1}{2}\lambda_R\left(R^j_{23}\left({}^{k}_{l}\hat{\boldsymbol{\theta}}\right)\right)^2$$
$$\Re_{6j-4}\left({}^{k}_{l}\hat{\boldsymbol{\theta}}\right)=\frac{1}{2}\lambda_R\left(R^j_{31}\left({}^{k}_{l}\hat{\boldsymbol{\theta}}\right)\right)^2 \tag{91}$$
$$\Re_{6j-3}\left({}^{k}_{l}\hat{\boldsymbol{\theta}}\right)=\frac{1}{2}\lambda_R\left(R^j_{12}\left({}^{k}_{l}\hat{\boldsymbol{\theta}}\right)\right)^2$$

where $j\in\{1,\ldots,N_{\mathcal{I}}\}$ and λ_R is the weight for residuals from Eq. (65). This constant weight is an algorithmic parameter included in the residual vector to ensure that its components are scaled to a similar order of magnitude (i.e., the components of $\mathbf{R}^j({}^{k}_{l}\hat{\boldsymbol{\theta}})$ are dimensionless while those of $\mathbf{d}^j({}^{k}_{l}\hat{\boldsymbol{\theta}})$ have units of length). The three components of the vector $\mathbf{d}^j({}^{k}_{l}\hat{\boldsymbol{\theta}})$, $j=1,\ldots,N_{\mathcal{I}}$, which must be zero for the constraint in Eq. (66) to be satisfied, provide the following components to the residual vector:

$$\Re_{6j-2}\left({}^{k}_{l}\hat{\boldsymbol{\theta}}\right)=\frac{1}{2}\lambda_d\left(d^j_1\left({}^{k}_{l}\hat{\boldsymbol{\theta}}\right)\right)^2$$
$$\Re_{6j-1}\left({}^{k}_{l}\hat{\boldsymbol{\theta}}\right)=\frac{1}{2}\lambda_d\left(d^j_2\left({}^{k}_{l}\hat{\boldsymbol{\theta}}\right)\right)^2 \tag{92}$$
$$\Re_{6j}\left({}^{k}_{l}\hat{\boldsymbol{\theta}}\right)=\frac{1}{2}\lambda_d\left(d^j_3\left({}^{k}_{l}\hat{\boldsymbol{\theta}}\right)\right)^2$$

where $j\in\{1,\ldots,N_{\mathcal{I}}\}$ and λ_d is the weight for residuals from Eq. (66).

3.5.2 Fold Angle Bounds. Additional components of $\boldsymbol{\mathcal{R}}({}^{k}_{l}\hat{\boldsymbol{\theta}})$ are included to ensure that the fold angles remain within prescribed upper and lower bounds during the continuous motion of the sheet. A penalty approach is used to implement the required fold angle bounds for each fold as in Ref. [40]. The lower bound for $\hat{\theta}_i$ is denoted $\hat{\theta}^L_i\in[-\pi,0]$ and the upper bound is denoted $\hat{\theta}^U_i\in[0,\pi]$. Conventional assignments for $\hat{\theta}^L_i$ and $\hat{\theta}^U_i$ are provided in Table 1.

The additional components of $\boldsymbol{\mathcal{R}}({}^{k}_{l}\hat{\boldsymbol{\theta}})$ required to enforce the lower bound of ${}^{k}_{l}\hat{\theta}_i$ consist of a penalty that is zero if ${}^{k}_{l}\hat{\theta}_i\geq\hat{\theta}^L_i$ and increases proportionally to the square of the difference between ${}^{k}_{l}\hat{\theta}_i$ and $\hat{\theta}^L_i$ when ${}^{k}_{l}\hat{\theta}_i<\hat{\theta}^L_i$

$$\Re_{6N_{\mathcal{I}}+2i-1}\left({}^{k}_{l}\hat{\boldsymbol{\theta}}\right)=\frac{1}{2}\lambda_B\max\left(0,-{}^{k}_{l}\hat{\theta}_i+\hat{\theta}^L_i\right)^2 \tag{93}$$

where $i\in\{1,\ldots,N_{\mathcal{F}}\}$ and λ_B is the weight for residuals from fold angle bound constraints. Similarly, to enforce the upper bound of $\hat{\theta}_i$, a penalty that is zero if ${}^{k}_{l}\hat{\theta}_i\leq\hat{\theta}^U_i$ and increases proportionally to the square of the difference between ${}^{k}_{l}\hat{\theta}_i$ and $\hat{\theta}^U_i$ when ${}^{k}_{l}\hat{\theta}_i>\hat{\theta}^U_i$ is included in the following components of $\boldsymbol{\mathcal{R}}({}^{k}_{l}\hat{\boldsymbol{\theta}})$:

$$\Re_{6N_{\mathcal{I}}+2i}\left({}^{k}_{l}\hat{\boldsymbol{\theta}}\right)=\frac{1}{2}\lambda_B\max\left(0,{}^{k}_{l}\hat{\theta}_i-\hat{\theta}^U_i\right)^2 \tag{94}$$

where $i\in\{1,\ldots,N_{\mathcal{F}}\}$.

3.5.3 Method of Solution. Following the generalized Newton's method [40], the first-order expansion of $\boldsymbol{\mathcal{R}}(\hat{\boldsymbol{\theta}})$ is used to determine the increment in $\hat{\boldsymbol{\theta}}$ required to minimize the components of the constraint residual vector $\boldsymbol{\mathcal{R}}(\hat{\boldsymbol{\theta}})$

$$\boldsymbol{\mathcal{R}}\left(\hat{\boldsymbol{\theta}}+\Delta\hat{\boldsymbol{\theta}}\right)=\boldsymbol{\mathcal{R}}\left(\hat{\boldsymbol{\theta}}\right)+\frac{\partial\boldsymbol{\mathcal{R}}\left(\hat{\boldsymbol{\theta}}\right)}{\partial\hat{\boldsymbol{\theta}}}\Delta\hat{\boldsymbol{\theta}}+\ldots=\mathbf{0}_{6N_{\mathcal{I}}+2N_{\mathcal{F}}} \tag{95}$$

Table 1 Conventional assignments for $\hat{\theta}^L_i$ and $\hat{\theta}^U_i$

Fold type	$\hat{\theta}^L_i$	$\hat{\theta}^U_i$
No assignment	$-\pi$	π
Valley	0	π
Mountain	$-\pi$	0
Rigidized fold	0	0

The following correction increment $\Delta\hat{\boldsymbol{\theta}}$ is obtained from the previous first-order expansion:

$$\Delta\hat{\boldsymbol{\theta}}=-\left(\frac{\partial\boldsymbol{\mathcal{R}}\left(\hat{\boldsymbol{\theta}}\right)}{\partial\hat{\boldsymbol{\theta}}}\right)^{\dagger}\boldsymbol{\mathcal{R}}\left(\hat{\boldsymbol{\theta}}\right) \tag{96}$$

where $(\cdot)^{\dagger}$ represents the Moore–Penrose pseudoinverse.

The lth set of guess fold angle increments is collected in the vector ${}^{IN}_{l}\Delta\hat{\boldsymbol{\theta}}\in\mathbb{R}^{N_{\mathcal{F}}}$. First, the guess fold angle vector for the lth increment (${}^{1}_{l}\hat{\boldsymbol{\theta}}$) is calculated as follows:

$${}^{1}_{l}\hat{\boldsymbol{\theta}}={}_{l-1}\hat{\boldsymbol{\theta}}+{}_{l}\Delta\hat{\boldsymbol{\theta}} \tag{97}$$

where the fold angles are first updated with the input fold angle increments ${}^{IN}_{l}\Delta\hat{\boldsymbol{\theta}}$ projected into the null space of the previous residual derivatives (see Ref. [40] for details)

$${}_{l}\Delta\hat{\boldsymbol{\theta}}=\left(\mathbf{I}_{N_{\mathcal{F}}}-\left(\frac{\partial\boldsymbol{\mathcal{R}}({}_{l-1}\hat{\boldsymbol{\theta}})}{\partial\hat{\boldsymbol{\theta}}}\right)^{\dagger}\left(\frac{\partial\boldsymbol{\mathcal{R}}({}_{l-1}\hat{\boldsymbol{\theta}})}{\partial\hat{\boldsymbol{\theta}}}\right)\right){}^{IN}_{l}\Delta\hat{\boldsymbol{\theta}} \tag{98}$$

If $\|\boldsymbol{\mathcal{R}}({}^{1}_{l}\hat{\boldsymbol{\theta}})\|/(6N_{\mathcal{I}}+2N_{\mathcal{F}})\geq\texttt{tol1}$, the fold angles are corrected iteratively as follows:

$${}^{k}_{l}\Delta\hat{\boldsymbol{\theta}}=-\left(\frac{\partial\boldsymbol{\mathcal{R}}\left({}^{k}_{l}\hat{\boldsymbol{\theta}}\right)}{\partial\hat{\boldsymbol{\theta}}}\right)^{\dagger}\boldsymbol{\mathcal{R}}\left({}^{k}_{l}\hat{\boldsymbol{\theta}}\right) \tag{99}$$

$${}^{k+1}_{l}\hat{\boldsymbol{\theta}}={}^{k}_{l}\hat{\boldsymbol{\theta}}+{}^{k}_{l}\Delta\hat{\boldsymbol{\theta}} \tag{100}$$

cf. Eq. (96). The correction process of Eqs. (99) and (100) is repeated until $\|\boldsymbol{\mathcal{R}}({}^{k+1}_{l}\hat{\boldsymbol{\theta}})\|/(6N_{\mathcal{I}}+2N_{\mathcal{F}})<\texttt{tol1}$ or $\|{}^{k}_{l}\Delta\hat{\boldsymbol{\theta}}\|/N_{\mathcal{F}}<\texttt{tol2}$, where `tol1` and `tol2` are numerical tolerances. Table 2 summarizes the numerical procedure used for the kinematic simulation of sheets with smooth folds.

4 Implementation Examples

The numerical procedure used for the simulation of the deformation of sheets with smooth folds presented in Sec. 3.5 is implemented in MATLAB. The smooth folds $\mathcal{F}^i_t$ are visualized using the MATLAB three-dimensional shaded surface plot function `surf` while the faces $\mathcal{P}^i_t$ are visualized as filled three-dimensional polygons using `fill3`. The complete MATLAB code for the kinematic simulation of origami with smooth folds and various input examples are included in the "Supplemental Materials" tab for this paper on the ASME Digital Collection.

Smooth folds having G^2 continuous joints with their adjacent faces are assumed for all the examples presented in this section. The formulation of the parametric curve $\hat{\mathbf{c}}^i(\zeta_1)$ that defines the cross-sectional shape of such smooth folds is provided in Eq. (34). Inextensible deformation and a symmetric parabolic curvature field are assumed for $\hat{\mathbf{c}}^i(\zeta_1)$ (see Appendix B for details). Also,

Table 2 Numerical procedure used to simulate the motion of sheets with smooth folds followed at the lth fold sequence increment

1	Determine ${}_{l}\Delta\hat{\boldsymbol{\theta}}$ from ${}^{IN}_{l}\Delta\hat{\boldsymbol{\theta}}$ using Eq. (98)
2	Calculate set of guess fold angles ${}^{1}_{l}\hat{\boldsymbol{\theta}}$ using Eq. (97)
3	`IF` $\|\boldsymbol{\mathcal{R}}({}^{1}_{l}\hat{\boldsymbol{\theta}})\|/N_{\mathcal{F}}<\texttt{tol1}$ `THEN` set ${}_{l}\hat{\boldsymbol{\theta}}={}^{1}_{l}\hat{\boldsymbol{\theta}}$ and `EXIT` `ELSE CONTINUE`
4	Determine correction of fold angles ${}^{k}_{l}\Delta\hat{\boldsymbol{\theta}}$ using Eq. (99)
5	Update ${}^{k+1}_{l}\hat{\boldsymbol{\theta}}$ using Eq. (100)
6	`IF` $\|\boldsymbol{\mathcal{R}}({}^{k+1}_{l}\hat{\boldsymbol{\theta}})\|/(6N_{\mathrm{I}}+2N_{\mathcal{F}})<\texttt{tol1}$ `OR` $\|{}^{k}_{l}\Delta\hat{\boldsymbol{\theta}}\|/N_{\mathcal{F}}<\texttt{tol2}$ `THEN` set ${}_{l}\hat{\boldsymbol{\theta}}={}^{k+1}_{l}\hat{\boldsymbol{\theta}}$ and `EXIT` `ELSE` set $k\leftarrow k+1$ and `GOTO` 4

the range of fold angle values assumed for all the examples presented in this section is the interval $[-\pi, \pi]$. It is noted that the aforementioned assumptions are taken for simplicity and do not present a limitation of the proposed model. Other assumptions on the extensibility and curvature field of the folds are also applicable as long as such assumptions do not violate the continuity conditions for $\hat{\mathbf{c}}^i(\zeta_1)$.

A sheet having eight smooth folds meeting at one interior fold intersection is shown in Fig. 13. The folds are enumerated in counterclockwise order. Various guess fold angle increments are considered ranging from simple to more complex. The folded configurations shown in Fig. 13(*a*) are obtained through the following guess fold angle increments:

$$ {}^{IN}_{l}\Delta\hat{\boldsymbol{\theta}} = \frac{\pi}{50}\begin{bmatrix}1 & 0 & 0 & 0 & 1 & 0 & 0 & 0\end{bmatrix}^{\top} \quad \forall l \in \{1, ..., 50\} \tag{101}$$

and the folded configurations shown in Fig. 13(*b*) are obtained through the following guess fold angle increments:

$$ {}^{IN}_{l}\Delta\hat{\boldsymbol{\theta}} = \frac{\pi}{50}\begin{bmatrix}0 & 1 & 0 & 0 & 0 & 1 & 0 & 0\end{bmatrix}^{\top} \quad \forall l \in \{1, ..., 50\} \tag{102}$$

The two previous guess fold angle increments represent simple examples, and the fold angle correction procedure (refer to Table 2) converged prior to performing an initial correction iteration (i.e., $\|\boldsymbol{\mathcal{R}}({}^{1}_{l}\hat{\boldsymbol{\theta}})\|/N_{\mathcal{F}} < \texttt{tol1} \forall l \in \{1, ..., 50\}$). Alternatively, an example of a more complex folding deformation resulting from guess fold angle increments that required iterative corrections is shown in Fig. 13(*c*). For this example, the guess fold angle increments are as follows:

$$ {}^{IN}_{l}\Delta\hat{\boldsymbol{\theta}} = \frac{\pi}{50}\begin{bmatrix}1 & -1 & 1 & -1 & 1 & -1 & 1 & -1\end{bmatrix}^{\top} \quad \forall l \in \{1, ..., 50\} \tag{103}$$

As shown in the fold angle versus increment plot in Fig. 13(*c*), the fold angles obtained from the simulation procedure differ

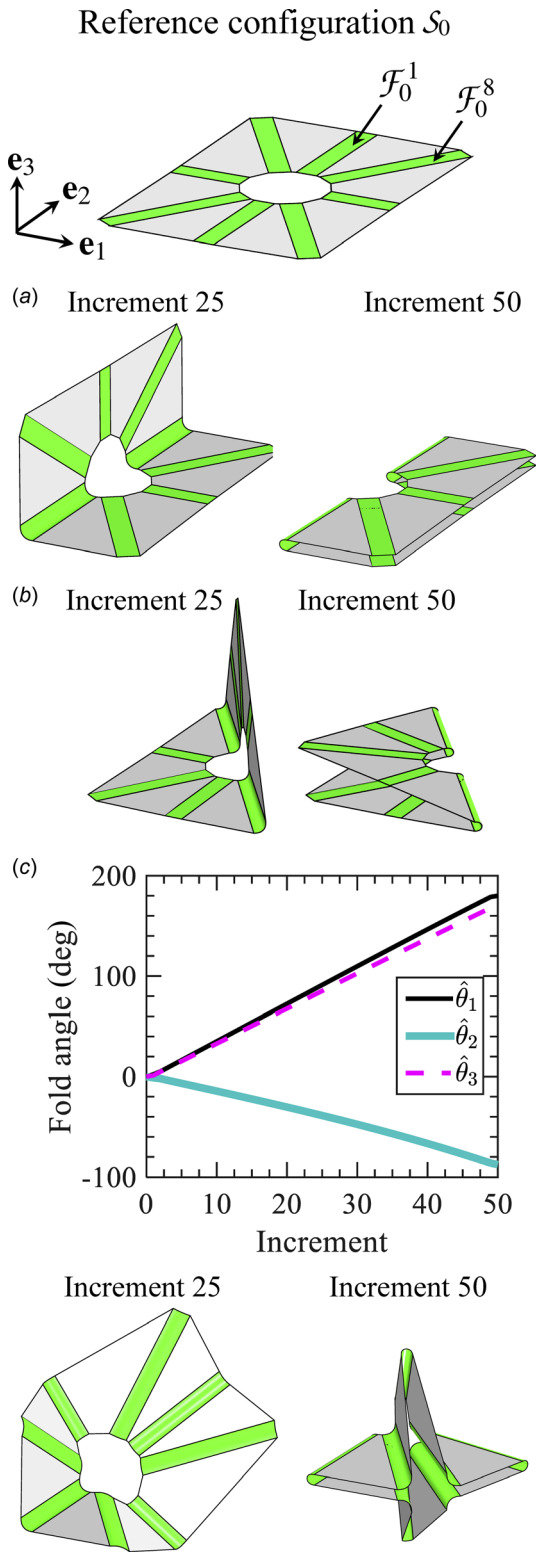

Fig. 13 (*a*) and (*b*): Configurations of a sheet having a single interior fold intersection obtained through the guess fold angle increments provided in Eqs. (101) and (102), respectively. (*c*) Fold angles versus increment number and configurations obtained through the guess fold angle increments provided in Eq. (103).

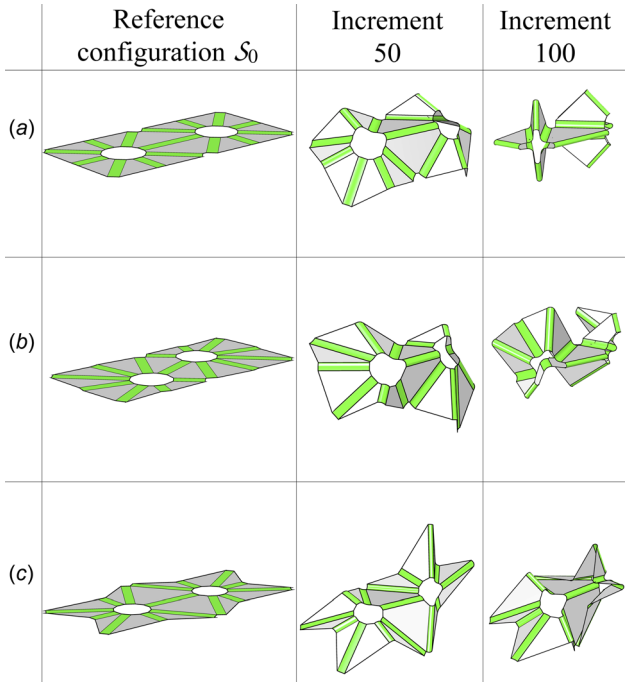

Fig. 14 Configurations for origami sheets with vertex coordinates and fold centerlines defined in Fig. 16: (*a*) sheet with the baseline fold pattern, (*b*) sheet with a fold pattern generated by modifying the interior vertex coordinates of the baseline fold pattern, and (*c*) sheet with a fold pattern generated by modifying the boundary vertex coordinates of the baseline fold pattern

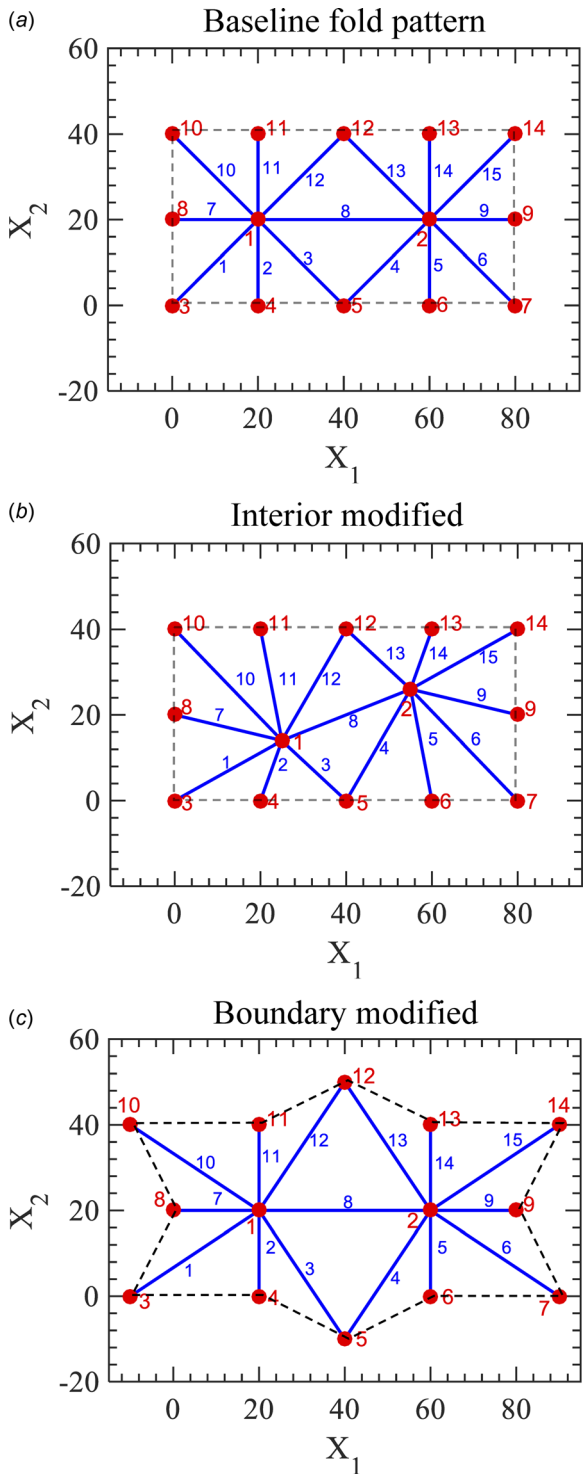

Fig. 15 Graphs showing the vertex coordinates and fold centerlines for the sheets shown in Fig. 14

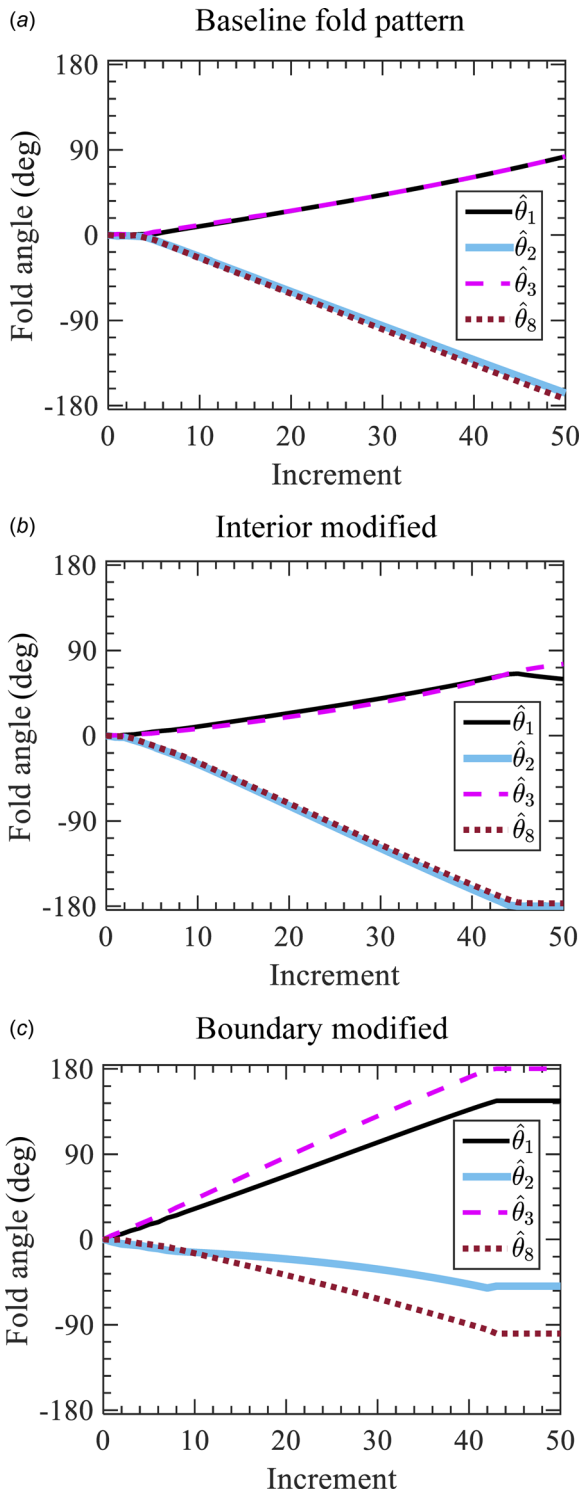

Fig. 16 Evolution of fold angles with increment number for the sheets shown in Fig. 14

from the simple addition of the guess fold angle increments. As observable in the configurations shown in Fig. 13(*c*), all the surface subdomains comprising the sheet remain joined through the deformation of the sheet. Thus, the simulation procedure presented in Sec. 3.5 successfully allows for the correction of the fold angles such that they satisfy the necessary constraints for a valid configuration presented in Eq. (76).

More complex examples of origami sheets having two interior fold intersections are shown in Fig. 14. The graphs of Fig. 15 show the vertices and fold centerlines associated with such sheets. Since the two interior fold intersections for these sheets share a common adjacent fold, their associated constraint equations are coupled. For all the three sheets, the guess fold angle increments are as follows (see Fig. 15 for the numbering of the folds):

$$
\begin{aligned}
&{}^{IN}_{l}\Delta\hat{\theta} \\
&= \frac{5\pi}{600}\begin{bmatrix} 1 & -1 & 1 & 1 & -1 & 1 & -1 & -1 & -1 & 1 & -1 & 1 & 1 & -1 & 1 \end{bmatrix}^{\top} \\
&\quad \forall l \in \{1, \ldots, 100\}
\end{aligned}
\tag{104}
$$

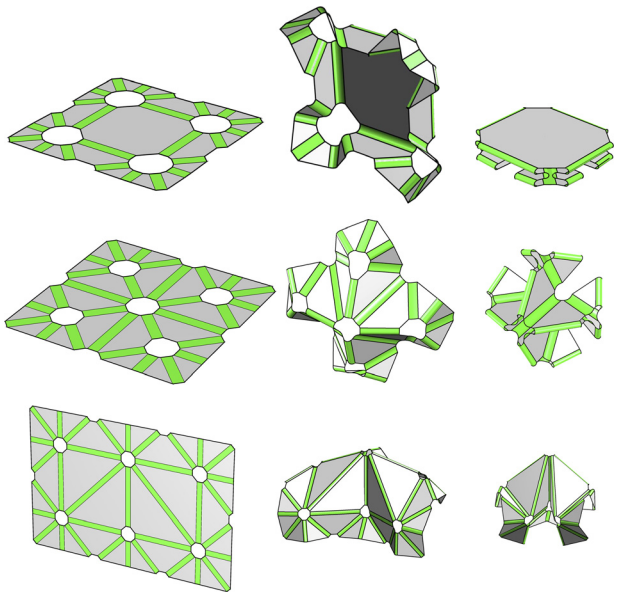

Fig. 17 Demonstration of constrained deformation associated with origami sheets having four, five, and six interior fold intersections. Note that configurations of substantial folding are captured without bending or stretching of the faces or tearing of the sheet.

The sheet with the baseline fold pattern shown in Fig. 14(*a*) exhibits a symmetric behavior, which is expected from the symmetry of the fold pattern and the guess fold angle increments. Sheets having fold patterns obtained by modifying the interior vertex coordinates and the boundary vertex coordinates of the baseline fold pattern are, respectively, shown in Figs. 14(*b*) and 14(*c*). It is observed that both sheets undergo dissimilar fold angle histories compared to the sheet having the baseline fold pattern as observed from both the folded configurations in Fig. 14 and the fold angle versus increment number plots in Fig. 16. These examples show the versatility of the present model that allows for simulation of sheets having arbitrary fold patterns and boundary shapes. This permits the potential application of the model in the design of origami-based structures and mechanisms constrained by realistic material and structural constraints.

The present model is also applicable for the simulation of sheets having arbitrary topology. To illustrate this, sheets having four, five, and six interior fold intersections are shown in Fig. 17.[10] Various configurations are shown for these examples. As observed from these schematics, the present model captures well the behavior of the folded sheets during their full range of motion (fold angles vary from 0 to $\pm\pi$ for various folds in these sheets). The sheet having four interior fold intersections exhibits a desired response that the proposed model captures well, which is of configurations having all the faces located in parallel tangent planes but not overlapping one another. This may aid ongoing efforts to model and design rigid origami structures with thick sheets (see Refs. [12,88–90]).

5 Summary and Conclusions

A model for the kinematic response of origami structures with smooth folds having nonzero sheet surface area and arbitrary order of geometric continuity was presented in this work. A brief review of an established model for rigid origami with conventional creased folds that is extended herein is provided in Sec. 2. The geometrical description of smooth folds was presented in Sec. 3.1, and the parametric representations of the fold cross-sectional shape for various orders of continuity were provided in Sec. 3.1.1. The fold pattern description (Sec. 3.2), the constraints on the sheet deformation for origami with smooth folds analogous to those for origami with creased folds (Sec. 3.3), and the map between reference and current configurations (Sec. 3.4) were also presented. The numerical implementation of the model allowing for simulation of the motion of sheets with arbitrary fold patterns was described in Sec. 3.5, and the implementation examples were provided in Sec. 4.

From the model formulation developed and the results presented in this work, a number of conclusions can be drawn. First, the proposed model successfully allows for the mathematical representation of origami with folds of nonzero sheet surface area and arbitrary order of geometric continuity (in terms of fold shape geometry, constraints on the fold shape variables, and mapping between reference and current configurations). The conventional rigid origami with creased folds of zeroth-order continuity represents a special case of this more general model and is captured as well. Furthermore, the arbitrary order of geometric continuity in the sheet considered in this work allows for the physical modeling of origami structures having significant thickness using plate or shell representations, which is a currently active research topic. Second, the present model and its associated numerical implementation allow for the simulation of sheets having arbitrary fold pattern geometry and topology and boundary shape. The careful consideration of constraints ensures that only meaningful valid configurations will be predicted. The proposed modeling and simulation framework readily allows for modifications to the fold pattern and folding sequence as demonstrated in the implementation examples provided in this work. These characteristics make such a framework useful in future fold pattern design and fold planning studies for origami structures and mechanisms having folds that cannot be accurately represented as creases.

Acknowledgment

This work was supported by the National Science Foundation and the Air Force Office of Scientific Research under Grant No. EFRI-1240483.

Appendix A: Derivation of the Constraint for Origami With Creased Folds

The constraint for origami with creased folds presented in Eq. (14) has been derived in the literature (see Refs. [36,37]) using an approach analogous to that used in Sec. 3.3 to derive the constraints for origami with smooth folds (Eqs. (65) and (66)). The purpose here is not to reproduce such a derivation from the literature but rather derive Eq. (14) as a special case of Eqs. (65) and (66) occurring when the smooth folds are degenerated to straight lines (corresponding to creased folds).

Since Eq. (14) is already accounted for in origami with smooth folds (cf. Eq. (65)), it is only needed to show that $\mathbf{d}^j = 0_3$ (Eq. (66)) holds for origami with creased folds if the constraint presented in Eq. (14) is met. A segment of a general path $\boldsymbol{\gamma}_j(\eta)$ enclosing an interior fold intersection (corresponding to a single point for origami with creased folds) crossing each of its incident folds once in a counterclockwise order is shown in Fig. 18. Using Fig. 18 as a reference, the vectors $\tilde{\mathbf{w}}^{jk}$ and $\tilde{\mathbf{l}}^{jk}$ (see Eqs. (61) and (62)) are, respectively, given as follows:

$$\tilde{\mathbf{w}}^{jk} = \begin{bmatrix} b_{jk} \\ 0 \\ 0 \end{bmatrix} \tag{A1}$$

[10]The example shown in Fig. 5 is also a simulation result obtained using the proposed model.

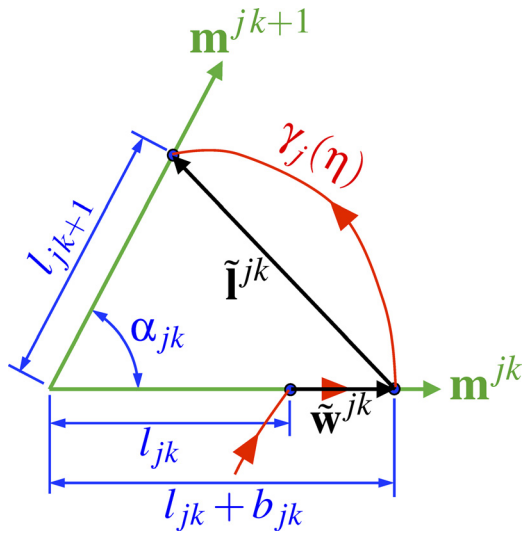

Fig. 18 Schematic showing two adjacent creased folds (along the vectors $\mathbf{m}^{jk}$ and $\mathbf{m}^{jk+1}$) incident to a common interior vertex. The vectors $\tilde{\mathbf{w}}^{jk}$ and $\tilde{\mathbf{l}}^{jk}$ are shown.

$$\tilde{\mathbf{l}}^{jk} = \begin{cases} \begin{bmatrix} l_{jk+1}\cos(\alpha_{jk}) - l_{jk} - b_{jk} \\ l_{jk+1}\sin(\alpha_{jk}) \\ 0 \end{bmatrix}; & k = 1, \ldots, n_j - 1 \\ \begin{bmatrix} l_{j1}\cos(\alpha_{jk}) - l_{jk} - b_{jk} \\ l_{j1}\sin(\alpha_{jk}) \\ 0 \end{bmatrix}; & k = n_j \end{cases} \tag{A2}$$

where $l_{jk} \in \mathbb{R}_{\geq 0}$, $b_{jk} \in \mathbb{R}$, and $l_{jk} + b_{jk} \geq 0$.

Substituting Eqs. (A1) and (A2) into the expression for $\mathbf{d}^j$ provided in Eq. (66) and utilizing the fact that $\mathbf{R}_1(\phi)\tilde{\mathbf{w}}^{jk} = \tilde{\mathbf{w}}^{jk}$ for the expression of $\tilde{\mathbf{w}}^{jk}$ in Eq. (A1), the following is obtained:

$$\begin{aligned} \mathbf{d}^j &= \sum_{k=1}^{n_j} \left(\left(\prod_{l=1}^{k-1} \mathbf{R}_1(\theta_{jl})\mathbf{R}_3(\alpha_{jl}) \right) \begin{bmatrix} b_{jk} \\ 0 \\ 0 \end{bmatrix} \right) \\ &+ \left(\sum_{k=1}^{n_j-1} \left(\left(\prod_{l=1}^{k-1} \mathbf{R}_1(\theta_{jl})\mathbf{R}_3(\alpha_{jl}) \right) \mathbf{R}_1(\theta_{jk}) \begin{bmatrix} l_{jk+1}\cos(\alpha_{jk}) - l_{jk} - b_{jk} \\ l_{jk+1}\sin(\alpha_{jk}) \\ 0 \end{bmatrix} \right) \right) \\ &+ \left(\left(\prod_{l=1}^{n_j-1} \mathbf{R}_1(\theta_{jl})\mathbf{R}_3(\alpha_{jl}) \right) \mathbf{R}_1(\theta_{jn_j}) \begin{bmatrix} l_{j1}\cos(\alpha_{jn_j}) - l_{jn_j} - b_{jn_j} \\ l_{j1}\sin(\alpha_{jn_j}) \\ 0 \end{bmatrix} \right) \\ &= \left(\sum_{k=1}^{n_j-1} \left(\left(\prod_{l=1}^{k-1} \mathbf{R}_1(\theta_{jl})\mathbf{R}_3(\alpha_{jl}) \right) \mathbf{R}_1(\theta_{jk}) \begin{bmatrix} l_{jk+1}\cos(\alpha_{jk}) - l_{jk} \\ l_{jk+1}\sin(\alpha_{jk}) \\ 0 \end{bmatrix} \right) \right) \\ &+ \left(\left(\prod_{l=1}^{n_j-1} \mathbf{R}_1(\theta_{jl})\mathbf{R}_3(\alpha_{jl}) \right) \mathbf{R}_1(\theta_{jn_j}) \begin{bmatrix} l_{j1}\cos(\alpha_{jn_j}) - l_{jn_j} \\ l_{j1}\sin(\alpha_{jn_j}) \\ 0 \end{bmatrix} \right) \end{aligned} \tag{A3}$$

The following equality is then utilized to simplify the previous expression:

$$\begin{bmatrix} l_{jk+1}\cos(\alpha_{jk}) \\ l_{jk+1}\sin(\alpha_{jk}) \\ 0 \end{bmatrix} = \mathbf{R}_3(\alpha_{jk})\mathbf{R}_1(\theta_{jk+1}) \begin{bmatrix} l_{jk+1} \\ 0 \\ 0 \end{bmatrix} \quad \forall\, k \in \{1, \ldots, n_j - 1\} \tag{A4}$$

Substituting Eq. (A4) into Eq. (A3), the following simplified expression is obtained:

$$\begin{aligned} \mathbf{d}^j &= \mathbf{R}_1(\theta_{j1}) \begin{bmatrix} -l_{j1} \\ 0 \\ 0 \end{bmatrix} + \left(\prod_{l=1}^{n_j-1} \mathbf{R}_1(\theta_{jl})\mathbf{R}_3(\alpha_{jl}) \right) \mathbf{R}_1(\theta_{jn_j}) \begin{bmatrix} l_{j1}\cos(\alpha_{jn_j}) \\ l_{j1}\sin(\alpha_{jn_j}) \\ 0 \end{bmatrix} \\ &= \begin{bmatrix} -l_{j1} \\ 0 \\ 0 \end{bmatrix} + \left(\prod_{l=1}^{n_j-1} \mathbf{R}_1(\theta_{jl})\mathbf{R}_3(\alpha_{jl}) \right) \mathbf{R}_1(\theta_{jn_j})\mathbf{R}_3(\alpha_{jn_j}) \begin{bmatrix} l_{j1} \\ 0 \\ 0 \end{bmatrix} \\ &= \begin{bmatrix} -l_{j1} \\ 0 \\ 0 \end{bmatrix} + \left(\prod_{l=1}^{n_j} \mathbf{R}_1(\theta_{jl})\mathbf{R}_3(\alpha_{jl}) \right) \begin{bmatrix} l_{j1} \\ 0 \\ 0 \end{bmatrix} = \begin{bmatrix} -l_{j1} \\ 0 \\ 0 \end{bmatrix} + \mathbf{R}^j \begin{bmatrix} l_{j1} \\ 0 \\ 0 \end{bmatrix} \end{aligned} \tag{A5}$$

The previous equation shows that $\mathbf{R}^j = \mathbf{I}_3 \Rightarrow \mathbf{d}^j = 0_3$ for origami with creased folds independently from the choice of the path $\gamma_j(\eta)$. Therefore, $\mathbf{d}^j = \mathbf{0}_3$ is a redundant constraint for origami with creased folds. This result shows that the constraints for origami with creased folds are a special case of the more general constraints for origami with smooth folds.

Appendix B: Determination of Fold Cross Section Shape Variables

As stated in Sec. 3.3, the full set of fold shape variables $\hat{\theta}_i$, $\hat{w}_i$, and $\hat{a}_i$, $i = 1, \ldots, N_{\mathcal{F}}$, is reduced for simplification to only the set of fold angles $\hat{\theta}_i$, $i = 1, \ldots, N_{\mathcal{F}}$, by determining relations $\hat{w}_i = \hat{w}_i(\hat{\theta}_i, \hat{w}_i^0)$ and $\hat{a}_i = \hat{a}_i(\hat{\theta}_i, \hat{w}_i^0)$. These relations are obtained by making assumptions on the extensibility and curvature field of the smooth folds. The process followed to determine such relations is outlined in this appendix.

Smooth folds having G^2 continuous joints with their adjacent faces are considered. The formulation of the parametric curve $\hat{\mathbf{c}}^i(\zeta_1)$ describing the cross-sectional shape for these smooth folds is provided in Eq. (34). In addition to $\hat{w}_i(\hat{\theta}_i, \hat{w}_i^0)$ and $\hat{a}_i(\hat{\theta}_i, \hat{w}_i^0)$, the relations $\beta^i_{L_1}(\hat{\theta}_i, \hat{w}_i^0)$, $\beta^i_{R_1}(\hat{\theta}_i, \hat{w}_i^0)$, $\beta^i_{L_2}(\hat{\theta}_i, \hat{w}_i^0)$, and $\beta^i_{R_2}(\hat{\theta}_i, \hat{w}_i^0)$ are also determined here since they are required to fully define the shape of the smooth folds (see Eqs. (29) and (31)) even though these variables do not appear in the constraints presented in Sec. 3.3.

To determine the fold shape variables for any value of fold width $\hat{w}_i^0$, the parametric curve $\hat{\mathbf{c}}^i(\zeta_1)$ is made nondimensional by $\hat{w}_i^0$ as follows:

$$\bar{\mathbf{c}}^i(\zeta_1) := \frac{\hat{\mathbf{c}}^i(\zeta_1)}{\hat{w}_i^0} \tag{B1}$$

This leads to the following nondimensional form of the parametric representation of $\hat{\mathbf{c}}^i(\zeta_1)$ presented in Eq. (34):

$$\begin{aligned} \bar{\mathbf{c}}^i(\zeta_1) = {} & h_{50}(\zeta_1)\bar{\mathbf{c}}^i_{L_0} + h_{51}(\zeta_1)\bar{\mathbf{c}}^i_{R_0} + h_{52}(\zeta_1)\bar{\mathbf{c}}^i_{L_1} \\ & + h_{53}(\zeta_1)\bar{\mathbf{c}}^i_{R_1} + h_{54}(\zeta_1)\bar{\mathbf{c}}^i_{L_2} + h_{55}(\zeta_1)\bar{\mathbf{c}}^i_{R_2} \end{aligned} \tag{B2}$$

where

$$\bar{\mathbf{c}}^i_{L_0} := \frac{\hat{\mathbf{c}}^i_{L_0}}{\hat{w}^0_i} = \begin{bmatrix} 0 \\ -\frac{1}{2}\frac{\hat{w}_i}{\hat{w}^0_i} \\ 0 \end{bmatrix}, \qquad \bar{\mathbf{c}}^i_{R_0} := \frac{\hat{\mathbf{c}}^i_{R_0}}{\hat{w}^0_i} = \begin{bmatrix} 0 \\ \frac{1}{2}\frac{\hat{w}_i}{\hat{w}^0_i} \\ 0 \end{bmatrix} \tag{B3}$$

$$\begin{aligned} \bar{\mathbf{c}}^i_{L_1} &:= \frac{\hat{\mathbf{c}}^i_{L_1}}{\hat{w}^0_i} = \frac{\beta^i_{L_1}}{\hat{w}^0_i} \begin{bmatrix} 0 \\ \cos(\hat{a}_i\hat{\theta}_i) \\ -\sin(\hat{a}_i\hat{\theta}_i) \end{bmatrix} \\ \bar{\mathbf{c}}^i_{R_1} &:= \frac{\hat{\mathbf{c}}^i_{R_1}}{\hat{w}^0_i} = \frac{\beta^i_{R_1}}{\hat{w}^0_i} \begin{bmatrix} 0 \\ \cos\left((1-\hat{a}_i)\hat{\theta}_i\right) \\ \sin\left((1-\hat{a}_i)\hat{\theta}_i\right) \end{bmatrix} \end{aligned} \tag{B4}$$

$$\begin{aligned} \bar{\mathbf{c}}^i_{L_2} &:= \frac{\hat{\mathbf{c}}^i_{L_2}}{\hat{w}^0_i} = \frac{\beta^i_{L_2}}{\hat{w}^0_i} \begin{bmatrix} 0 \\ \cos(\hat{a}_i\hat{\theta}_i) \\ -\sin(\hat{a}_i\hat{\theta}_i) \end{bmatrix} \\ \bar{\mathbf{c}}^i_{R_2} &:= \frac{\hat{\mathbf{c}}^i_{R_2}}{\hat{w}^0_i} = \frac{\beta^i_{R_2}}{\hat{w}^0_i} \begin{bmatrix} 0 \\ -\cos\left((1-\hat{a}_i)\hat{\theta}_i\right) \\ -\sin\left((1-\hat{a}_i)\hat{\theta}_i\right) \end{bmatrix} \end{aligned} \tag{B5}$$

Equations (B3)–(B5) show that the nondimensional fold cross section $\bar{\mathbf{c}}^i(\zeta_1)$ is a function of the nondimensional variables $\hat{\theta}_i$, $\hat{w}_i/\hat{w}^0_i$, $\hat{a}_i$, $\beta^i_{L_1}/\hat{w}^0_i$, $\beta^i_{R_1}/\hat{w}^0_i$, $\beta^i_{L_2}/\hat{w}^0_i$, and $\beta^i_{R_2}/\hat{w}^0_i$.

The nondimensional arc length of $\bar{\mathbf{c}}^i(\zeta_1)$, denoted $\bar{s}^{\text{tot}}_i$, is determined as follows:

$$\bar{s}^{\text{tot}}_i = \frac{s^{\text{tot}}_i}{\hat{w}^0_i} = \int_{-1}^{1} \left\| \frac{\mathrm{d}\bar{\mathbf{c}}^i(\zeta_1)}{\mathrm{d}\zeta_1} \right\| \mathrm{d}\zeta_1 \tag{B6}$$

and the nondimensional curvature of $\bar{\mathbf{c}}^i(\zeta_1)$, denoted $\bar{\kappa}_i(\zeta_1)$, is given as follows:

$$\bar{\kappa}_i(\zeta_1) := \hat{w}^0_i \kappa_i(\zeta_1) = \left\| \frac{\mathrm{d}\bar{\mathbf{c}}^i(\zeta_1)}{\mathrm{d}\zeta_1} \times \frac{\mathrm{d}^2\bar{\mathbf{c}}^i(\zeta_1)}{\mathrm{d}\zeta_1^2} \right\| \Big/ \left\| \frac{\mathrm{d}\bar{\mathbf{c}}^i(\zeta_1)}{\mathrm{d}\zeta_1} \right\|^3 \tag{B7}$$

The nondimensional signed curvature of $\bar{\mathbf{c}}^i(\zeta_1)$, denoted $\bar{\kappa}^s_i(\zeta_1)$, is given as

$$\bar{\kappa}^s_i(\zeta_1) = \hat{w}^0_i \kappa^s_i(\zeta_1) = \bar{\kappa}_i(\zeta_1)\,\mathrm{sgn}\left(\left(\frac{\mathrm{d}\bar{\mathbf{c}}^i(\zeta_1)}{\mathrm{d}\zeta_1} \times \frac{\mathrm{d}^2\bar{\mathbf{c}}^i(\zeta_1)}{\mathrm{d}\zeta_1^2} \right) \cdot \hat{\mathbf{e}}^i_1 \right) \tag{B8}$$

The next step is to provide assumptions on the extensibility and curvature field of the fold cross section exhibited during folding. Inextensible deformation is assumed here. It should be noted that inextensibility of the folds is not a restriction of the present model but rather assumed for simplicity. Thus, the goal arc length of the fold cross section, s^{totG}_i, is constant

$$s^{\text{totG}}_i = \hat{w}^0_i \tag{B9}$$

A parabolic form for the goal signed curvature field $\kappa^{sG}_i(\zeta_1)$ is assumed

$$\kappa^{sG}_i(\zeta_1) := \kappa^{\max}_i \left(-\frac{4s_i(\zeta_1)^2}{\left(\hat{w}^0_i\right)^2} + \frac{4s_i(\zeta_1)}{\hat{w}^0_i} \right) \tag{B10}$$

where $s_i(\zeta_1)$ is defined in Eq. (23). Note that $\kappa^{sG}_i(\zeta_1) = 0$ at $s_i(\zeta_1) = 0$ and $s_i(\zeta_1) = \hat{w}^0_i$.

The nondimensional form of Eq. (B9) yields the following nondimensional goal arc length for $\bar{\mathbf{c}}^i(\zeta_1)$, denoted $\bar{s}^{\text{totG}}_i$:

$$\bar{s}^{\text{totG}}_i = \frac{s^{\text{totG}}_i}{\hat{w}^0_i} = 1 \tag{B11}$$

The nondimensional form of the goal signed curvature field in Eq. (B10), denoted $\bar{\kappa}^{sG}_i(\zeta_1)$, is the following:

$$\bar{\kappa}^{sG}_i(\zeta_1) = \hat{w}^0_i \kappa^{sG}_i(\zeta_1) = \bar{\kappa}^{\max}_i \left(-4\bar{s}_i(\zeta_1)^2 + 4\bar{s}_i(\zeta_1) \right) \tag{B12}$$

where

$$\bar{\kappa}^{\max}_i := \hat{w}^0_i \kappa^{\max}_i \tag{B13}$$

$$\bar{s}_i(\zeta_1) = \frac{s_i(\zeta_1)}{\hat{w}^0_i} = \int_{-1}^{\zeta_1} \left\| \frac{\mathrm{d}\bar{\mathbf{c}}^i(\zeta)}{\mathrm{d}\zeta} \right\| \mathrm{d}\zeta \tag{B14}$$

Once the assumptions on extensibility and curvature field are selected, the nondimensional variables $\hat{\theta}_i$, $\hat{w}_i/\hat{w}^0_i$, $\hat{a}_i$, $\beta^i_{L_1}/\hat{w}^0_i$, $\beta^i_{R_1}/\hat{w}^0_i$, $\beta^i_{L_2}/\hat{w}^0_i$, and $\beta^i_{R_2}/\hat{w}^0_i$ are fitted to satisfy such assumptions. For the symmetric smooth folds resulting from the selected assumptions, the variables to fit are simplified as follows:

$$\hat{a}_i = \frac{1}{2}, \quad \frac{\beta^i_{L_1}}{\hat{w}^0_i} = \frac{\beta^i_{R_1}}{\hat{w}^0_i} =: \frac{\beta^i_1}{\hat{w}^0_i}, \quad \frac{\beta^i_{L_2}}{\hat{w}^0_i} = \frac{\beta^i_{R_2}}{\hat{w}^0_i} =: \frac{\beta^i_2}{\hat{w}^0_i} \tag{B15}$$

For a given value of $\bar{\kappa}^{\max}_i$, the error between the goal arc length ($\bar{s}^{\text{totG}}_i$) and the arc length of $\bar{\mathbf{c}}^i(\zeta_1)$ ($\bar{s}^{\text{tot}}_i$), and the error between $\bar{\kappa}^s_i$ and $\bar{\kappa}^{sG}_i$ are minimized as follows:

$$\begin{aligned} &\text{Find} && \hat{\theta}_i \in [0,\pi], \quad \frac{\hat{w}_i}{\hat{w}^0_i} \in (0,1] \\ &&& \frac{\beta^i_1}{\hat{w}^0_i} \in (0,n], \quad \frac{\beta^i_2}{\hat{w}^0_i} \in [0,n] \\ &\text{that minimize} && f\left(\hat{\theta}_i, \frac{\hat{w}_i}{\hat{w}^0_i}, \frac{\beta^i_1}{\hat{w}^0_i}, \frac{\beta^i_2}{\hat{w}^0_i} \right) \end{aligned} \tag{B16}$$

where

$$f\left(\hat{\theta}_i, \frac{\hat{w}_i}{\hat{w}^0_i}, \frac{\beta^i_1}{\hat{w}^0_i}, \frac{\beta^i_2}{\hat{w}^0_i} \right) = \frac{\left(\bar{s}^{\text{totG}}_i - \bar{s}^{\text{tot}}_i\right)^2}{\left(\bar{s}^{\text{totG}}_i\right)^2} + \frac{\int_{-1}^{1} \left(\bar{\kappa}^{sG}_i(\zeta_1) - \bar{\kappa}^s_i(\zeta_1)\right)^2 \mathrm{d}\zeta_1}{\int_{-1}^{1} \left(\bar{\kappa}^{sG}_i(\zeta_1)\right)^2 \mathrm{d}\zeta_i} \tag{B17}$$

It is assumed that the fold shape variables $\hat{w}_i/\hat{w}^0_i$, $\beta^i_1/\hat{w}^0_i$, and $\beta^i_2/\hat{w}^0_i$ are equal for folds having the same fold angle absolute value $|\hat{\theta}_i|$. Thus, the range for fold angles in the bounds of the optimization problem in Eq. (B16) only includes non-negative numbers.

The minimization problem in Eq. (B16) is repeated for a set of values of $\bar{\kappa}_{\max}$ to obtain values of $\hat{\theta}_i$, $\hat{w}_i$, β^i_1, *and* β^i_2 associated with such a maximum nondimensional curvature, which satisfy the assumptions on extensibility and curvature field. The problem is solved for each value of $\bar{\kappa}_{\max}$ using the gradient-based optimization algorithm in MATLAB `fmincon`. The upper bound n for $\beta^i_1/\hat{w}_i$ and $\beta^i_2/\hat{w}_i$ is selected as 10, which is far from the actual values obtained for these parameters, and thus, it resulted in an

inactive bound. Afterward, approximations for $\hat{w}_i(\hat{\theta}_i, \hat{w}_i^0)$, $\beta_1^i(\hat{\theta}_i, \hat{w}_i^0)$, $\beta_2^i(\hat{\theta}_i, \hat{w}_i^0)$ and $\kappa_i^{\max}(\hat{\theta}_i, \hat{w}_i^0)$ are interpolated from the data obtained by solving Eq. (B16) for a set of values for $\bar{\kappa}_i^{\max}$.

References

[1] Lang, R. J., 2007, "The Science of Origami," Phys. World, **20**(2), pp. 30–31.
[2] Demaine, E. D., 2001, "Folding and Unfolding Linkages, Paper, and Polyhedra," *Discrete and Computational Geometry*, Springer-Verlag, Berlin, pp. 113–124.
[3] Demaine, E. D., and O'Rourke, J., 2007, *Geometric Folding Algorithms*, Cambridge University Press, Cambridge, UK.
[4] Cromvik, C., and Eriksson, K., 2009, "Airbag Folding Based on Origami Mathematics," Fourth International Meeting of Origami Science, Mathematics, and Education, Origami 4, Pasadena, CA, Sept. 8–10, pp. 129–139.
[5] Pandey, S., Gultepe, E., and Gracias, D. H., 2013, "Origami Inspired Self-Assembly of Patterned and Reconfigurable Particles," J. Visualized Exp., **72**, p. e50022.
[6] Morgan, J., Magleby, S. P., Lang, R. J., and Howell, L. L., 2015, "A Preliminary Process for Origami-Adapted Design," ASME Paper No. DETC2015-47559.
[7] Gray, S., Zeichner, N., Kumar, V., and Yim, M., 2011, "A Simulator for Origami-Inspired Self-Reconfigurable Robots," Fifth International Meeting of Origami Science, Mathematics, and Education, Origami 5, CRC Press, Taylor & Francis Group, Boca Raton, FL, pp. 323–333.
[8] Hawkes, E., An, B., Benbernou, N. M., Tanaka, H., Kim, S., Demaine, E. D., Rus, D., and Wood, R. J., 2010, "Programmable Matter by Folding," Proc. Natl. Acad. Sci., **107**(28), pp. 12441–12445.
[9] Lang, R. J., 2009, "Computational Origami: From Flapping Birds to Space Telescopes," 25th Annual Symposium on Computational Geometry, Aarhus, Denmark, June 8–10, ACM, New York, pp. 159–162.
[10] Wilson, L., Pellegrino, S., and Danner, R., 2013, "Origami Sunshield Concepts for Space Telescopes," AIAA Paper No. 2013-1594.
[11] Pohl, D., and Wolpert, W. D., 2009, "Engineered Spacecraft Deployables Influenced by Nature," Proc. SPIE, **7424**, p. 742408.
[12] Zirbel, S. A., Lang, R. J., Thomson, M. W., Sigel, D. A., Walkemeyer, P. E., Trease, B. P., Magleby, S. P., and Howell, L. L., 2013, "Accommodating Thickness in Origami-Based Deployable Arrays," ASME J. Mech. Des., **135**(11), p. 111005.
[13] Cheng, Q., Song, Z., Ma, T., Smith, B. B., Tang, R., Yu, H., Jiang, H., and Chan, C. K., 2013, "Folding Paper-Based Lithium-Ion Batteries for Higher Areal Energy Densities," Nano Lett., **13**(10), pp. 4969–4974.
[14] Nam, I., Kim, G.-P., Park, S., Han, J. W., and Yi, J., 2014, "All-Solid-State, Origami-Type Foldable Supercapacitor Chips With Integrated Series Circuit Analogues," Energy Environ. Sci., **7**(3), pp. 1095–1102.
[15] Song, Z., Ma, T., Tang, R., Cheng, Q., Wang, X., Krishnaraju, D., Panat, R., Chan, C. K., Yu, H., and Jiang, H., 2014, "Origami Lithium-Ion Batteries," Nat. Commun., **5**, p. 3140.
[16] White, P. J., Latscha, S., Schlaefer, S., and Yim, M., 2011, "Dielectric Elastomer Bender Actuator Applied to Modular Robotics," IEEE/RSJ International Conference on Intelligent Robots and Systems (IROS), San Francisco, CA, Sept. 25–30, pp. 408–413.
[17] Lee, D.-Y., Kim, J.-S., Kim, S.-R., Koh, J.-S., and Cho, K.-J., 2013, "The Deformable Wheel Robot Using Magic-Ball Origami Structure," ASME Paper No. DETC2013-13016.
[18] Snyder, M. P., Sanders, B., Eastep, F. E., and Frank, G. J., 2009, "Vibration and Flutter Characteristics of a Folding Wing," J. Aircr., **46**(3), pp. 791–799.
[19] Cheung, K. C., Tachi, T., Calisch, S., and Miura, K., 2014, "Origami Interleaved Tube Cellular Materials," Smart Mater. Struct., **23**(9), p. 094012.
[20] Silverberg, J. L., Evans, A. A., McLeod, L., Hayward, R. C., Hull, T., Santangelo, C. D., and Cohen, I., 2014, "Using Origami Design Principles to Fold Reprogrammable Mechanical Metamaterials," Science, **345**(6197), pp. 647–650.
[21] Schenk, M., and Guest, S. D., 2013, "Geometry of Miura-Folded Metamaterials," Proc. Natl. Acad. Sci., **110**(9), pp. 3276–3281.
[22] Fuchi, K., Diaz, A. R., Rothwell, E. J., Ouedraogo, R. O., and Tang, J., 2012, "An Origami Tunable Metamaterial," J. Appl. Phys., **111**(8), p. 084905.
[23] Filipov, E. T., Tachi, T., and Paulino, G. H., 2015, "Origami Tubes Assembled Into Stiff, Yet Reconfigurable Structures and Metamaterials," Proc. Natl. Acad. Sci., **112**(40), pp. 12321–12326.
[24] Thrall, A. P., and Quaglia, C. P., 2014, "Accordion Shelters: A Historical Review of Origami-Like Deployable Shelters Developed by the U.S. Military," Eng. Struct., **59**, pp. 686–692.
[25] Martínez-Martín, F. J., and Thrall, A. P., 2014, "Honeycomb Core Sandwich Panels for Origami-Inspired Deployable Shelters: Multi-Objective Optimization for Minimum Weight and Maximum Energy Efficiency," Eng. Struct., **69**, pp. 158–167.
[26] Turner, N., Goodwine, B., and Sen, M., "A Review of Origami Applications in Mechanical Engineering," Proc. Inst. Mech. Eng., Part C, **230**(14), pp. 2345–2362.
[27] Peraza-Hernandez, E. A., Hartl, D. J., Malak, R. J., Jr., and Lagoudas, D. C., 2014, "Origami-Inspired Active Structures: A Synthesis and Review," Smart Mater. Struct., **23**(9), p. 094001.
[28] Lebée, A., 2015, "From Folds to Structures, A Review," Int. J. Space Struct., **30**(2), pp. 55–74.
[29] Tachi, T., 2009, "Simulation of Rigid Origami," Fourth International Meeting of Origami Science, Mathematics, and Education, Origami 4, Pasadena, CA, Sept. 8–10, pp. 175–187.
[30] Evans, T. A., Lang, R. J., Magleby, S. P., and Howell, L. L., 2015, "Rigidly Foldable Origami Gadgets and Tessellations," R. Soc. Open Sci., **2**(9), p. 150067.
[31] Abel, Z., Cantarella, J., Demaine, E. D., Eppstein, D., Hull, T. C., Ku, J. S., Lang, R. J., and Tachi, T., 2015, "Rigid Origami Vertices: Conditions and Forcing Sets," e-print arXiv:1507.01644.
[32] Tachi, T., 2010, "Geometric Considerations for the Design of Rigid Origami Structures," International Association for Shell and Spatial Structures (IASS) Symposium, Shanghai, China, Nov. 8–12, Vol. 12, pp. 458–460.
[33] Tachi, T., 2013, "Designing Freeform Origami Tessellations by Generalizing Resch's Patterns," ASME J. Mech. Des., **135**(11), p. 111006.
[34] Tachi, T., 2013, "Freeform Origami Tessellations by Generalizing Resch's Patterns," ASME Paper No. DETC2013-12326.
[35] Wu, W., and You, Z., 2010, "Modelling Rigid Origami With Quaternions and Dual Quaternions," Proc. R. Soc. London, Ser. A, **466**(2119), pp. 2155–2174.
[36] Belcastro, S.-M., and Hull, T. C., 2002, "Modelling the Folding of Paper Into Three Dimensions Using Affine Transformations," Linear Algebra Appl., **348**(13), pp. 273–282.
[37] Belcastro, S.-M., and Hull, T. C., 2002, "A Mathematical Model for Non-Flat Origami," Third International Meeting of Origami Mathematics, Science, and Education, Origami 3, pp. 39–51.
[38] Tachi, T., 2007, "Rigid Origami Simulator," TSG, University of Tokyo College of Arts and Sciences, Komaba, Tokyo, Japan.
[39] Tachi, T., 2010, "Freeform Origami," TSG, University of Tokyo College of Arts and Sciences, Komaba, Tokyo, Japan.
[40] Tachi, T., 2010, "Freeform Variations of Origami," J. Geom. Graphics, **14**(2), pp. 203–215.
[41] Schenk, M., and Guest, S. D., 2011, "Origami Folding: A Structural Engineering Approach," Fifth International Meeting of Origami Science, Mathematics, and Education, Origami 5, pp. 291–304.
[42] Demaine, E., Demaine, M., Koschitz, D., and Tachi, T., 2011, "Curved Crease Folding: A Review on Art, Design and Mathematics," IABSE-IASS Symposium: Taller, Longer, Lighter (IABSE-IASS2011), London, Sept. 20–23, pp. 20–23.
[43] Demaine, E. D., Demaine, M. L., Huffman, D. A., Koschitz, D., and Tachi, T., 2015, "Characterization of Curved Creases and Rulings: Design and Analysis of Lens Tessellations," Origami 6: I. Mathematics, pp. 209–230.
[44] Dias, M. A., Dudte, L. H., Mahadevan, L., and Santangelo, C. D., 2012, "Geometric Mechanics of Curved Crease Origami," Phys. Rev. Lett., **109**(11), p. 114301.
[45] Francis, K. C., Rupert, L. T., Lang, R. J., Morgan, D. C., Magleby, S. P., and Howell, L. L., 2014, "From Crease Pattern to Product: Considerations to Engineering Origami-Adapted Designs," ASME Paper No. DETC2014-34031.
[46] Fuchi, K., and Diaz, A. R., 2013, "Origami Design by Topology Optimization," ASME J. Mech. Des., **135**(11), p. 111003.
[47] Kergosien, Y. L., Gotoda, H., and Kunii, T. L., 1994, "Bending and Creasing Virtual Paper," IEEE Comput. Graphics Appl., **14**(1), pp. 40–48.
[48] Solomon, J., Vouga, E., Wardetzky, M., and Grinspun, E., 2012, "Flexible Developable Surfaces," Comput. Graphics Forum, **31**(5), pp. 1567–1576.
[49] Hwang, H.-D., and Yoon, S.-H., 2015, "Constructing Developable Surfaces by Wrapping Cones and Cylinders," Comput.-Aided Des., **58**, pp. 230–235.
[50] Schreck, C., Rohmer, D., Hahmann, S., Cani, M.-P., Jin, S., Wang, C. C., and Bloch, J.-F., 2015, "Nonsmooth Developable Geometry for Interactively Animating Paper Crumpling," ACM Trans. Graphics, **35**(1), p. 10.
[51] Zhu, L., Igarashi, T., and Mitani, J., 2013, "Soft Folding," Comput. Graphics Forum, **32**(7), pp. 167–176.
[52] Fuchi, K., Ware, T. H., Buskohl, P. R., Reich, G. W., Vaia, R. A., White, T. J., and Joo, J. J., 2015, "Topology Optimization for the Design of Folding Liquid Crystal Elastomer Actuators," Soft Matter, **11**(37), pp. 7288–7295.
[53] Fuchi, K., Buskohl, P. R., Ware, T., Vaia, R. A., White, T. J., Reich, G. W., and Joo, J. J., 2014, "Inverse Design of LCN Films for Origami Applications Using Topology Optimization," ASME Paper No. SMASIS2014-7497.
[54] Peraza Hernandez, E. A., Hu, S., Kung, H. W., Hartl, D., and Akleman, E., 2013, "Towards Building Smart Self-Folding Structures," Comput. Graphics, **37**(6), pp. 730–742.
[55] Peraza-Hernandez, E. A., Hartl, D. J., and Malak, R. J., Jr., 2013, "Design and Numerical Analysis of an SMA Mesh-Based Self-Folding Sheet," Smart Mater. Struct., **22**(9), p. 094008.
[56] Peraza-Hernandez, E., Hartl, D., Galvan, E., and Malak, R., 2013, "Design and Optimization of a Shape Memory Alloy-Based Self-Folding Sheet," ASME J. Mech. Des., **135**(11), p. 111007.
[57] Peraza Hernandez, E., Hartl, D., Malak, R., and Lagoudas, D., 2015, "Analysis and Optimization of a Shape Memory Alloy-Based Self-Folding Sheet Considering Material Uncertainties," ASME Paper No. SMASIS2015-9001.
[58] Ahmed, S., Ounaies, Z., and Frecker, M., 2014, "Investigating the Performance and Properties of Dielectric Elastomer Actuators as a Potential Means to Actuate Origami Structures," Smart Mater. Struct., **23**(9), p. 094003.
[59] McGough, K., Ahmed, S., Frecker, M., and Ounaies, Z., 2014, "Finite Element Analysis and Validation of Dielectric Elastomer Actuators Used for Active Origami," Smart Mater. Struct., **23**(9), p. 094002.
[60] Liu, Y., Boyles, J. K., Genzer, J., and Dickey, M. D., 2012, "Self-Folding of Polymer Sheets Using Local Light Absorption," Soft Matter, **8**(6), pp. 1764–1769.

[61] Mailen, R. W., Liu, Y., Dickey, M. D., Zikry, M., and Genzer, J., 2015, "Modelling of Shape Memory Polymer Sheets That Self-Fold in Response to Localized Heating," Soft Matter, **11**(39), pp. 7827–7834.
[62] Davis, D., Mailen, R., Genzer, J., and Dickey, M. D., 2015, "Self-Folding of Polymer Sheets Using Microwaves and Graphene Ink," RSC Adv., **5**(108), pp. 89254–89261.
[63] Ionov, L., 2013, "Nature-Inspired Stimuli-Responsive Self-Folding Materials," *Intelligent Stimuli-Responsive Materials: From Well-Defined Nanostructures to Applications*, Wiley, New York, pp. 1–16.
[64] Demaine, E. D., and Demaine, M. L., 2002, "Recent Results in Computational Origami," Third International Meeting of Origami Mathematics, Science, and Education, Origami 3, pp. 3–16.
[65] Fuchi, K., Buskohl, P. R., Bazzan, G., Durstock, M. F., Reich, G. W., Vaia, R. A., and Joo, J. J., 2015, "Origami Actuator Design and Networking Through Crease Topology Optimization," ASME J. Mech. Des., **137**(9), p. 091401.
[66] Lang, R. J., 1996, "A Computational Algorithm for Origami Design," 12th Annual Symposium on Computational Geometry, Philadelphia, PA, May 24–26, ACM, New York, pp. 98–105.
[67] Tachi, T., 2010, "Origamizing Polyhedral Surfaces," IEEE Trans. Visualization Comput. Graphics, **16**(2), pp. 298–311.
[68] Peraza Hernandez, E., Hartl, D., Malak, R., Akleman, E., Gonen, O., and Kung, H., 2016, "Design Tools for Patterned Self-Folding Reconfigurable Structures Based on Programmable Active Laminates," ASME J. Mech. Rob., **8**(3), p. 031015.
[69] Peraza-Hernandez, E., Frei, K., Hartl, D., and Lagoudas, D., 2014, "Folding Patterns and Shape Optimization Using SMA-Based Self-Folding Laminates," Proc. SPIE, **9057**, p. 90571G.
[70] Zhou, X., Wang, H., and You, Z., 2015, "Design of Three-Dimensional Origami Structures Based on a Vertex Approach," Proc. R. Soc. London, Ser. A, **471**(2181), p. 20150407.
[71] Saito, K., Tsukahara, A., and Okabe, Y., 2016, "Designing of Self-Deploying Origami Structures Using Geometrically Misaligned Crease Patterns," Proc. R. Soc. London, Ser. A, **472**(2185), p. 20150235.
[72] Song, G., and Amato, N. M., 2004, "A Motion-Planning Approach to Folding: From Paper Craft to Protein Folding," IEEE Trans. Rob. Autom., **20**(1), pp. 60–71.
[73] Amato, N. M., Dill, K. A., and Song, G., 2003, "Using Motion Planning to Map Protein Folding Landscapes and Analyze Folding Kinetics of Known Native Structures," J. Comput. Biol., **10**(3–4), pp. 239–255.
[74] Xi, Z., and Lien, J.-M., 2014, "Folding Rigid Origami With Closure Constraints," ASME Paper No. DETC2014-35556.
[75] Xi, Z., and Lien, J.-M., 2015, "Folding and Unfolding Origami Tessellation by Reusing Folding Path," IEEE International Conference on Robotics and Automation (ICRA), Seattle, WA, May 26–30, pp. 4155–4160.
[76] Xi, Z., and Lien, J.-M., 2015, "Plan Folding Motion for Rigid Self-Folding Machine Via Discrete Domain Sampling," IEEE International Conference on Robotics and Automation (ICRA), Seattle, WA, May 26–30, pp. 2938–2943.
[77] Kuribayashi, K., Tsuchiya, K., You, Z., Tomus, D., Umemoto, M., Ito, T., and Sasaki, M., 2006, "Self-Deployable Origami Stent Grafts as a Biomedical Application of Ni-Rich TiNi Shape Memory Alloy Foil," Mater. Sci. Eng.: A, **419**(12), pp. 131–137.
[78] Horn, R. A., and Johnson, C. R., 1991, *Topics in Matrix Analysis*, Cambridge University Press, Cambridge, UK.
[79] Pressley, A. N., 2010, *Elementary Differential Geometry*, Springer-Verlag, London.
[80] Calladine, C. R., 1989, *Theory of Shell Structures*, Cambridge University Press, Cambridge, UK.
[81] Akleman, E., and Chen, J., 2006, "Insight for Practical Subdivision Modeling With Discrete Gauss–Bonnet Theorem," International Conference on Geometric Modeling and Processing, Pittsburgh, PA, July 26–28, Springer-Verlag, Berlin, pp. 287–298.
[82] Sullivan, J. M., 2008, "Curvatures of Smooth and Discrete Surfaces," *Discrete Differential Geometry*, Birkhauser, Basel, Switzerland, pp. 175–188.
[83] Tachi, T., 2015, "Rigid Folding of Periodic Origami Tessellations," Origami 6: I. Mathematics, American Mathematical Society, Providence, RI, pp. 97–108.
[84] Barsky, B. A., and DeRose, T. D., 1984, "Geometric Continuity of Parametric Curves," Computer Science Division, University of California, Berkeley, CA, Technical Report No. UCB/CSD 84/205.
[85] Barsky, B. A., Bartels, R. H., and Beatty, J. C., 1987, *An Introduction to Splines for Use in Computer Graphics and Geometric Modeling*, M. Kaufmann Publishers, Los Altos, CA.
[86] Cheney, W., and Kincaid, D., 1996, *Numerical Analysis. Mathematics of Scientific Computing*, Brooks & Cole Publishing Company, Pacific Grove, CA.
[87] McRobie, F., and Lasenby, J., 2000, "The Kinematics of Large Rotations Using Clifford Algebra," IUTAM-IASS Symposium on Deployable Structures: Theory and Applications, Springer Science+Business Media Dordrecht, The Netherlands, pp. 271–280.
[88] Ku, J. S., and Demaine, E. D., 2015, "Folding Flat Crease Patterns With Thick Materials," ASME Paper No. DETC2015-48039.
[89] Chen, Y., Peng, R., and You, Z., 2015, "Origami of Thick Panels," Science, **349**(6246), pp. 396–400.
[90] Tachi, T., 2011, "Rigid-Foldable Thick Origami," Fifth International Meeting of Origami Science, Mathematics, and Education, Origami 5, CRC Press, Boca Raton, FL, pp. 253–264.